

Universidad de Antioquia



**UNIVERSIDAD
DE ANTIOQUIA**
1803

Martian Ice Sample Return Mission

Project Haba-Sulue



Undergraduate Space Design Competition

Aerospace Engineering

2021



J. Elias Montoya

J. Elias Montoya
Faculty Advisor



Santiago A. Velez

Santiago A. Velez
Team Leader
Member #: 1241089



Juan José Mejía

Juan J. Mejía
Team Leader
Member #: 1241095



Laura Duque

Laura Duque
Mars Surface Operations
Member #: 1241094



Jorge M. Serna

Jorge M. Serna
Mars Surface Operations
Member #: 1241100



Sebastián Zapata

Sebastián Zapata
Orbits
Member #: 1241154



Luisa F. Mendoza

Luisa F. Mendoza
Orbits
Member #: 1241098



Sebastián León Serna

Sebastián León
Orbits
Member #: 1241099



Juan Carlos Rojas

Juan C. Rojas
Atmospheric Flight
Member #: 1241096



Manuela Zapata

Manuela Zapata
Mars Surface Operations
Member #: 12441102



Mario Silva

Mario Silva
Atmospheric Flight
Member #: 1241155

Special thanks for their collaboration and support, without them this would not be possible.



Samuel Cadavid



Maria A. Botero



Jhon Amaya

Contents

1	Summary	1
1.1	Prologue	1
1.2	Motivation	1
1.3	Executive summary	1
1.4	Mission Overview	4
2	Landing Site and Season	5
2.1	Mars Landing Site Selection	5
3	Orbital Mechanics	7
3.1	Timeline	7
3.2	Key trades	7
3.3	Launch vehicle	9
3.4	Trajectory	11
3.5	Interplanetary Transfer Vehicle	17
4	Mars Surface Operations	28
4.1	Entry, Descent and Landing	28
4.2	Modified Skycrane Lander Descent Stage	29
4.3	Surface Vehicle, Rover - Technology Offset	36
4.4	Drilling and Coring	54
4.5	Conservation of the Ice-Core Samples	58
4.6	Mass and Costs Budget	65
5	Mars Ascent Vehicle	66
5.1	Key Trades	66
5.2	MAV Options	67
5.3	Fuel Selection	70
5.4	Motor Design	70
5.5	MAV Guidance, Navigation and Control	71
5.6	MAV Systems	76
6	Earth Entry Vehicle (EEV)	78
6.1	System Overview	78
6.2	Alternatives and Decision	79
6.3	TPS and EEV Geometry	79
6.4	Temperature Passive Control and External Thermal Performance	80
6.5	Heat Transfer Calculations	82
6.6	Results	83
6.7	EEV systems and components	84
7	Mission Analysis	84
7.1	Mission overall cost	84
7.2	Mission risks and Compliance Matrix	86
	Bibliography	90

List of Figures

1.1	Main mission steps	4
2.1	Depth to the top of the water ice table derived from MCS data	6
3.1	Mission timeline.	8
3.2	Launch vehicle and payload overview.	10
3.3	Round-trip rendezvous mission to Mars with optimal parameters	13
3.4	Outbound trajectory model	15
3.5	Circularizing maneuver to parking orbit	16
3.6	Return trajectory model	17
3.7	ITV at launch configuration.	18

3.8	ITV exploded view and components.	18
3.9	Falcon 9 load factors.	20
3.10	ITV Communications access with Earth – DSN	22
3.11	Communication overview between the DSN and a relay station and communication between the rover and the ITV.	22
3.12	Maximum communication range between the ITV and rover.	23
3.13	ITV attitude at WCH.	26
3.14	COM primary dimensions.	27
3.15	COM operational concept.	27
4.1	MSL Aeroshell Measures.	28
4.2	Trajectory profile of MSL EDL	29
4.3	Lander on mars surface.	30
4.4	Lander Requirements.	30
4.5	Photography of original sky crane used in the MSL.	31
4.6	Original sky crane design viewed from below.	32
4.7	Original sky crane and backshell interface.	32
4.8	Modified sky crane and backshell interface.	32
4.9	Beams stress simulation from Fusion 360.	33
4.10	Novel approach for the lander legs	34
4.11	Erection Mechanism.	35
4.12	MAV erection process from stowed to erect.	36
4.13	Surface Vehicle Requirements.	39
4.14	Instrumentation and avionics inside WEB	40
4.15	REMS' Booms Location	41
4.16	Downhill slope considerations	42
4.17	Cross hill slope considerations	42
4.18	Position of center of mass in sample handling operations.	43
4.19	Position of center of mass in traverse operation.	43
4.20	Calculated Rocker-Bogie dimensions.	43
4.21	Drilling operations	43
4.22	Mars 2020 rover chassis truss form	44
4.23	Rover-TO cantilever truss.	44
4.24	Main truss simulations.	45
4.25	Rover Navigation Cameras	46
4.26	Rover-DSN Daily Access.	51
4.27	Rover-Orbiter Daily Access.	52
4.28	Auto-Gopher II concept of autonomous sampling system	56
4.29	Auto Gopher II: Drill Parts and concept on MSL rover.	57
4.30	Cross-Section of the Orbiting Sample Sub-Assemblies.	58
4.31	Cross-Sections of the Orbiting Sample Capsules	59
4.32	Sample Tubes	61
4.33	Transfer of the Ice-Core to the Sample Tubes.	62
4.34	Caching Sequence.	62
4.35	Rover Arm holding the OS.	63
5.2	MAV Requirements.	66
5.1	Haba Sulue Designed MAV at Mars Surface.	66
5.3	SSTO Bi Propellant CAD Model	67
5.4	SSTO Hybrid Rocket Motor	68
5.5	TSTO Solid Rocket Motor.	68
5.6	STAR 13B. First Stage Solid Rocket Motor.	70
5.7	STAR 17. Second Stage Solid Rocket Motor.	70
5.8	MSR Solid Vehicle Nominal Flight.	72
5.9	TSTO Solid Rocket Motor Trajectory Plot Using Designed Interface.	73
5.10	MAV Dynamic Pressure Plot.	73
5.12	MAV avionics	75
5.13	Second Stage RCS.	76
5.14	MAV Stowed inside Igloo.	77
5.15	Heaters and Thermometers for Thermal Control Inside Igloo	77
6.1	EEV configuration.	80
6.2	EEV's General Dimensions	80
6.3	Thermal Design of HSRC from JAXA	81
6.4	Heat Flux, no Rigid Flares and Rigid Flares	82
6.5	Heat Flux vs Time	82
6.6	Temperature vs time	83

List of Abbreviations

ΔV	Delta V	OS	Orbiting Sample
ACS	Attitude Control System	PAF	Payload Attach Fitting
ADCS	Attitude Determination and Control System	PCEC	Project Cost Estimation Capability
AFT	Allowable Flight Temperature	PCM	Phase Change Material
AHP	Analytic Hierarchy Process	PDC	Polycrystalline Diamond Compact
ATS	Atmospheric Temperature Sensor	PICA	Phenolic Impregnated Carbon Ablator
C&DH	Command and Data Handling	PIXL	Planetary Instrument for X-ray Lithochemistry
CFD	Computational Fluids Dynamics	PLF	Payload Fairing
CLG	Closed-Loop Guidance	PLS	Phoenix Landing Site
CNSA	China National Space Administration	PP	Planetary Protection
COM	Capture and Orient Module	PPL	Propulsive Platform Lander
Comm	Communications	PRTs	Platinum Resistance Thermometers
COSPAR	Committee On Space Research	PS	Pressure Sensor
CPS	Cross-Product Steering	RAMP	Rover Avionics Mounting Panel
CV	Containment Vessel	RCS	Reaction Control Systems
DSN	Deep Space Network	REMS	The Rover Environmental Monitoring Station
EDL	Entry, Descent and Landing	RFP	Request For Proposal
EEV	Earth Entry Vehicle	RIMFAX	Radar Imager for Mars' subsurFACE eXperiment
EMT	Estimated Mission Time	RIPAS	Rover Integrated Pump Assembly
EPS	Electrical Power Subsystem	RLGA	Rover Low Gain Antenna
ERM	Earth Return Module	ROP	Rate Of Penetration
ERO	Earth Return Orbiter	Rover-TO	Rover- Technology Offset
FCM	Flexure Claw Mechanism	RTG	Radioisotope Thermoelectric Generator
GLOM	Gross Lift-Off Mass	SCHERLOC	Scanning Habitable Environments with Raman & Luminescence for Organics & Chemicals
GNC	Guidance Navigation and Control	SDL	Sky Crane Delivered Lander
GPR	Ground Penetrating Radar	SDST	Small Deep-Space Transponders
GPS	Global Positioning System	SIRCA	Silicon Impregnated Reusable Ceramic Ablator
GTO	Geostationary Transfer Orbit	SMAD	Space Mission Analysis and Design
GTS	Ground Temperature Sensor	SOI	Sphere of Influence
HGA	High Gain Antenna	SRC	Samples Reentry Capsule
HS	Humidity Sensor	SSTO	Single Stage to Orbit
ICRF	International Celestial Reference Frame	STA	Sample Transfer Arm
ICU	Instrument Control Unit	STK	Systems Tool Kit
IMU	Inertial Measurement Unit	SXS	Simple Cross-product Steering
ISP	Specific Impulse	TCS	Thermal Control System
ISPT	In-Space Propulsion Technology	TLR	Technology Level Readiness
ISS	International Space Station	TPS	Thermal Protection System
ITV	Interplanetary Transfer Vehicle	TPW	Triple Point of Water
JAXA	Japan Aerospace Exploration Agency	TRL	Technology Readiness Level
JPL	Jet Propulsion Laboratory	TTSTO	Two Stage To Orbit
JSC	Johnson Space Center	TT&C	Telemetry, Tracking and Command
LRO	Lunar Reconnaissance Orbiter	TVC	Thrust Vectoring Control
MAV	Mars Ascent Vehicle	TWTA	Traveling Wave Tube Amplifier
Max Q	Maximum Dynamic Pressure	UBL	Unknown But Low
MECO	Main Engine Cut-Off	USDC	Ultrasonic/Sonic Drill/Corer
MEDA	Environmental Dynamics Analyzer	UVS	Ultraviolet Sensor
MERV	Mars Earth Return Vehicle	VIP	Vacuum Insulation Packs
MEV	Mars Entry Vehicle	WCC	Worst Case Cold
MMRTG	Multi-Mission Radioisotope Thermoelectric Generator	WCH	Worst Case Hot
MOMA	Mars Organic Molecule Analyser	WEB	Warm Electronics Box
MOS	Missions On Site	WISDOM	Water Ice and Subsurface Deposit Observation on Mars
MPA	MAV Payload Assembly	WOB	Weight On Bit
MPW	Melting point of water	WS	Wind Sensor
MRO	Mars Reconnaissance Orbiter		
MSL	Mars Science Laboratory		
NASA	National Aeronautics and Space Administration		
NDEAA	NonDestructive Evaluation and Advanced Actuators		
NGAVGS	Next Generation Advanced Video Guidance Sensor		

1 Summary

1.1 Prologue

Haba-Sulue is a team of students of the aerospace engineering program at Universidad de Antioquia. This is the first aerospace engineering undergraduate program in the country, and this is the first time that a Colombian team enters the competition. We look forward to participating in this and other AIAA competitions every year, and would greatly appreciate if the reader could provide their feedback regarding this proposal, which can be sent to salberto.velez@udea.edu.co

1.2 Motivation

Reasons for reaching outer space are getting quotidian for humanity, generation by generation, year by year, while the world develops every day more confident than ever, but still keeps facing the inevitable challenges of nature, like those lived throughout 2020 and the ongoing 2021 pandemic. Reaching outer space is necessary to advance, to survive, and to understand our place as whole humankind. But for these outstanding views and those fierce moments to come from space exploration, as individuals the day of today, we might not be present. Despite this, we still reach for space and stars. We reach space and we risk thriving on it for a very different reason beyond need or survival. Today, we accept these challenges "...not because they are easy, but because they are hard because that goal will serve to organize and measure the best of our energies and skills...". As students, we would like to understand the words of President John F. Kennedy as a call to accept the challenge, because only by emerging through it we find the best version of ourselves. This is what a still-young history of the National Aeronautics and Space Administration (NASA) has taught around a still divided world. Being better to yourself is reached only by making others around you better, and the best version of ourselves knows that best is only achieved as a team.

1.3 Executive summary

Project Haba-Sulue team, in the opportunity of challenge, submits this proposal to the American Institute of Aeronautics and Astronautics (AIAA), aimed to accomplish a formal proposition to NASA of a round trip involving the concept of a planetary sampling campaign with a Mars Sample Return (MSR) mission. The name of our project, in honor to the Kogi, an ancient culture of Colombia that worships snow among their Gods and gave it the name of Haba-Sulue, reflects the main goal of the mission, retrieving ice cores from Mars, and from then on, the start of MSR operations.

To date, NASA's Mars Sample Return is being executed in various stages, starting with Mars 2020 Rover collecting geological samples from Mars, but a sole round trip aimed to accomplish it is being thought only for 2030 as a crewed mission that will precisely sample ice cores and return them back to Earth. To achieve this level of precision of a manned mission, the team followed the constraints imposed for the Request for Proposal (RFP), for which a special emphasis was put on Planetary Protection.

To achieve this proposal the team performed trade studies with models like Analytic Hierarchically Process (AHP), a structured technique for organizing and analyzing complex decisions, based on mathematics that finds applications in group decision making. AHP process developed used quantitative values but also it was used qualitative values compared from logic, experts advisory and knowledge gained as the mission was evolving. this decision-making process can be found within subsystems sections. For some cases, the team had the chance to directly discard some of the concepts and architectures based on facts and literature. all decision processes and down select were based paramount trades such as cost, low complexity and design and development time, as well as specific drivers found on every system.

Regarding launch architecture, two cases were assessed, one launch architecture and multiple launch architecture ongoing right now by NASA and ESA. This last option was discarded considering convenience, mission success probability and also that cost and time were out of range for Space Design constraints. A single architecture was then responsible to carry at least the main systems needed for the round trip, being these the Mars Ascent Vehicle (MAV), the coring and sampling systems, and the conservation of sample systems. Over this wide spectrum of possibilities, multiple architectures were evaluated for each of these systems.

Regarding MAV the hybrid versus solid propellant architecture selection, a wide variety of investigation was carried out considering hybrid efforts made by NASA and its different partner contractors. Hybrid MAV was desired due to its low Allowable Flight Temperature (-72°C) and potentially even go as low as -100°C . This condition is even more relevant when is considered that the MAV need to survive near pole temperatures. On the other hand, it was found that Hybrid option was less GLOM sensible compared with the solid solution. Despite these characteristics, hybrid option was discarded considering its low technology readiness level (TRL) and little time available for development, testing and certification, all of this before 2026 selected launch window. This and that solid rocket motor was found to have a high TRL, its selected propellant has flight heritage, and it was the complex, costliest and needed the least time to be ready. the designed rocket is a Two Stage To Orbit (TSTO) rocket equipped with Reaction Control System (RCS), Thrust Vectoring Control (TVC) and high heritage TP-H 3062 (16% Al) propellant that withstands temperatures as low as -58°C

Regarding coring and sampling, on the drill matter two options were considered, resulting auto-gopher as the best option given that there was scarce literature information and therefore other drills could not be compared properly. The Auto-gopher is a deep drill design and developed by honeybee robotics, the same company that designed the MSL curiosity and perseverance drills. Once the drill selected different robotic arms were assessed, Johnson Space Center proposed that an arm equipped with a claw was used but literature review on this type of arms was outdated and their functionality was

limited to this mission in particular, meaning no heritage. Considering this the Canada arm was selected due to its low cost is currently working on the ISS. The overall selected system allowed for low complexity and convenience given that it only needs two steps to drill and save the extracted sample inside the capsule, whereas discarded alternatives would need at least five steps to achieve the same goal.

Regarding the rover versus lander options, a lander was selected due to its low cost and low complexity. Modifying the descent stage sky crane used in MSL and Mars 2020 to serve as lander as well was found to meet the requirements and key trades, whereas the rover architecture, despite having the ability to launch the MAV at any time regardless of the rover being stuck, it the costliest option and carrying a +400 kg MAV system would need a large and robust rover, impacting negatively on complexity and packaging options. On conservation system the OS with active vs passive thermal regulation resulted that other systems could provide thermal control assistance and thus the OS would not need thermal active system, a thermal study was made and found that the OS would be secure in every stage of the mission, having the rover with thermal active assistance as well as Earth Return Module (ERM). The OS is well sealed and hermetic, and it uses a white coating as a passive thermal control while orbiting around mars until catching with ERM.

From these trades, a final configuration based on saving of space, mass, and costs was found optimal, as it was the less risky option for its extensive use of heritage components, or if not, at least already proven in-flight systems. This configuration based on heritage components results in a less costly mission due to less testing and design considerations. To confirm this, various analyses based on reliability and costs were performed throughout the systems. At the end of the trade studies, the solution was delivered by three systems: an electrically propelled spacecraft with the capacity of being an orbiter and a round trip shuttle, based on Stardust, Osiris Rex, and Mars Reconnaissance Orbiter (MRO) missions. This spacecraft will circularize around Mars with aid of the Martian Atmosphere and will deliver the payload into coordinates 68.22N, 234.25E, Green Valley, Phoenix landing site. An EDL system, which has the twice proven Aeroshell of MSL class missions with no changes to its configuration will perform the entry with its autonomous guidance systems and will hand the last landing stage to the Powered Descent Stage (PDS) of this very MSL class EDL. This vehicle will be the same as in previous missions but with two structural modifications that allow it to carry the MAV and to land it in a safely condition, still being able to perform the skycrane maneuver to deposit on Mars surface the operations vehicle. This operations vehicle is a rover of considerable size to weight ratio and made up of heritage components of the two previous NASA rover classes MER and MSL. This rover is specifically designed to carry the Auto-Gopher II drill, a wireline autonomous coring system developed by JPL in association with Honeybee Robotics, the company responsible for the two drills that are right now in operation on Mars surface aboard the two MSL class rovers. The rover will return the samples to a solid propellant MAV system that survived Martian poles thanks to a brand-new igloo thermal system, and to design components that can stand the selected environment. Finally, the most critical stage of the mission, the conservation of the samples, was achieved by choosing adequate latitude and season for landing. This conjunction permitted the ice to remain stable at environment changes, being supported in extreme temperature cases by the Mechanically Pumped Fluid Loop (MPFL) aboard the rover.

The following stages include the accomplishing of a novel orbital maneuver, tested already on ISS facilities, known as the "catching", in which the orbiter will perform attitude control till the OS (Orbiting Sample), a little canister of about 20 cm in diameter and about 25 cm tall, is found optically after surviving on-orbit conditions, and then brought inside the spacecraft into an environment suited for the sample preservation during the trip back to Earth.

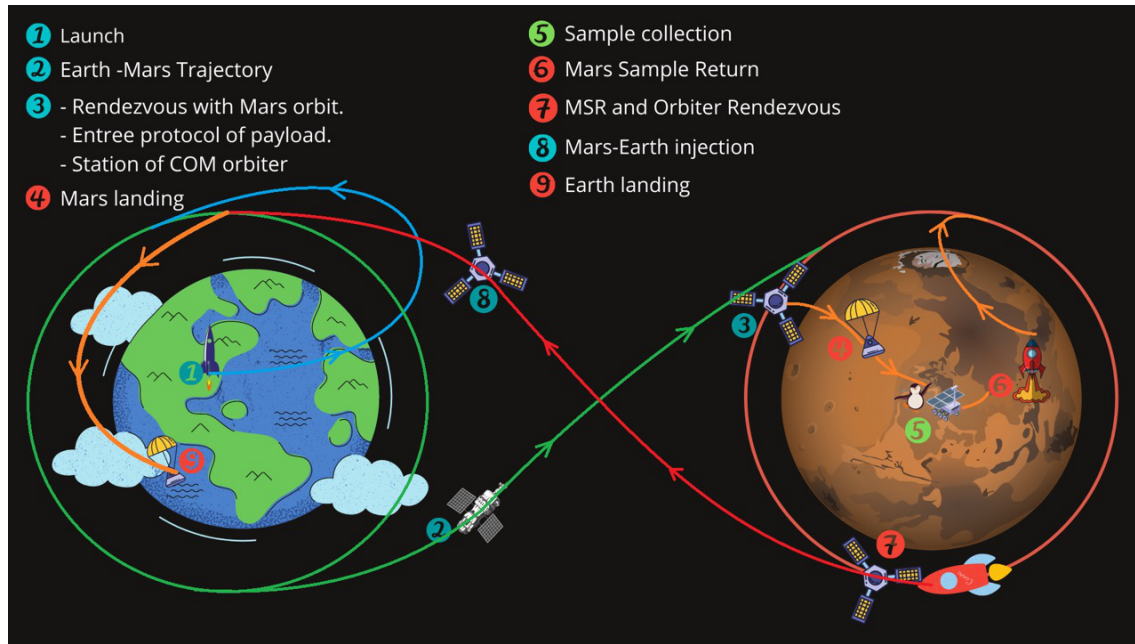


FIGURE 1.1: The main mission steps considered by the Team in a very basic scheme.

1.4 Mission Overview

1.4.1 Project management and Mission Design

Haba-Sulue Mission Design was broken up into three main phases. System requirements review and literature review, Preliminary Design Review and Critical Design Review. Initially, the team brought together the required deliverables, key deadlines, estimates of required work effort and team organization. Initially, the team was tasked with recognizing the required deliverables, key deadlines and a general study of the effort and time required to meet deadlines. Starting in November 2020 and after doing a literature review of the mission, the team was divided into three main groups, sample extraction and mars campaign, atmospheric flight and orbital mechanics, each responsible for mission decisions pertinent to each area. Once the working groups were established, a 3-month time frame was given, the preliminary work was focused on conceptual design, performing an extensive literature review of each system, identifying the key trades for each of these. Initially, meetings between teams took place every week to accumulate knowledge through dialogue, during the week the

activity, apart from advancing in the research, consisted of writing down the main findings and identifying the interface needs with other systems. Starting the Preliminary Design Review in February 2020, 3 meetings were held per week, a general meeting to evaluate the status of the mission, the meeting of each group, where the needs were identified and a space for a third interface meeting with the other teams. During this stage, we held consultancies with different experts on the subject, some compatriots who work at NASA and some professors of the program. By the end of March, a written PDR was ready. April and May consisted of the Critical Design Review and the final drafting of the proposal.

1.4.2 Needs Analysis

For several decades, scientists have advocated the return of geological samples from Mars. To bring Mars closer to Earth, NASA has declared a Mars Sample Return mission the main goal for this decade. Samples of particular interest are ice core samples; these samples have accumulated information of interest throughout millions of years about Mars history and the formation of life. MSR mission will pave the way for future exploration of Mars and allow manned missions to the red planet in the forthcoming years. Considering that some stages of this mission have never been done, there are many challenges that need to be addressed for the success of this mission. Ice cores sample survivability from extraction to the laboratories on Earth, sample handling and transfer to lander, MAV flight ascension and OS injection to target orbit are among them.

2 Landing Site and Season

Where to land on Mars proved to be the most critical part for the planning of this mission. On this decision relies all aspects over vehicles, orbits and budget and the decisions to follow. Therefore, several alternatives have been considered for the landing site based on studies about the distribution of ice deposits on Mars. At first hand the team the sites selected according to the above include areas such as glaciers in the middle latitudes, northern craters, Arcadia Planitia, the North Pole and its environments at whole Vastias Borealis.

It should be mentioned that the south of the planet and associated latitudes were not considered due to the surface relief they present and the large changes in height due to the number of craters it has, which for a type of mission like ours is quite critical and presents many difficulties to access them.

2.1 Mars Landing Site Selection

For the selection of the landing site on Mars, as mentioned above, the main interest is focused on the confirmation of the existence of solid ice at the site, however, aspects that could be seen as impediments during the development of the mission or that could affect any of the associated systems, that is, the place should have at least environmental conditions where

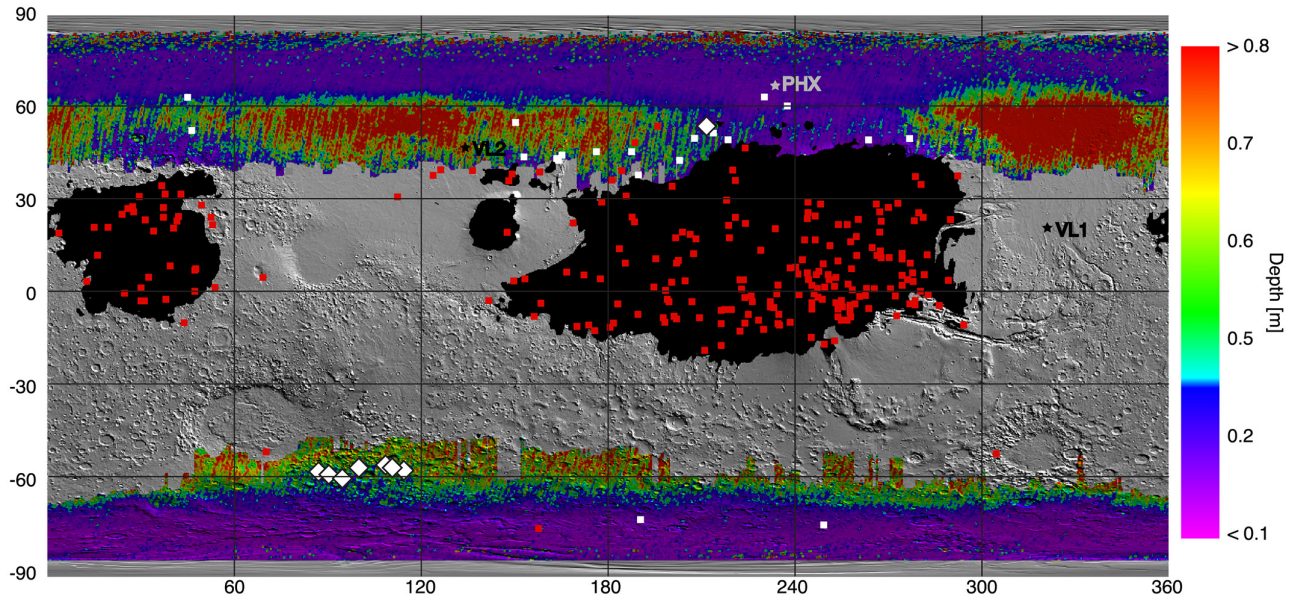


FIGURE 2.1: Depth to the top of the water ice table derived from MCS data. Background is a MOLA shaded relief. Low thermal inertia regions unsuitable for landing are masked out. PHX, VL1, and VL2 indicate the landing site locations for Phoenix, Viking Lander 1, Viking Lander.

the pressure and temperature are not so extreme and can be controlled in the vehicles that operate on the surface through the system of thermal control these, low or zero slopes on the ground to facilitate the mobility of the rover and the range of the landing ellipse, be located at a latitude and with altitude MOLA accessible for the EDL and for the launch of the MAV, finally that it does not have planetary protection restrictions that prevent the operation of instruments that are planned to be implemented in that area.

In accordance with the above, the option of the northern polar craters is ruled out due to their surface relief that compromises landing and operational physical support [1]. Glaciers, even though is ideally suitable for this task, are ruled out due to the lack of certainty about the depth of the ice and its composition [2]. The North Pole, despite being one of the best consolidated candidates in terms of the presence, shape and depth in which the ice is found, presents planetary protection and location restrictions that make access and survival difficult, for that is also discarded [3, 4].

Finally, the two places with the most suitable conditions for landing are reduced to Arcadia Planitia and the Phoenix landing site. The first been promising for human colonies settlement, ancient ice [5, 6], but the latter being the one chosen for the certainty of finding ice, its shape and stability with respect to Arcadia [7, 8]. In addition to having the information and characterization that the Lander [9] carried out, which allows us to propose the systems with greater certainty of the environmental conditions they will be faced with.

TABLE 2.1: Reliability Study for Mars Landing Site.

Alternatives	Ice Composition	%P of Finding Ice	Surface Free Obstacles	-
Weight	0.16794	0.75138	0.08067	AHP
North Pole	0.47011	0.32471	0.56002	0.36812
Arcadia Planitia	0.05215	0.05085	0.04399	0.05052
Craters	0.27396	0.32471	0.23533	0.30898
PLS	0.20377	0.29971	0.16065	0.27238

TABLE 2.2: Trade Study for Mars Landing Site.

Alternatives	MOS	Pressure / Temperature	PP	Mean Slope (°)	EMC	Reliability	-
Weight	0.134	0.264	0.114	0.12	0.15	0.22	AHP
North Pole	0	11 mbar/205 K	0	0ř	UBL	0.36812	0.08216
Arcadia Planitia	0	0-18 mbar/205 K	1	5.7ř	1281 suns	0.05052	0.12504
Craters	0	11 mbar/205 K	0	0-20ř	UBL	0.30898	0.06896
PLS	1	7-11 mbar/175.3-253.4 K	0	0.2-0.3ř	150 suns	0.27238	0.19328

3 Orbital Mechanics

3.1 Timeline

An overview of the mission timeline is shown in Fig. 3.1.

3.2 Key trades

3.2.1 Decision to Dock or Catch Mars samples

A first proposal for the on-orbit collection of samples was studied. It required MAV to be adapted to carry out a docking maneuver with the orbiter, which implies increases in the mass and the electrical power consumption for both vehicles since it must integrate components that allow the proper interface between both spacecraft environments of MAV and EEV.

However, several Orbiting Sample (OS) capture systems for MSR have been studied at JPL [10]. Therefore, a Capture and orient module (COM) concept was selected because of its improvements on interfacing phases and achieving different goals compared to the concepts studied before. In this architecture, the geometry of the OS concept is roughly a cylinder with spherical caps. This allows a safe preservation of the samples but also simplifies the complexity of the rendezvous

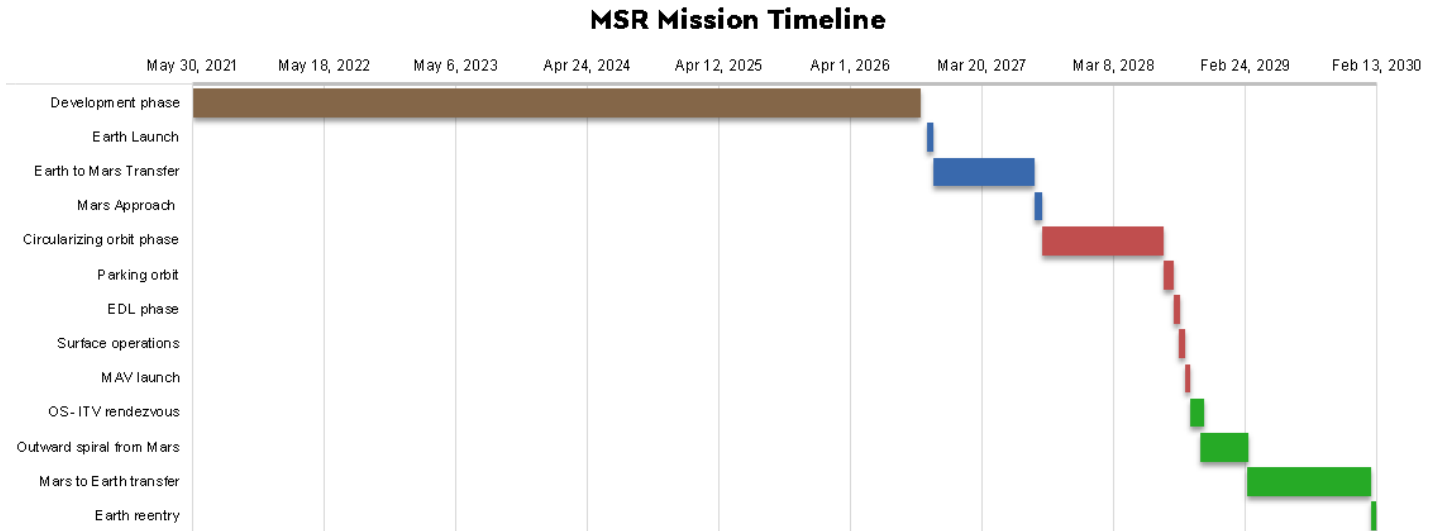


FIGURE 3.1: Mission timeline.

with the ITV as the MAV only has to put in orbit the OS capsule instead of performing a docking maneuver, thus saving mass and power budgets. Additionally, this alternative allows for greater mission reliability since the OS has undefined orbit time due its coatings, which can be modified to withstand prolonged/shorter times, this allows for greater capture opportunities in the event of an unsuccessful phasing maneuver.

3.2.2 Propulsion system

Interplanetary missions have been characterized by an increased use of chemical propulsion as the main propulsion system. Due to its high thrust and its impulsive characteristic, chemical propulsion allows a simpler and more precise development of maneuvers during the mission. In addition, it allows the temporary reduction of mission phases and the use of more effective correction maneuvers. Despite all this, chemical fuels have a low specific impulse that causes excessive consumption for each maneuver. The fuel in an interplanetary mission with a chemical propulsion system can reach 110% of the dry mass.

In recent missions, the use of low thrust and high specific thrust propulsion systems has become useful in order to reduce propellant mass at the expense of increasing mission flight time. Ionic electric propulsion is characterized by its high specific impulse and greater thrust compared to other low-thrust propulsion systems. This system has been used in missions such as Deep space I and Bepicolombo. A trade study about propulsion system is shown in Table 3.1 using a dry mass estimation of 3,600 kg at the initial state and 600 kg at the final state of mission. Bepicolombo system and AMBR rocket are considered for calculus.

The Ion electric Propulsion System was selected due to its greater reduction in fuel consumed, reducing the total mission mass and allowing the use of a medium-lift launch vehicle as Falcon 9, at the expense of greater mission complexity and

TABLE 3.1: Propulsion trade study.

Propulsion	Δv [km/s]	Mass [kg]	Cost [M USD]	Time of fly [days]
Chemical	4.0	2700	0.84	627
Electric	12.7	525	1.57	760

TABLE 3.2: Launch vehicle trade study.

Alternatives	Cost [M USD]	Payload volume [m^3]	Payload mass to GTO [kg]	Reliability	-
Weight	0.498	0.097	0.322	0.083	APH
Ariane V	137	186	10865	100	0.322
Atlas V	121	89	8290	100	0.157
Delta IV	164	85	6160	100	0.063
Falcon 9	62	145	8300	100	0.457

greater flight time.

3.3 Launch vehicle

3.3.1 Launch Vehicle Selection

Historically, the most used launcher for Mars missions has been the Atlas V. However, due to the limited Payload Fairing (PLF) volume, its cost and the development of new launchers in recent years, it has been decided to also consider launchers such as Ariane 5, Delta V and Falcon 9 Block 5. To fulfil the design constraints, only medium-lift launchers were taken into account in the selection process as their capabilities, both in mass and volume, are sufficient to meet the mission requirements.

Table 3.2 presents the analyzed criteria and their respective weights, prioritizing the launch cost and the mass payload since they are the main drivers of the mission. On the other hand, all candidates have the ability to send a payload to Mars with sufficient reliability as they all comply with category 3 of NASA Launch Vehicle Certification [11], which is awarded to launchers that have the minimum risk of failure and are capable of holding highly complex scientific payloads (eg, category A) [12]. It is worth mentioning that in addition to this type of certification, each launcher must have a special allow to be able to send a payload that contains nuclear material. In this permit tests and structural analysis contemplate the worst failure scenarios and the harmful effects of spreading nuclear material in the atmosphere.

In this sense, the AHP method was applied, obtaining Falcon 9 Block 5 (Fig. 3.2a) as the best option. This decision is justified due to its low cost and sufficient payload to Geostationary transfer orbit (GTO) orbit, which represents a 4,020 kg payload capability to Mars. Although SpaceX's Falcon 9 has not yet launched payloads towards Mars, it has shown to have a great operational capacity and precision demonstrated with its 116 successful launches since 2010 and especially in

TABLE 3.3: Standard launch integration schedule.

Estimated Schedule	Title
L-24 months	Contract signature
L-22 months	Mission integration kickoff
L-12 months	Completion of mission-unique design and analyses
L-3 months	Launch campaign kickoff
L-2 days	Launch readiness review
Separation + TBD minutes	Orbit injection report
Launch + 8 weeks	Flight report

3.4 Trajectory

3.4.1 Alternatives

There is an extensive catalog of possibilities to go and go back from Mars: bi-elliptic transfer, Hohmann transfer, lunar flyby, Venus flyby.

Bi-elliptic trajectory:

Is a maneuver that consists of two half-elliptic orbits. It may require less delta-v than other maneuvers like Hohmann transfer maneuver. There are two parameters that are necessary to optimize a bi-elliptic trajectory: Ratio of radii ($R = r_2/r_1$) and alfa ($\alpha = r_b/r_1$) where r_1 is the radius of the initial orbit, r_2 is the radius of the final orbit and r_b is the radius of the elliptic auxiliary orbit [14]. when the ratio of radii is less than 11.94, Hohmann transfer is always better than bi-elliptic transfer [15]. The ratio of radii between Earth and Mars is 1.53, therefore, bi-elliptic transfer is not profitable.

Hohmann transfer

The maneuver par excellence. Consist in a half-elliptic orbit in the ideal case, but in real cases exist two cases: when the path is less than half-elliptic orbit and when the path is more than half-elliptic orbit [16]. It often uses the least amount of propellant. Its simplicity and cost savings make it the most used trajectory.

Lunar and Venus flyby

Lunar flyby consist in perform a gravity assist around the moon before starting the trajectory to Mars with the objective to get an impulse from the satellite. It may require less ΔV than other Hohmann transfers but generally it require approximately 1.44 km/s more delta-v than optimal Hohmann transfers (ΔV of 7.148–8.006 km/s) [17]. Similar to Lunar flyby, Venus flyby consist in perform a gravity assist around Venus before arriving to Mars. This trajectory enables to carry out multiple science missions in Venus and offer numerous safe-return-to-earth options [18]. Despite of the scientific mission, crewed Venus missions are more useful than robotic mission like this. Additionally, the ΔV necessary for Venus flyby is not less than 9 km/s [19, 20].

Other trajectories like low-thrust impulse were discarded because its higher cost in time or because of its lack of reliability and technology readiness. Due to costs and simplicity, Hohmann transfer was selected like the trajectory to go and go back from Mars.

3.4.2 Selection process

With the purpose to estimate the characteristics of the trajectory, the tool trajectory browser of NASA was used. The search parameters were: Mission type round-trip rendezvous, launch year between 2022-2030, max duration of 5 years, max ΔV of 20 km/s and minimize the ΔV [20].

For analysis of all trajectories obtained with the trajectory browser, a trade study was carried out. The parameters considered were the elapsed days from PDR, the season of arrival, the stay time, the total time of flight and the total ΔV . Having the main drivers and its weight of importance on Table 3.4, two trade studies were made. Considering stay time parameter directly proportional to the score, the results of three best trajectories can be appreciated in first part of Table 3.5. In the other hand, having stay time parameter indirectly proportional to the score, the results of four best trajectories can be appreciated in the second part of Table 3.5. These options correspond to Hohmann type II trajectories. The results of trade study are shown in Table 3.6.

TABLE 3.4: Best trajectories.

Driver	Criteria	Weight(%)
Mars Arrival Season	Extraction operations of samples	0.132
Stay time	Extraction operations of samples	0.2
Time of flight	Batteries	0.15
Total ΔV	Fuel	0.3
Earth Departure	Preparation time	0.218

TABLE 3.5: Best trajectories.

#	Eart Departure	Elapsed Days From PDR	Season	Elapsed Seasons	Earth Return	Stay time (days)	Total time of flight (days)	Total ΔV (km/s)
First Study								
1	01/10/2024	1236	Summer	7	09/06/2029	1104	608	4.90
2	01/10/2024	1236	Summer	7	24/05/2029	1104	592	4.92
3	17/10/2024	1252	Summer	7	24/05/2029	1088	592	5.04
Second Study								
4	08/11/2026	2004	Summer	3	27/07/2029	352	640	4.85
5	08/11/2026	2004	Summer	3	09/06/2029	368	576	4.90
6	08/11/2026	2004	Summer	3	24/05/2029	368	560	4.91
7	08/11/2026	2004	Summer	3	08/05/2029	368	544	5.14

TABLE 3.6: Trade study about trajectories

Trajectory #	Elapsed days from PDR	Season	Stay time	Total time of flight (days)	Total ΔV (km/s)	Total score
1	6.07	10	9.86	7.63	9.88	8.72
2	6.07	10	9.86	7.84	9.84	8.74
3	6.15	10	9.71	7.84	9.60	8.66
4	9.84	10	3.18	7.25	9.98	8.18
5	9.84	10	3.04	8.06	9.88	8.25
6	9.84	10	3.04	8.29	9.86	8.27
7	9.84	10	3.04	8.53	9.42	8.18

3.4.3 Chosen alternative and details

Despite of the three trajectories of 2024 having a better score than trajectories of 2026, the critical ORR stage can take more longer than expected. For that reason, only the trajectories of 2026 were considered and the trajectory #5 was selected due to high score, but in the next steps, the trajectory #2, that have the best score, is considered in case of any estimate of development and ORR stage time. Another trajectories with more development time were discarded due to its great fuel consume. additionally, in Fig. 3.3 the trajectory selected is shown.

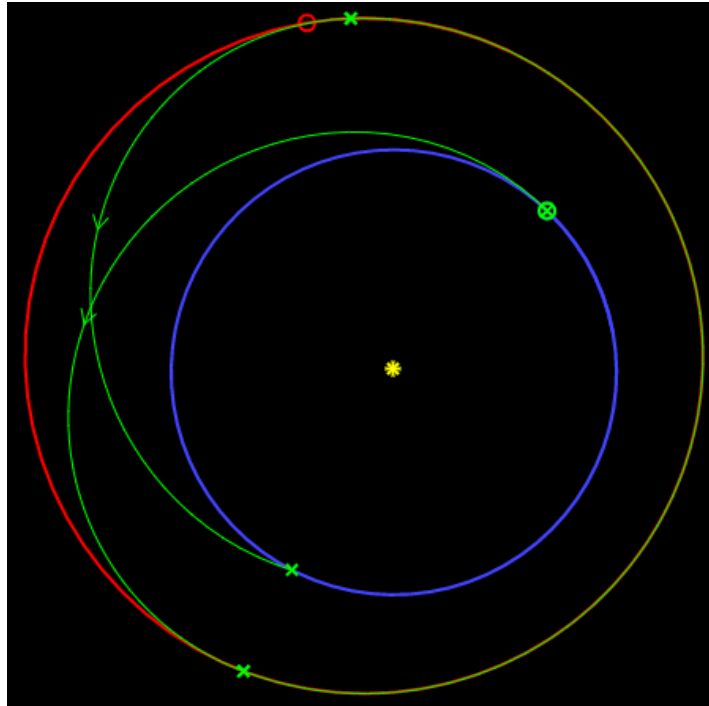


FIGURE 3.3: Round-trip rendezvous mission to Mars with optimal parameters [20].

3.4.4 Trajectory Design

The trajectory obtained with trajectory browser does not fully apply to our current mission strategy due to 1) it implements impulsive maneuvers (instead of using finite burns), and 2) the return date of the samples has been changed. For these reasons, the final trajectory has been redesigned. STK software has been selected to design, model, and analyze the complete trajectory. Astrogator module was used to develop and solve the trajectory stages of the vehicle. The ΔV values obtained with astrogator trajectories were translated at mass cost using rocket's equation.

Interplanetary Outbound trajectory design

The objective of the Outbound trajectory is to match the position and velocity relative to Mars that are necessary to stay in an elliptical orbit around it. The path obtained with trajectory browser for the Outbound trajectory is a Hohmann transfer type II, perfect for low thrust maneuver due to greater tangency between the target body's path and the satellite at the end state. Low thrust maneuvers have a greater difficulty than impulsive maneuvers which lies in the thrust's temporary effect. For that reason, the outbound trajectory is divided in four segments after the departure of Earth: coast, correction, braking and capture.

The coast segment lasts approximately 180 days. During this time, the ITV has enough time to perform an appropriate system deployment and checks, to calculate corrections of the next steps in the trajectory. After these 180 days, the correction phase starts with a low thrust burn for 106 days that provides to the system the necessary ΔV and direction to match Mars in the next segments. Immediately after of this maneuver, the ITV is turned in the opposite direction of speed with the objective to do a brake phase and approximate to Mars with the right speed. Last, the capture segment reduces the ITV's speed relative to Mars. This maneuver ensures that the ITV is captured in an elliptical and polar orbit around Mars. Elliptical orbit allows a posterior aerobraking sub-phase. A summary of the outbound trajectory segments is presented in the Table 3.7 and a 2D general view in the Fig. 3.4.

TABLE 3.7: Outbound trajectory summary.

Maneuver	ΔV (km/s)	Propellant Mass(kg)	Duration(months)
Coast	0	0	6
Correction	2.7	243	3.5
Braking	0.16	14	0.2
Capture	0.044	4.0	0.1
Total	2.9	261	9.8

Parking Orbit Design

The phase to achieve a parking polar orbit around Mars is divided in 3 segments: stable orbit, circularizing and increasing. The capture orbit has an eccentricity near to 1. To reduce this parameter is necessary to do a low thrust burn during the

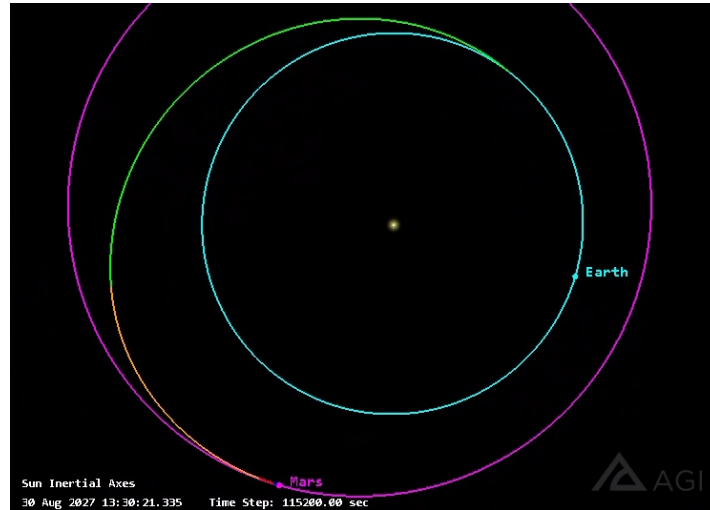


FIGURE 3.4: Interplanetary outbound trajectory model with STK software.

first orbit to achieve a stable orbit with a period of around 1.9 days. This first maneuver increases the periapsis from 100 to 650 km, allowing a correct development of the circularizing maneuver. The circularizing phase consist in two parts: one, a reduction of periapsis using low thrust maneuvers, and a second part using aerobraking. Aerobraking maneuver is a highly mass-efficient method that reduce energy spend using the atmospheric drag force. For that reason, aerobraking is selected as a part of the circularizing phase above increase use of low thrust.

In the Second orbit, the ITV burns between windows of -90 and $+90$ degrees true anomaly along the velocity vector starting to reduce the apoapsis of its orbit. This maneuver not only affects its apoapsis, but also reduces its periapsis slowly. After 500 orbits the ITV reach an 0.3-eccentricity orbit with a period of 3 hours and periapsis of 113 km. the aerobraking starts during these 500 orbits while the periapsis reduces and become significant around a periapsis of 150 km. Then, the ITV starts his increasing phase, that consists in a low thrust maneuver along the velocity vector. After 70 orbits, the vehicle reaches a circular orbit with radius of 310 km and a period about 2 hours. These parameters allow the correctly development of the descending and catching phase. The Table 3.8 shows the main parameters of the parking orbit sub-phases and Fig. 3.5 is a visual 2D representation of the trajectory obtained.

TABLE 3.8: Parking Orbit summary.

Maneuver	ΔV (km/s)	Propellant Mass(kg)	Duration(months)
Stable Orbit	0.04	4	0.06
Circularizing	0.53	46	9.6
Increasing	0.15	13	1.2
Total	0.72	62	10.8

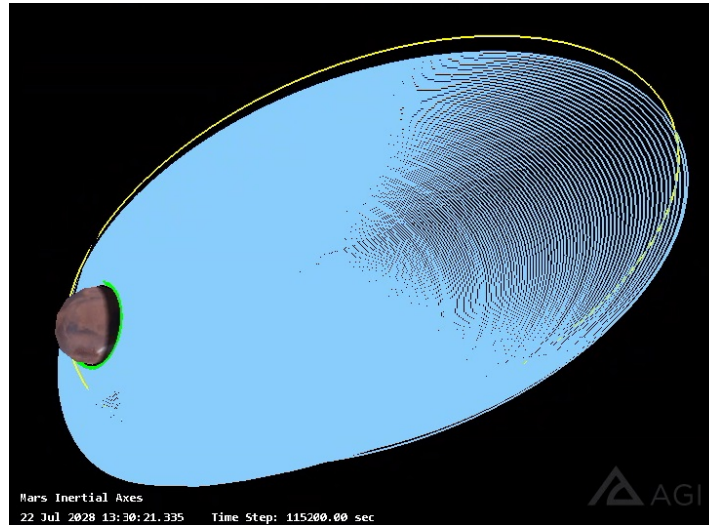


FIGURE 3.5: Circularizing maneuver to parking orbit, model with STK software.

Sample Rendezvous

Around 30 days later, after the sampling process and posterior MAV launch, the sample rendezvous phase will start. The MAV can deliver the OS in a polar 300 km parking orbit with an uncertainty of ± 1 degrees and ± 10 km of altitude. The rendezvous phase will have a maximum duration of 40 days [21]. To minimize the time and error of the catching, attitude thrusters are selected for the maneuver. A 20 km maximum altitude correction are considered due to the ITV parking orbit. The inclination correction was considered to a maximum of 5 degrees in the case of an emergency with the OS locating or significant gravitational perturbations. The ΔV calculus of inclination and altitude maneuvers gives a value of 59 and 9 m/s, respectively. The total mass for the ITV rendezvous maneuvers with an additional 10% of security factor is 26 kg of hydrazine.

Return trajectory design

The return trajectory has the difference with the outbound trajectory in that the return trajectory go out from mars with a low thrust maneuver, adding an extra maneuver and increasing the energy and complexity in all trajectory. The 4 phases of this trajectory are: Departure, decreasing, elevating, and intercepting. The departure phase is the additional sub-phase and consists in an increasing spiral orbit to match the hyperbolic excess speed in the SOI surroundings necessary to escape of the Mars gravitational field. This maneuver takes around 128 days of low thrust burn along the velocity vector. After escape of the Mars SOI, the decreasing phase starts with the objective to reduce the orbit around the sun to match the earth orbit. This phase requires a burn oriented in the opposite direction of ITV's velocity relative to sun.

Then, the elevating sub-phase does a burn oriented in a 90-degrees elevation respect to the ICRF coordinate system. This maneuver has the main purpose to change the inclination of the return trajectory to the needed for earth orbit interception. Last, the intercepting sub-phase realizes a burn with a direction near to the anti-velocity vector to correct

the trajectory and achieve a successful interception with the earth. The reentry speed is about 16 km/s. Table 3.9 and fig. 3.6 summarize the return trajectory. Table 3.10 gives a estimation of ΔV and mass of propellant.

TABLE 3.9: Return trajectory summary.

Maneuver	ΔV (km/s)	Propellant Mass (kg)	Duration (months)
Departure	3.3	54	4.3
Decreasing	4.5	72	5.0
Elevating	0.7	12	0.9
Interception	4.4	71	5.3
Total	12.9	208	15.5



FIGURE 3.6: Return trajectory model with STK software.

TABLE 3.10: ITV Propulsion summary.

Propellant	ΔV (km/s)	Mass (kg)	Mass with reserves (kg)
Xenon	16.5	532	585
Hydrazine	0.08	26	28
Total	16.6	558	613

3.5 Interplanetary Transfer Vehicle

3.5.1 System Overview

The Interplanetary Transfer Vehicle (ITV) has three main functions: the first one is to transport and deploy the Entry, Descent and Landing (EDL) capsule into Mars, which carries with it the Lander, Rover and Mars Ascent Vehicle (MAV); the second one is to link the communications between Mars operations and Earth; and the third one is to return the Mars ice core samples back to Earth through the Orbiting Sample (OS) within the Earth Entry Vehicle (EEV).

3.5.2 Configuration

Fig. 3.7 shows the ITV at launch configuration, its coordinates axes and its general dimensions. Its design is inherited by OSIRIS-Rex and MAVEN designs. Also, it shares some similarities with Mars Reconnaissance Orbiter (MRO). The ITV configuration consists of an aluminum honeycomb cylindrical structure, with 1.3 meters of diameter and 3 m of height, surrounded tangentially and radially by four and two aluminum honeycomb panels respectively. Additionally, two panels are disposal at top and bottom of the cylinder.

In order to fit the spacecraft into the Falcon 9 payload volume, the EDL is disposed at the top of the ITV. This also makes the center of mass to be along the central axis, which results in a better performance of the structure supporting the stresses generated at launch. Within the cylinder is the xenon tank for the two T6 Gridded Ion Thrusters which in turn are positioned at the bottom, fulfilling the function of main engine. Surrounding the main engine is the 1.575 meters of diameter Payload Attachment Fitting (PAF) for the ITV with the Falcon 9 [13].

At - y-axis panel is the Capture and Orient Module (COM) oriented vertically. The COM is in charge of catching the Orbiting Sample (OS), for that reason, the COM lid is pointing to the + z-axis in order to avoid main engine plume at rendezvous with the OS. Additionally, at the + y-axis panel is mounted the 1.9 meters diameter high antenna. Fig. 3.8 shows an exploded view of the ITV and its components.

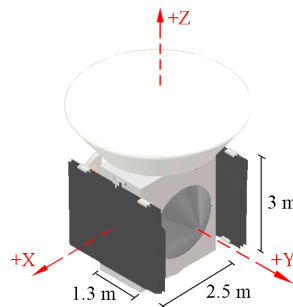


FIGURE 3.7: ITV at launch configuration.

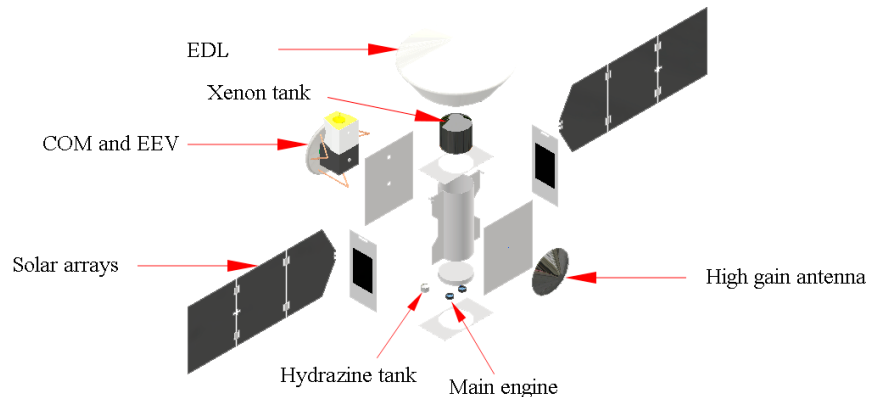


FIGURE 3.8: ITV exploded view and components.

3.5.3 Structure

The ITV structure is a legacy of MAVEN and OSIRIS-REx. It consist of a main cylinder of 1.3 meters of diameter and 3 meters of height, which in turn is composed by two panels of 20 millimeters of thickness, 0.6 meters large, and 3 meters height, disposed radially pointing to +/- x-axis. Those two radially panels are disposed in order to reduce lateral stresses due to high slenderness ratio, and also to serve as support for the solar arrays and instruments. Each radial panel has a reduced cross area in order to minimize overall mass. All the structure, as MAVEN and OSIRIS-REx, is made of aluminum honeycomb sandwiched between graphite sheets [22]. In order to know the performance of the structure, an axial stress analysis is made using the tool for structural analysis of Autodesk Inventor [23] with the objective of knowing the safety factor of the structure. The critical phase where ITV is submitted to the highest stresses is at launch. For that purpose, Table 3.11 shows the mass budget of the ITV. Additionally, Fig. 3.9, taken from the Falcon 9 User Manual, shows the load factors on units of gravity acceleration (g) that the payload experiments on launch. With that, a mass of 1,190 kg and an load factor of 8.5 is taken for the analysis, showing that the structure has a minimum safety factor for axial stress of 3.91.

TABLE 3.11: ITV mass and cost budget.

Subsystem	Mass (kg)	Cost (M USD)
Structure	72.0	1.2
Propulsion (no fuel)	65.0	72.7
EPS	83.4	1.6
C&DH	6.6	12.8
Communications	21.2	8.9
AD&C	41.4	12.8
TCS	25.0	0.5
COM	108.2	0.5
EEV	153.9	-
Drymass	576.7	112.7
Fuel (xenon and hydrazine)	613.0	1.7
infrastructure and testing	-	3.9
Operations	-	86.3
Total	1189.7	202.9

3.5.4 Propulsion

Three types of propulsion systems are considered: chemical, ion electric and hall effect thrusters. Chemical propulsion was discarded from an early stage due to the low payload ratio that translate in a higher mass consume. The propellant mass represents about 110 of dry mass in interplanetary missions. A similar scenario is presented with hall effect propulsion. Instead the hall effect propulsion generates higher thrust than ion electric propulsion, the low specific impulse reduces the payload ratio significantly. For all these reasons the ion thruster was selected as the ITV's main propulsion system.

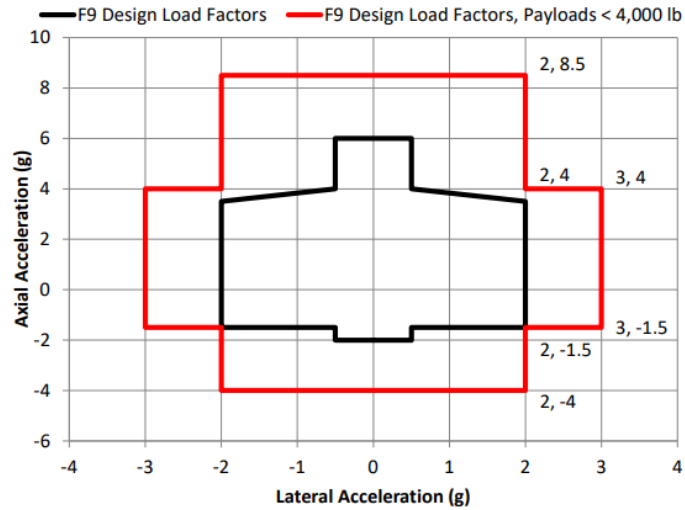


FIGURE 3.9: Falcon 9 load factors.

There are many options of ion electric propulsion that can be considered to the mission. NSTAR is one of the most popular ionic thrusters because Dawn and Deep space 1 missions. It presents a specific impulse of 3100 s. Another recent thruster is the Qinetiq-T6 which is used in Bepicolombo mission. It can perform a specific impulse over 4000 s. Other thrusters like NEXT was directly discarded due to its low specific impulse reducing the payload ratio and increase fuel consume. Qinetiq-T6 was selected because its highest payload ratio and specific impulse that reduces fuel mass significantly.

The configuration of the propulsion system is similar than used in BepiColombo mission. ITV will use two thrusters to generate a maximum thrust of 290 mN. The maximum specific impulse is about 4,600 seconds and the combine power operating range is between 5 and 9.2 kW. The mass and radius of each thruster are 8.9 kg and 22 cm [24].

3.5.5 Attitude Determination and Control (AD&C)

The attitude determination and control subsystem is responsible of the ITV 3-axis stabilization knowledge and correction. The sensors used to determine the spacecraft spatial orientation are 4 SELEX-EX A-STR star trackers, used in multiple mission such as Lunar Reconnaissance Orbiter (LRO), mission which least more than 11 years; 2 ACSS Advanced Coarse Sun Sensor sun trackers, built by Solar MEMS Technologies, which has been proven and has a TRL of 9; and the Northrop Grumman LN-200s FOG IMU [22, 23, 25, 26]. The attitude accuracy of the A-STR star tracker is 3.6 arcseconds at the beginning of mission, satisfying the 6 arcsecond requirement of JPL's orbiter concept [27]. The ACSS sun tracker is necessary for the continuous and correct solar arrays pointing towards sun. The accuracy of these sensors are less than 0.5 degrees, under the JPL's requirement. Finally, the LN-200 IMU is employed as a redundant sensor in the emergency situations where the star trackers are unable to determine the attitude state of the ITV and the sun tracker is at Mars orbit eclipse zone.

In order to achieve the control of the ITV systems requiring addressing, such as communication system or solar arrays, it is necessary to have an AD&C system. The possible options are thrusters, reaction wheels and control mounted gyroscopes. Reaction wheels and control mounted gyroscopes are used to change the ITV's axis direction and the thrusters are used to do an impulsive maneuver in any of the ITV's axis. Reaction wheels are selected over control mounted gyroscopes because there are more options on the market. Moreover, reaction wheels are less mechanically complex and much simpler operational compared to gyroscopes [28]. Comparison between more common aerospace reaction wheels is shown in Table 3.12. Both Collins Aerospace RSI 45 and RSI 12 generate the momentum necessary to keep the direction of ITV in any of the mission maneuvers. However, RSI 12 reaction wheel was selected due to its less mass, sacrificing effect time, which is compensated with the low thrust thrusters in order to have an coupled system [29].

TABLE 3.12: Reaction wheels comparison.

Reference	Power (W)	Mass (kg)	Momentum (Nms)	Torque (mNm)
RSI 45	90	7.7	45	75
RSI 12	90	4.85	12	75

On the other hand, thrusters are the only method capable of doing translation and rotation movements in any axis of the ITV. For that reason, these serves for trajectory correction maneuvers in a short time that ion electric propulsion is not able to do. Also, thrusters play an important role in the catching phase, since they allow a fast radius or inclination changes of the orbit of the ITV. Table 3.13 shows a comparison between the three more known space thrusters. Aerojet Rocketdyne MR-103D was selected in view of the fact that it has significantly lower mass and power against the other options [30].

TABLE 3.13: Thrusters comparison.

Reference	Power (W)	Mass (kg)	Propellant	Thrust (N)	ISP (s)
MR-401	11.95	0.6	Hydrazine	0.09	180
MR-103D	8.25	0.33	Hydrazine	1.02	224
MR-107S	34.8	1.01	Hydrazine	360	225

3.5.6 Communications

Communication requirements for the orbiter are based on the needs contemplated for this mission, focusing on communication between the orbiter and Earth, and communication between the orbiter and elements on the surface of Mars. Earth Communications will use a High Gain Antenna, 2,100 mm X-Band with a dual axis mechanism and a Low Gain omnidirectional antenna for communications in close distance to Earth . These communications will be integrated with two Bosch Traveling Wave Tube Amplifier (TWTA) [31] that will provide 100 Watts to the High and Low Gain antennas as required. In addition, there will be two General Dynamics Small Deep-Space transponders (SDST) [32] designed by JPL specifically for deep space probes. All communication to and from Earth for the orbiter will be carried out by NASA's

Deep Space Network (DSN). As such, we conclude that all the chosen equipment is compatible with transmission and reception of signals through this network. In assessing the risks for these kinds of mission it is important to incorporate redundancy in the systems. The equipment mentioned before is to be doubled to assure redundancy. The DSN consists of three equidistant stations, located at approximately 120° long over the Earth. The sites are in California, Madrid, and Canberra [33]. This location allows an ITV continuous communications coverage, which was confirmed by an access report done in STK. In Fig. 3.10 shows how the communications with Earth are constant with a mean duration of 3000 seconds and a waiting time of 50 minutes between every access.

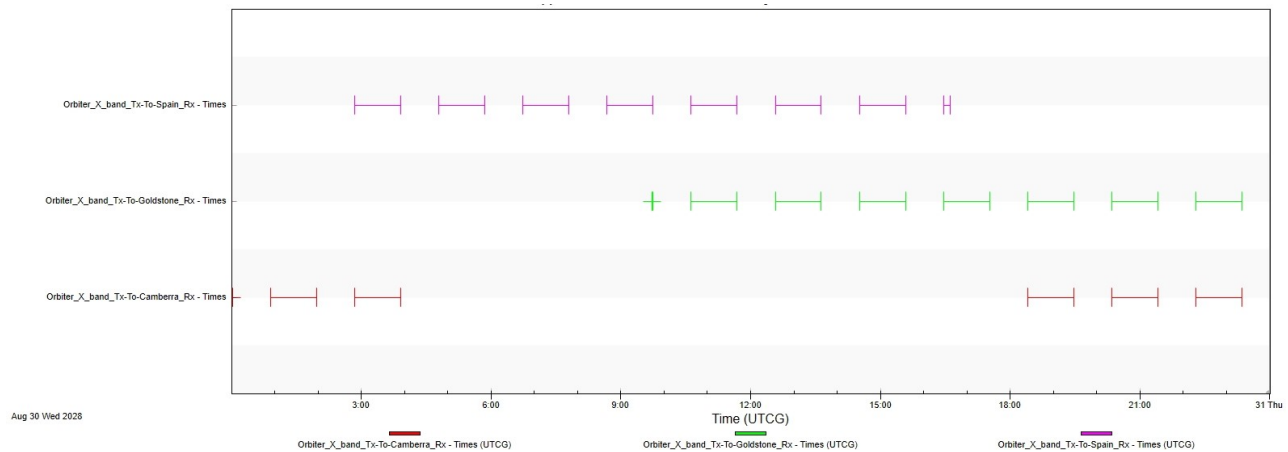


FIGURE 3.10: ITV communication access with Earth DSN.

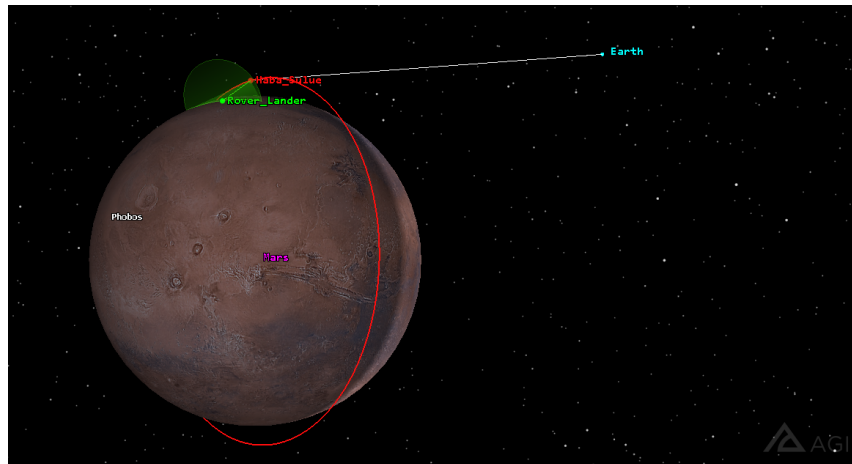


FIGURE 3.11: Communication overview between the DSN and a relay station and communication between the rover and the ITV.

As for communication between elements on the surface of Mars and the ITV, the UHF band will be used via the Electra transponder, with a quadrifilar helix antenna, that will be in contact with the rover's Electra Lite. A distance analysis of these communications was performed on STK allowing a maximum range of 1600 km between ITV and Mars Rover as shown in Fig. 3.12.

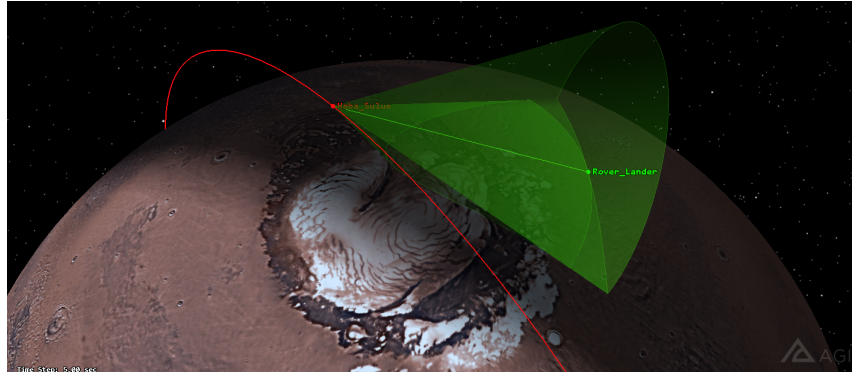


FIGURE 3.12: Maximum communication range between the ITV and rover.

The total mass and power budget required is 21.2 kg and 492.6 W respectively for communications can be found on Table 3.14:

TABLE 3.14: ITV communication bands and components.

ITV X- band communications				
Element	Reference	Size	Mass (kg)	Power (W)
Amplifier	Bosch Travelling Wave Tube Amplifier	375 L x 72 W \varnothing 110 (mm)	1.1 X 2	396
Transmitter	Small Deep-Space Transponder	18.1 L x 16.6 W x 11.4 H (cm)	3.2 X 2	15.8
Antenna	Parabolic	2.1 m \varnothing	5	–
Antenna	Low Gain omnidirectional Antenna	–	2.5	–
ITV UHF communications				
Tranceiver	Electra	21.7 L, 20.1 W, 11.6 H (cm)	5	65
Antenna	Quadrifilar helix	5 cm \varnothing	0.1	–
Total			21.2	492.6

The characteristics for transmitting and receiving data from each of the antennas used are presented in Table 3.15. The uplink data rate from Mars operations is 5 Mbps and 200 kbps for the downlink data rate to Earth using a 2100 mm high gain antenna.

TABLE 3.15: Data Transmission and Reception specifications.

X-band antenna	
Size (m)	2.1
Frequency (GHz)	8.4
Data rate (kb/s)	200
Polarization	Right Hand Circular
UHF antenna	
Size (m)	0.05
Frequency (GHz)	0.45
Data rate (Mb/s)	2
Polarization	Right Hand Circular

3.5.7 Command and Data Handling (C&DH)

The Command and Data Handling subsystem for the ITV is controlled by the BAE RAD750 processor, which works at frequencies between 133 and 166 MHz and has been produced in order to resist the high radiation conditions in space. This processor has been employed in various successful missions, such as Mars Reconnaissance Orbiter (MRO) and MAVEN, missions that have lasted more than 14 and 6 years respectively, proving a TRL of 9. The RAD750 coupled with the 6U CompactPCI computer provide the main brain of the ITV, where all data and instructions are processed. Added to the processor and computer, the 197A807 PROM will serve as a redundant memory for the data collected [34, 35, 36]. Table 3.16 shows power requirements and mass for each component.

TABLE 3.16: Command and Data Handling power and mass budget.

Component	Power (W)	Mass (kg)
BAE RAD750 processor	10	
CompactPCI computer	7.5	0.92
197A807 5V PROM	0.25	5.67
Total	17.75	6.59

3.5.8 Electrical Power Subsystem (EPS)

The Electrical Power Subsystem (EPS) consists of two gimbaled arrays with two EaglePicher SAR-10197 Lithium Ion batteries (one redundant). The solar arrays have a similar design to MRO's. Fixed solar arrays were also considered, but rendezvous maneuvers and communications required a constant energy supply, also making AD&C system less sturdy and less expensive. Nickel Hydrogen and Nickel Cadmium batteries were considered, nevertheless Li-ion batteries technology offers a significant energy density advantage, in this case 104.3 W-hr/kg, and also providing a much wider operating temperature range (-5 to 35 °C). RTGs energy generation were also considered, but due to their high mass (38 kg) and having high power capacities, it exceeds the ITV requirements. Additionally, taking into account that the ITV will have an Earth reentry and burn up at return, using RTGs were forbidden for the ITV mission due to it would contaminate the Earth atmosphere with nuclear material [37, 38, 39].

Table 3.17 shows the components and total power needed for the ITV operations. With the aim of knowing the arrays area needed to supply the components and keep the ITV operative, an analysis is made using sunlight and eclipse time periods and electrical power. Such procedure is driven by the Space Mission Design and Analysis recommendations [3]. Taking into account that the electrical power needed at sunlight intervals will be the entire components, and at eclipse intervals will be just the necessary power needed for correct operation (around 500 W), a solar arrays area of 65.3 m² is necessary using the Spectrolab 30.7% XTJ Prime solar cells. This type of solar cells were selected due to its high efficiency

TABLE 3.17: ITV Total power budget.

Item	Power (W)
Propulsion	9,256
C&DH	7.7
AD&C	259.6
Thermal control	300
Communications	492.6
Payload	86
Total	10,400.9

at Beginning of Life (BOL) and a low degradation grade, being a value of 0.01 for the mission time [40]. The XTJ cells have a cell mass of 84 mg/cm², thus total solar arrays mass is around 60 kg.

3.5.9 Thermal Control System (TCS)

In order to sustain operational conditions, the ITV must have an independent Thermal Control System (TCS) that complies with the requirements shown in the Table 3.18.

TABLE 3.18: ITV Temperature Ranges.

Component	Operational Range (°C)	Survival Range (°C)
Batteries	-5 to 35	-15 to 40
AD&C	0 to 40	-10 to 50
C&DH	-20 to 60	-40 to 75
Thrusters, propellant and lines	15 to 40	5 to 50
Antennas	-100 to 100	-120 to 120
Structure	-45 to 65	

According to that requirements, a heating transfer analysis is done following the procedure given by the SMAD book, so as to achieve maintaining the ITV on a 15 °C temperature, value where every component remains on an operable state. Taking into account that the main way of heating transfer at space is radiation, Stefan Boltzmann Law is used. Two cases are consider: in order to know the isolation material for the ITV panels and the radiators area, a Worst Case Hot (WCH) is considered, where main engine and electronics are operating at sunlight, on Mars polar orbit; in the other hand, in order to obtain the power of the heating patches, the Worst Case Cold (WCC) scenario is considered, where just the necessary electronics are operating and the ITV is on Mars orbit eclipse.

At WCH, the electronics and propulsion waste heat due to inefficiencies in power conversion and transmission is consider to be 20% (around 2 kW) of the total EPS power [41]. Fig. 3.13 shows the ITV attitude at WCH, where - y-axis is pointing towards sun, having the incident solar flux on a projected area of 7.5 m². This ITV attitude also makes radiators to be at +/- x-axis, so radiators do not have incident solar flux. Considering a Mars albedo of 0.25 [42], the isolation material selected is the Multilayer Kapton, which has a α_{abs} of 0.09 and a e_{IR} of 0.15 [41]. Additionally, the radiators area needed to

exhaust the waste heat is 3.12 m^2 . At WCC, the waste heat by electronics is considered to be 5% of the total EPS power (0.52 kW). With that, heaters must exhaust around 290 W to components in order to have a $15 \text{ }^\circ\text{C}$ temperature.

Additionally to the radiators and heaters, the ITV must provide thermal protection to the OS in order to keep the ice core samples below the MPW. For that, the ITV must contain a MPFL which will be in contact with the catching system. With that requirement and assuming a WCH, the minimum power MPFL must transmit to the OS is 9 W.

Having all the above, Table 3.19 shows the TCS power requirements and its respective mass.

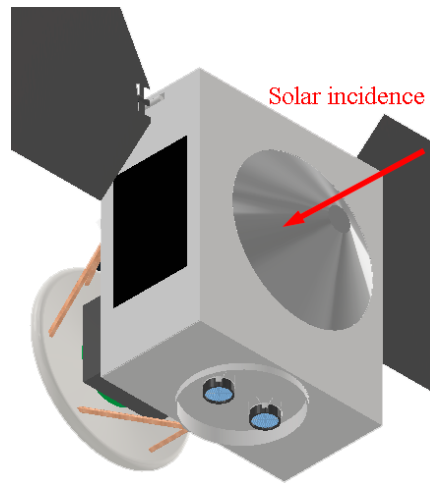


FIGURE 3.13: ITV attitude at WCH.

TABLE 3.19: Thermal control system total power requirement.

Component	Power (W)	Mass (kg)
Heaters and Radiators	290	0.2
MPFL	30	15
Total	320	15.2

3.5.10 On-Orbit Sample Capture and Orient System

The main function of the capture and orient module (COM) is to catch the OS and transfer it to the EEV, and also providing Planetary Protection. According to JPL, "Several OS capture systems for MSR has been studied... ...COM concept was selected because of its improvements on interfacing phases and achieving different goals compared to the concepts studied before" [10]. Those goals are the need of orienting the OS and to perform capture before contact. Orientation goal was a determinative characteristic due to the shape of the OS is cylindrical instead of spherical. The COM concept has been developed at half and full-scale in order to validate its architecture, but it has not been applied to a real mission, leading the COM to a TRL of 5.

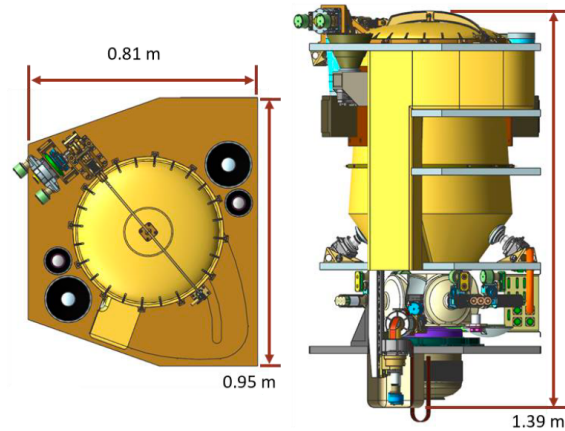


FIGURE 3.14: COM primary dimensions.

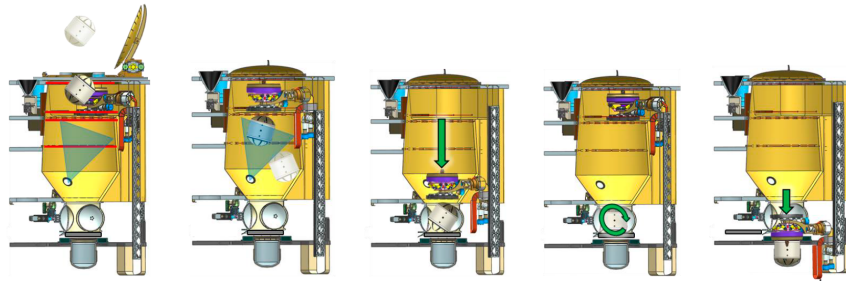


FIGURE 3.15: COM operational concept.

As seen in Fig. 3.14, the COM is 1.39 meters of large, 0.81 meters of height and 0.95 meters of width. It counts with a lid through where the OS enters. The COM firstly detects the OS by the use of the the Next Generation Advanced Video Guidance Sensor (NGAVGS), which is a LIDAR sensor [43], and then achieves capture without contact on its diverging-converging cylinder work space with multiple cameras disposed around the structure of the COM. Then, a transfer mechanism cages and transfer the OS into the orientation mechanism, which centers the OS to the desired orientation in two rotational degrees of freedom. After that, transfer mechanism encloses the OS with a containment vessel (CV) in order to have a correct attachment and mechanical protection with the Earth Entry Vehicle (EEV). Fig. 3.15 shows the COM operational concept described [44].

The transfer mechanism plays an important role since it has to maintain the OS on the desirable conditions, it is keeping the OS on temperatures below zero $^{\circ}\text{C}$. For that, transfer mechanism must count with a MPFL which is in contact with the OS extracting the heating waste generated by the gradient of temperature between the ITV and the COM. This contact will remain until reentry operations begin, in order to maintain the desired conditions to the OS on the entire return flight.

Placed at the + y-axis panel of the ITV, the lid of the COM is + z-axis directed in order to avoid main engine plume and heating waste. This configuration is possible taking into account that the EDL will not be attached to the + y-axis panel during rendezvous with the OS. COM concept complies with the desirable requirements, having a total mass of 108.3 with the instruments required for its operation, which in turn need a total power of 84 W.

4 Mars Surface Operations

4.1 Entry, Descent and Landing

Once the capsule reaches the Martian orbit, it is necessary to execute an entrance maneuver, followed by the breaking assisted by the atmosphere, using a heat-shield and then a supersonic parachute; when the speed is slow enough begins to operate the landing stage, in this case a SkyCrane modification. This procedure is called Entry Descent and Landing (EDL).

4.1.1 Aeroshell

Since the Viking missions the materials and geometry of the Aeroshell for the Martian EDL systems have been very similar resulting from the high performance reliability they have proved. For this case, the main restrictions were the volume the capsule is able carry, the diameter for the heat-shield (so it can suit in the launching rocket) and the geometry, so the MAV can fit inside of it.

The Aeroshell used in the MSL and Mars 2020 missions satisfy these necessities, given its reliability and high TRL, it was chosen. As seen in Fig. 4.1 the MSL aeroshell has a 4.5 m diameter for the heat-shield on a 70 degree sphere-cone [45]. For hypersonic descent, and with a zero angle of attack (the worst setting possible) it has a Drag Coefficient C_D of approximately 1.68 [46].

The heatshield thermal protection system is made of phenolic impregnated carbon ablator, and the back shell uses an ablative material called SLA-561V [45], which does not need to be modified. As well as the thermal protection, the instrumentation would remain the same as in the original design. There are some approximated constrains that relate the mass with the possible landing site. As seen in the Table 4.1 for a MOLA elevation of -2.0 km and a mass of 1000 kg there is a maximum hyper-sonic ballistic coefficient (β) of 160 kg/m² [46]. The parachute will retain geometry and dimensions of the one used in Mars2020, the Supersonic Disk-Gap-B and Parachute made of Nylon and Kevlar Web, with 21.5 m diameter, that allows deploy at a maximum speed of approximately Mach 2.7.

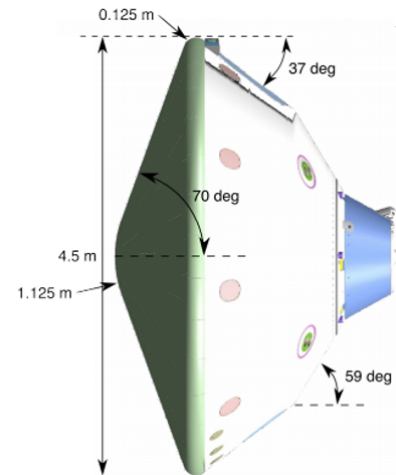


FIGURE 4.1: MSL Aeroshell Measures.

TABLE 4.1: Approximate landed mass constraint as a function of elevation [46].

Surface elevation, MOLA km	Maximum β , kg/m^2	Landed mass for 2.65-m-diam aeroshell	Landed mass for 4.5-m-diam aeroshell
-2.0	160	350	1000
0.0	135	300	850
+2.0	115	250	750

The β can relate when the parachute is deployed, and with a lower β the system will have a lower peak heat rate. For an entry mass of approximately 2,700 kg, a C_D of 1.68 and an area of $15.9 m^2$, the β value is $101.01 kg/m^2$; this considering the MOLA elevation of 4.0 km of the landing site, indicates that the system complies the requirements and it is safe.

$$\beta = \frac{m}{C_D A} \quad (4.1)$$

For an atmosphere entry speed of 6km/s and a Lift-to-Drag ratio of 0.18, using Eq. (4.1) it can be estimated the altitude deploy between 10 km to 15 km, altitude enough for the require deceleration.

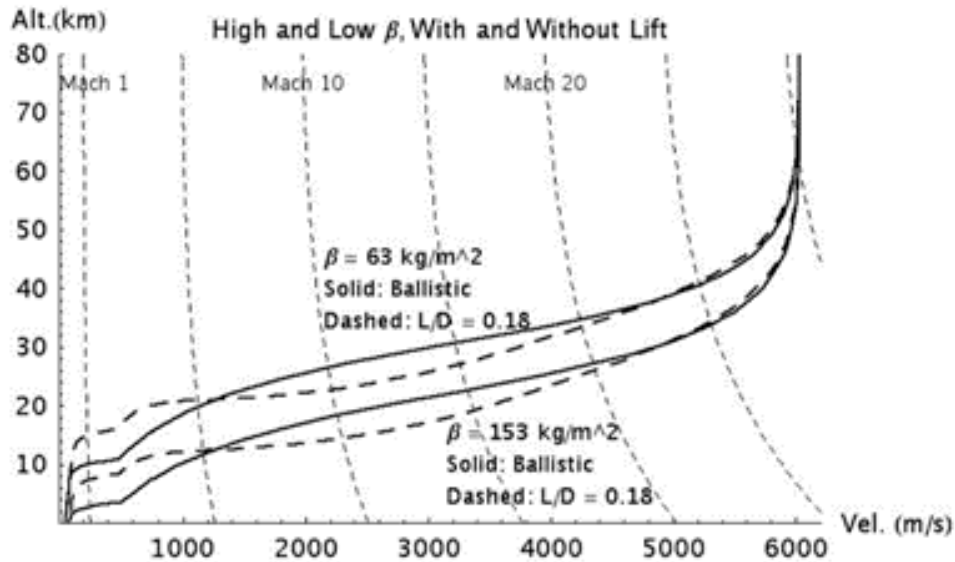


FIGURE 4.2: Trajectory profile of MSL EDL.[46]

4.2 Modified Skycrane Lander Descent Stage

As mentioned in EDL section one of the main restrictions was the touchdown mass capability for different existing Landing technologies, being SkyCrane used in MSL and Mars 2020 missions the most capable over configurations as Retrorockets or Airbags. Due to the high mass needs of the mission and having TRL as a constrain, three lander concepts were studied: A

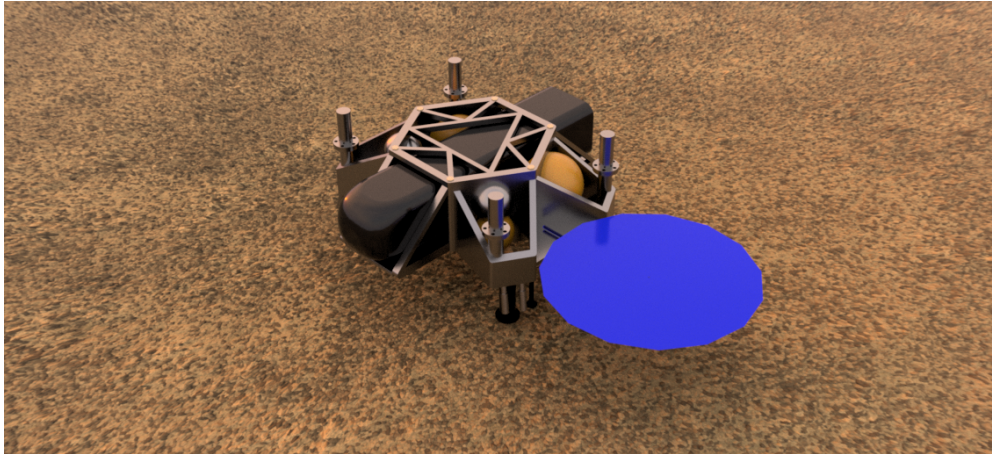


FIGURE 4.3: Lander on mars surface.

Propulsive Platform Lander (PPL), a Sky Crane Delivered Lander (SDL) and a modified sky crane. The sample retrieval lander must land on Mars, deploy the Sample Rover and maintain the MAV within safe operating conditions, including temperatures, while the rover retrieves the mission sample tubes. Once the rover returns with the tubes the following operations would be conducted: transfer tubes to the OS in the MAV Payload Assembly (MPA), using the Sample Transfer Arm (STA), assemble the MPA to the MAV, prepare the MAV for launch (heat to operational temperatures and erect); and execute the MAV launch. The launch sequence would be coordinated between the Earth Return Orbiter (ERO) and ground control and will include the capability for launch abort and retry.

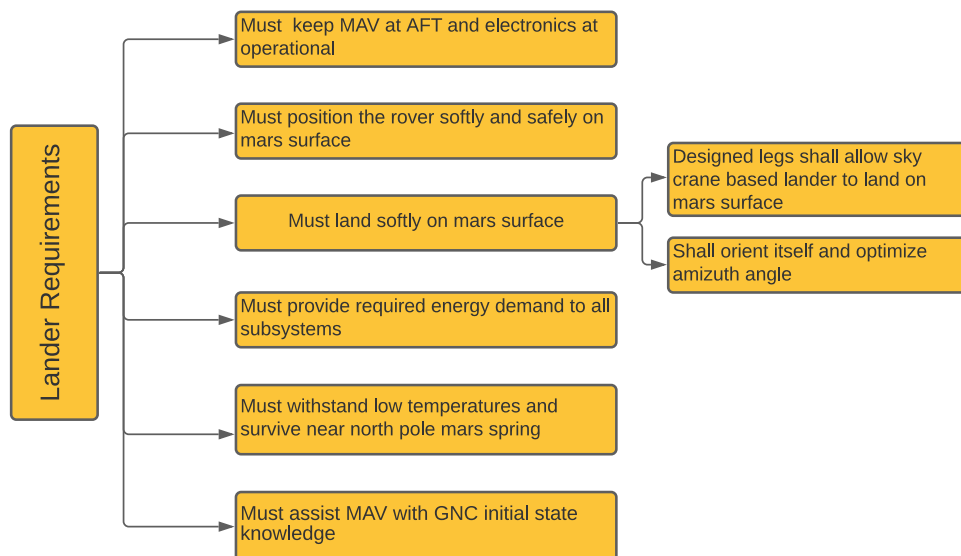


FIGURE 4.4: Lander Requirements.

As seen in Fig. 4.3, the lander consists of a sky crane that was refurbished to be able to land on mars instead to fly away and crash. this concept was chosen considering cost, landed mass capabilities and packaging and complexity. These

TABLE 4.2: Lander qualitative assessment matrix.

Options	Cost	Development time	Accommodation issue	Volume packaging
Modified Sky Crane	Low	Low	Low	Moderate
SDL	High	Moderate	Moderate	High
PPL	High	High	Moderate	High

modified sky crane as acting as lander will be responsible for placing the rover on mars surface the same way as with the original sky crane, collect and provide energy for the MAV thermal control and avionics using a solar array, prepare the MAV for launch (heat to operational temperatures and erect), provide MAV with initial knowledge and assist MAV launch. The launch sequence would be coordinated between the ERO and ground control and will include the capability for launch abort and retry.

4.2.1 Lander Selection

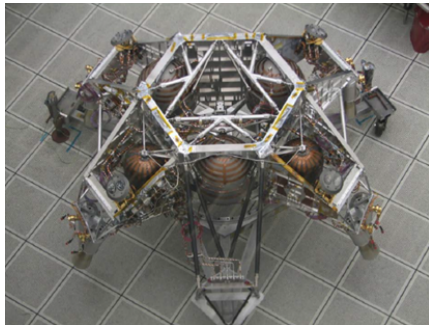


FIGURE 4.5: Photography of original sky crane used in the MSL.

Most of the entry, descent and landing technology is common to the three options and is based on Mars Science Laboratory and Mars 2020. The key drivers for the selection of the lander are cost, landed mass and packaging as well as common key elements common to every option such as accommodation of the MAV and the rover. PPL and SDL utilize a slightly larger, 4.7m spherical heatshield. Although it has been used in previous Mars landers [47] this presents issues with the space available in the Falcon 9 rocket used for launch. Likewise, this provides significant additional volume inside the aeroshell that is critical to accommodate the Lander payloads. The PPL concept employs an EDL more similar to Viking or INSIGHT, using the descent and landing propulsion elements from Mars 2020, as part of the platform

itself. However, both concepts present problems with MAV and rover accommodation considering that the mission will not use a small fetch rover but rather a considerably larger rover. These two concepts also present cost and packaging inside the EDL capsule issues. On the other hand, the third option, the modified sky crane consists of accommodating the MAV inside the sky crane structure and the rover below just like the MSL and Perseverance rovers. This option has the advantage of low cost as there is no need to make all its development and testing considering that a big part of the vehicle is already proven functional and requires minor changes. However, despite being low cost and solving the MAV and rover accommodation, this option presents packaging issues. A qualitative assessment matrix is shown in Table 4.2.

4.2.2 Structural Design

Comparing the modified sky crane with the original shown in Fig. 4.6. it can be appreciated that the structural design needed different propellant tanks accommodation, lay a platform in the middle of the system to accommodate the MAV, added landing legs and studies to find whether the structure could still withstand EDL loads. Initial studies showed issues packaging inside aeroshell.

First, it is important that the rearrange of propellant tanks does not affect the sky crane center of mass and thus the stability. In the original design, the tanks are arranged as shown in Fig. 4.5. The three hydrazine tanks have a triangular arrange while the two smaller helium tanks are accommodated on both sides for static stability. It was needed that the hydrazine tank on the sensor slot was removed for MAV platform clearance. The solution found for this matter was to divide the hydrazine tank into two smaller tanks and take advantage of the space found in the helium tanks slots. This way there was no need of removing the tank from the equilibrium plane it was before.

Considering the MSL and perseverance missions, the sky crane is attached to the back shell the sky crane top structure leaves little to no space on the back shell, as can be seen in Fig. 4.6.



FIGURE 4.7: Original sky crane and back-shell interface.

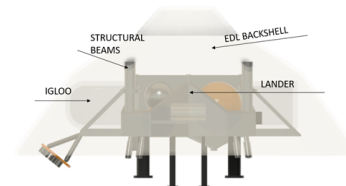


FIGURE 4.8: Modified sky crane and back-shell interface.

This does not allow the MAV to fit inside the aeroshell, making it necessary to lower the sky crane in height. For this, the proposed design consists of 4 vertical beams that accomplish the job of lock the sky crane and make it still for the journey and EDL stage. The interface between sky crane and back shell is the same, the difference is that in order to lower the sky crane and allow the MAV to fit into the aeroshell, the original grips were elongated vertically, as shown in Fig. 4.7.

To assess the viability of this solution, simulations were carried out using Autodesk Fusion 360 simulation environment. The bigger stress suffered in the sky crane grips happens when the parachute is fully opened, provoking a huge deceleration, and thus transmitting that force to the grips. The dynamic pressure exerted on the parachute at that time is 570 Pa, the parachute diameter is 19.7 meters [48] and the drag coefficient for a shaped body like the MSL parachute is 0.64

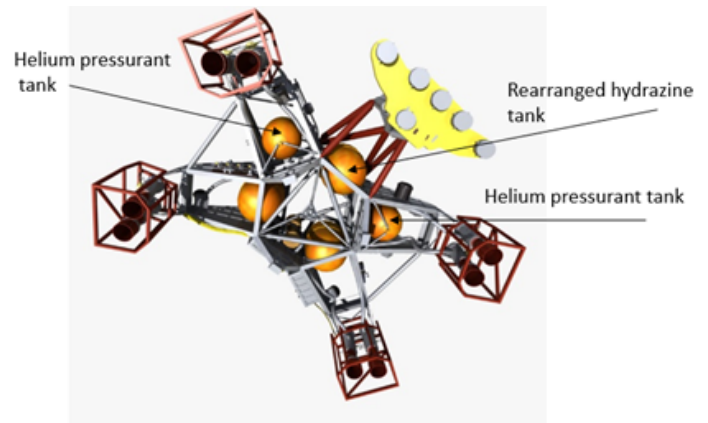


FIGURE 4.6: Original sky crane design viewed from below.

approximately. the force subjected on the grips could be found with the drag equation $F_D = P_D C_D A$, where F_D is drag force, P_D dynamic pressure, C_D drag coefficient and A the cross area.

Using the event simulation environment, which dynamically simulates the event, it was found that the structural beams resisted the loads acting upon them during descent stage and that Von Misses stress is low, as shown in Fig. 4.9.

Finally, the upper hexagonal structure encloses the igloo as shown in Fig. 4.8 when the MAV is to be erected, this structure must be removed out for erection clearance. The solution found was to use well known technology pyrotechnic bolts and a simple signal sent from lander avionic would blow the bolts and set free this hexagonal structure.

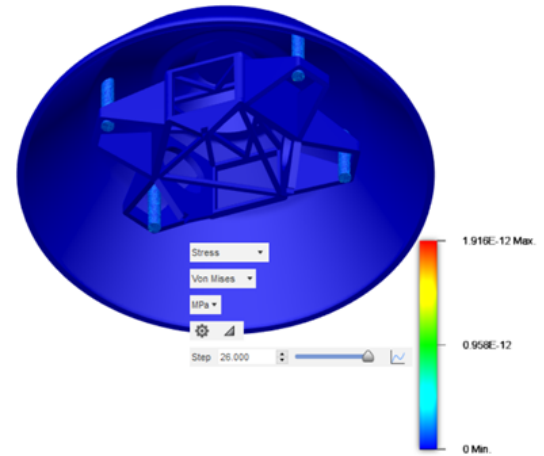


FIGURE 4.9: Beams stress simulation from Fusion 360.

4.2.3 Lander Legs

To understand the landing dynamics of a lander on mars, it is important to find out more about the past missions to the moon as well as other landers which had made it successfully to other planets. Landing systems used in these landers were reviewed and reusability of shock absorbers was investigated.

The Viking 1 lander was the first spacecraft to achieve soft landing successfully on Mars's surface as part of the NASA Viking program in 1976. The landing system had a system which included a main strut assembly, secondary struts assembly and a footpad for each leg. The main strut assembly contained five stages of crushable honeycomb tube core for main energy absorption. The secondary strut inboard ends were attached to load limiters which deformed upon reaching the designed limit load to protect the main body structure and onboard electronics components [49].

Landers after Viking have used a similar approach with crushable material as attenuator. However, considering the capabilities of the sky crane and a considerably high weight on the modified sky crane (1.3 tons), utilizing the historical approach was discarded given that the legs would need to be substantially large considering the few available space on the aeroshell capsule and that all crushable bumper landers having aluminum honeycomb, foam plastic, airbags, and crushable carbon fibers present this issue.

In response to that, a novel approach for the lander legs was required. Different options were identified such as Metal Bellows Shock Absorber [50], electromagnetic absorber [51], electromechanical absorber [52], and novel hydraulic absorber [53]. All options but hydraulic absorber are shown in Fig. 4.10.

To evaluate these options, extensive literature review was made, and advantages and disadvantages identified are presented in Table 4.3.

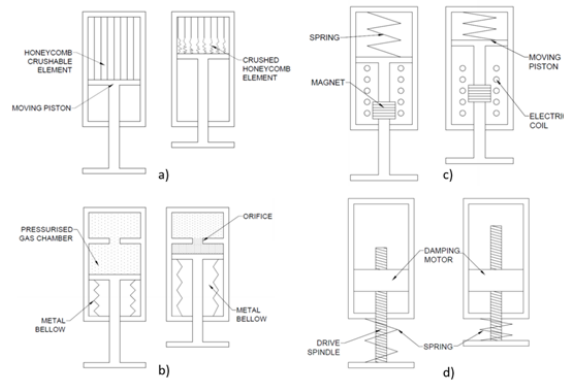


FIGURE 4.10: Novel approach for the lander legs: a) honeycomb crushable element b) metal Bellows shock absorber c) electromagnetic absorber d) electromechanical absorber [53].

Looking at table 4.3 it can be seen that despite some interesting advantages like relative low mass and operations at cryogenic conditions, the most important advantages are found in the novel hydraulic absorber and thus this concept was selected to be incorporated in the modified sky crane lander legs.

The chosen option consists of eight landing legs in both inner square lines. Each leg comprising of primary attenuator with a spring-damper and secondary attenuator with a hydraulic damper. The primary attenuator incorporates a spring holder and a helical compression spring as well as a secondary attenuator incorporates a hydraulic cylinder and a piston rod. Total setup is confined within a retractable cylinder which completes the entire lander leg setup [53].

During the landing phase, after the halt of retrorockets, the lander gets dropped from 7.5 to 5 m, and the lander contacts the ground from a vertical direction. It gets subjected to vertical impact now the spring damper inside primary attenuator starts working and gets pressed downwards. The maximum impact gets absorbed by the spring. After a short layoff, it transfers the same energy to a secondary attenuator, obeying Newton's second law. Secondary attenuator encounters maximum impact which in turn makes its piston to move upwards so that the hydraulic damper can dissipate maximal impact [53].

4.2.4 Lander Systems

Power

For power supply, solar arrays and RTG were considered. The solar array consists of one 6.2 meters deployed ultra-flex GaAs solar panel similar to that used on the Phoenix mission with two 50 A-Hr Li-Ion batteries with 900 Wh per sol [54] available for all subsystems. On the other hand, there is a 22.5 kg, 1330 Wh per sol RTG unit.

Comparing these two options, even if lighter, RTG was an over-engineered option for lander requirements as it can be seen at table 4.5. The solar array provides enough energy for the lander power requirements at spring, just as Phoenix

TABLE 4.3: Landing legs option analysis.

Options considered	Advantages	Disadvantages
Metal Bellows Shock Absorber	Withstand harsh environments. Designed to operate at cryogenic conditions. Relatively low mass	Less effective means of energy absorption as compared to the honeycomb absorbers. Requires similar space as with crushable method.
Electromagnetic Absorber	No hydraulic or pneumatic system is required. Reusable shock absorber in space applications	The use of magnets and coils add a considerable amount of mass to the shock absorber.
Electromechanical Absorber	Can be resettable	Substantially complex. Adds considerable mass.
Novel Hydraulic Absorber	Commercial-Off-The-Shelf components. Safe and large scale mass landings on the surface of Mars. Compatible with available volume inside aeroshell. Works well with vertical landing. Good shock absorption	More components are needed than crushable technology. More weight than traditional approach.

solar array did. Finally, although safe as described below at section 4.2.6, RTG represents a bigger risk to the mission than a solar array, and already one RTG is being sent in the same EDL.

Considering these reasons, the solar array was selected as power supply for the lander.

Erection Mechanism

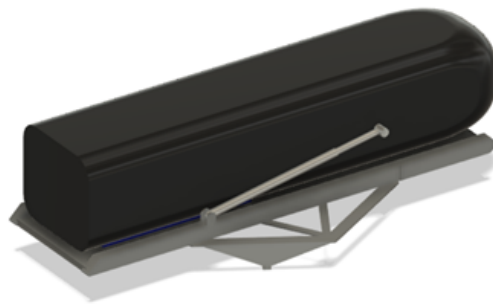


FIGURE 4.11: Erection Mechanism.

The elevation mechanism shown in Fig. 4.11, consists of a 1-axis rotator, similar to that used by the MER lander [56], two linear actuators and two sliders in the platform to allow free displacement of the igloo while the erecting process takes effect. In this configuration, the system can expand and contract thermally without inducing unintended clamping loads on the bearings.

TABLE 4.4: Erection mechanism estimation characteristics [55]

Parameter	Value
Torque (Nm)	3,000
Mass (kg)	30
Range (deg)	90
Power (W)	75
Actuation time (min)	20

Regarding the erection system, the erector pivot transfers the loads from the MAV to erector, with no load transfer or sharing to the launch tube. It connects the primary actuator to the MAV, while the lineal actuators slide the MAV towards the center. This combined movement completes the erection shown in figure 10. A pyrotechnic pin puller prevents the MAV from sliding forward prior to elevation. Parameter values for the erection mechanism are exhibited on Table 4.4.

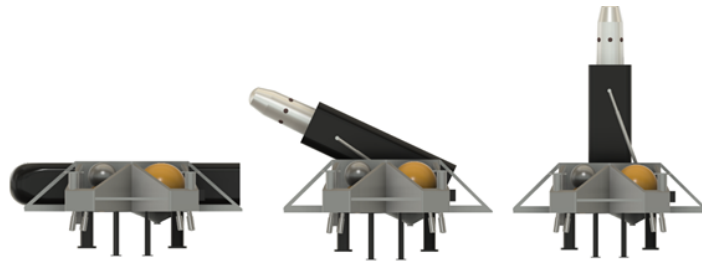


FIGURE 4.12: MAV erection process from stowed to erect.

4.2.5 Budget

Mass and Power Budget

To corroborate whether the solar array was enough for all lander subsystems, calculations regarding battery charge cycles were made and it was found that on idle mode, for the battery to reach critical power level, it would take approximately 14.8 hours and 8.7 hours to be fully charged.

Cost Budget

In the first instance, only the costs related to the sub-systems were estimated as shown in Table 4.5. Consequently, the costs related to the operating and ground systems, integration and testing, planetary protection were estimated to obtain a total cost as shown in the Table 4.6.

4.3 Surface Vehicle. Rover - Technology Offset

TABLE 4.5: Lander mass and power budget estimation.

System Element	Mass [kg]	Average ~Power (W)	Normal-IDLE (24h)	MAV lifting (0.33 Hr)	Landing (0.12 Hr)~	Comm (0.3 Hr)	Costs (M USD)
Payload	385.0	15.0	12.0	12.0	12.0	12.0	-
MAV	300.0	-	-	-	-	-	-
MAV support	85.0	-	-	-	-	-	-
Avionics	27.8	10.0	10.0	10.0	10.0	10.0	
Command ~Data ~Handling	4.0	-	-	-	-	-	12.34
Power control	6.6	-	-	-	-	-	
Power distribution	12.6	-	-	-	-	-	
Pyro switches	4.6	-	-	-	-	-	
Telecommunications	3.8	65.0	-	-	-	65.0	7.38
UHF hardware	3.8	-	-	-	-	-	
Power	28.0	82.0	-	-	-	-	1.93
Solar array	15.0	-	-	-	-	-	
Battery	13.1	-	-	-	-	-	-
Thermal control	19.0	36.0	36.0	36.0	36.0	36.0	1.36
Attitude control	46.0	334.0	-	-	334.0	-	16
Mecanical	306.6	75.0	-	75.0	-	-	6.91
Structure	286.6	-	-	-	-	-	
Mechanisms	20.0	-	-	-	-	-	3.03
Cabling	25.7	-	-	-	-	-	5.09
Propulsion	480.0	-	-	-	-	-	
Dry mass	190.0	-	-	-	-	-	26.76
Wet mass	290.0	-	-	-	-	-	
Total	1321.9	208.0	58.0	133.0	392.0	123.06	83,06

TABLE 4.6: Total lander cost budget estimation.

Description	Costs (M USD)
Ground operations	20.79
Integration and test	24.21
Ground systems	39.65
Planetary Protection	23.48
Subtotal subsystems costs	83.06
Total	191.19

4.3.1 System Overview

Rover- Technology Offset (Rover-TO) stands for the use of combined heritage technologies with the intention of amplifying its reach to that of the mission. Key factor of the selection of this technologies was the stability of the rover during operations while allowing a lighter design, reducing the traditional landed mass in comparison with the occupied volume and for this, offering an increase on operational capabilities to those of handling the Auto-Gopher II drill, as will be discussed at section 4.4.

The rover programmed for 7 modes of power operation: Drilling and sampling, geophysics studies, two communications and data handling modes, regular field traversing, charging mode (idle mode) and secondary mission mode. In the following sections a deepening on this topics will be performed.

4.3.2 Requirements

Following RFP requirements, Rover-TO was design to fulfill:

1. Being an autonomous system capable of performing drilling operations on mars surface with the express purpose of retrieving ice cores.
2. Storing the ice cores in a frozen state during surface operations.
3. Maximize the data return within cost and schedule constraints.

To fulfill those requirements Rover-TO has been design to withstand Auto-Gopher's size and mass with an effective mass dsitribution. For reaching this size and this low mass Rover-TO was inspired on Rosalind Franklin rover, a very light and spacious design. Also Rover-TO had to have at least the power of MSL class rovers to power the drill [57]. To achieve effective sample conservation, Rover-TO had to be designed with an active thermal system capable of both, heat and freeze. RIPAS reliable and capable technology from MSL class rovers was taken for this matter. Finally, to maximize data return,

Rover-TO will make use of the deep drilling capabilities of Auto-Gopher II and reach beyond 6 mts of depth into the ice table at phoenix landing site, limit established by curiosity's team in which life could survive to radiation, allowing this mission, for once and for all, to determinate if life has survived mars surface radiation by hiding in the depths of the ground, [58]. Also, a secondary lasta mission is proposed for Rover-TO. After finishing primary mission operations by delivering the sample canister to MAV startin MSR mission sequence, Rover-TO will travel to where remains of Phoenix lander are, and there it will inspect for the results on Planetary protection donde on Phoenix by searching for signs of life.

Besides this general requirements some specific requirements thought for the mission of the rover were condensed on Fig. 4.13.

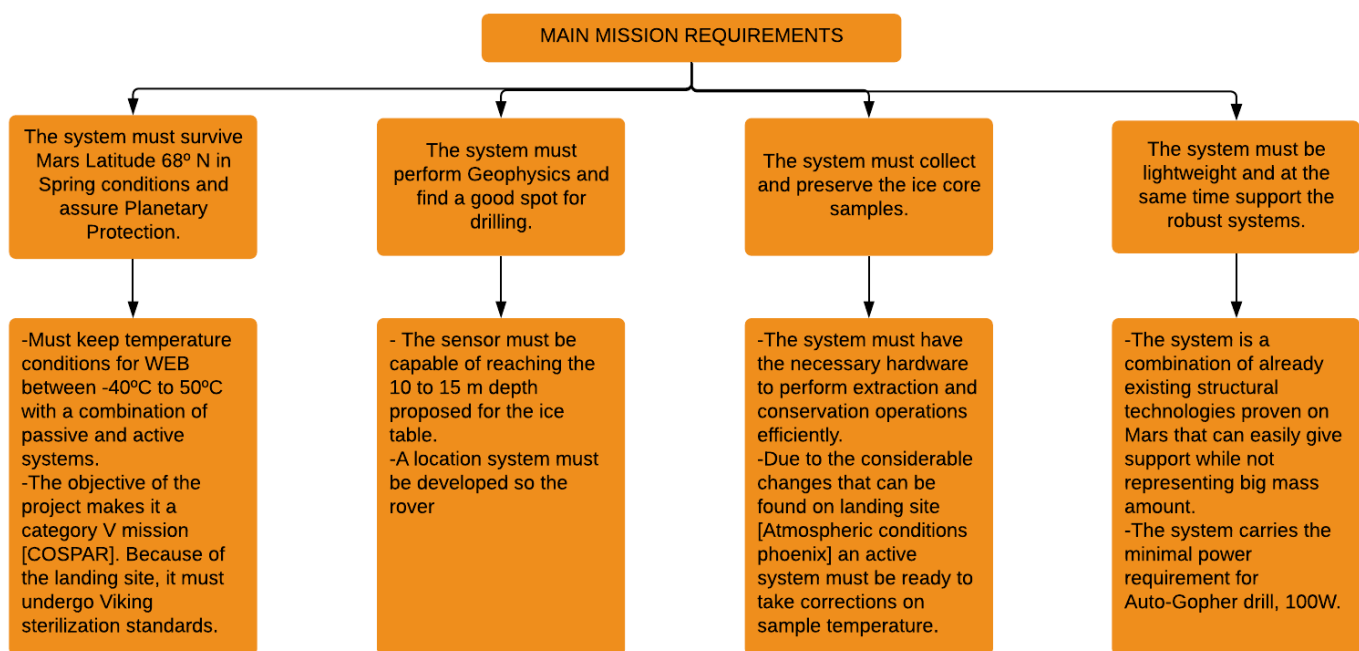


FIGURE 4.13: Surface Vehicle Requirements.

4.3.3 Instrumentation

Being drilling and sampling its primary mission, Rover-TO was focused on this operations based on automated hardware, leaving the necessity for instrumentation to only three science payload instruments: The one chosen for geophysics studies, RIMFAX, the one suited for temperature, pressure and air speed measurements, REMS, and the one capable of detecting life signs, SHERLOC.

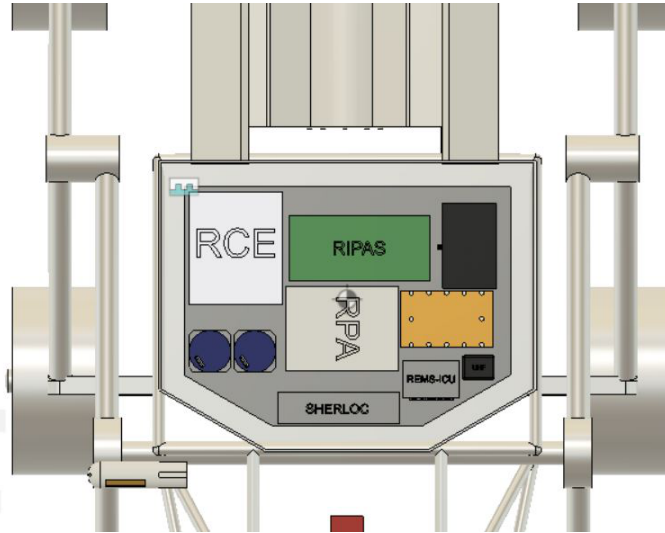


FIGURE 4.14: Instrumentation and avionics inside WEB. Notice the center of the instruments, its stability determined the dimensions and shape of the WEB. RIMFAX main instrumentation chosen for this mission, corresponds to the golden rectangular box.

TABLE 4.7: Trade Study for Ground Penetrating Radar.

Alternatives	Mass [Kg]	Dimensions [mm]	Estimated Cost [M USD]	Depth Range [m]	-
Weight	0,2	0,1	0,3	0,4	AHP
WISDOM	(WEU) 0,811	145x163x55 (WEU) 410x200x180 (WAA)	0,9850	2-3	0,3935
DAN	2,1	204x61x212	2,9234	1	0,1688
RIMFAX	3	196x120x66	3,0887	10	0,4353

About RIMFAX

The Radar Imager for Mars' subsurFACE eXperiment (RIMFAX), mission's main instrumentation, is in charge of the geophysical study that will find the best spot for drilling. It was selected based on a trade study between 3 instruments that have been deployed or are currently being deployed on Mars missions: ESA's WISDOM, NASA's RIMFAX, Roscosmos' DAN, and CNSA's. The features compared can be found at Table 4.7. RIMFAX is an ultra-wideband design GPR, which can provides a vertical resolution of 14.2 cm in free space and a depth range of 10 m perfect for the needed depth of 6 m [59]. the radar generates radio frequency electromagnetic waves that penetrate the subsurface. The dielectric properties of the subsurface materials cause the reflection of part of the propagated wave back to the antenna, allowing to verify the composition below the surface [60]. The RIMFAX, has a mass of 3 kg and can operate while the rover is in motion at speeds of 80 and 150 m/h [61] consuming 10W of power. Typical sweep time over the full bandwidth is between 1 and 20 ms [59], depending on the mode of operation. It should be should be noted that RIMFAX was designed with the same concept as WISDOM [62], both developed by Dr. Svine-Erik Hamran, which gives a possible innovation advantage to RIMFAX.

About REMS

For the environmental monitoring station, the team implemented REMS station from Curiosity rover. The sensor array allows simultaneous data acquisition of UV irradiance, pressure, wind speed, humidity, and atmospheric and surface temperature [63]. This station, with a total mass of 2.04 kg, is designed to survive a temperature range of $-130\text{ }^{\circ}\text{C}$ to $+70\text{ }^{\circ}\text{C}$ falling inside the range of expected temperatures at Phoenix landing site. This power consumption will depend on REMS activity and ambient temperature [63], staying at an average of 9.5 W.

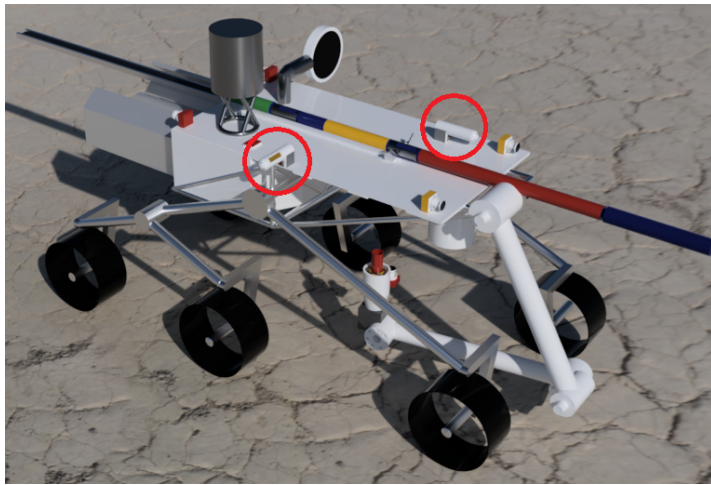


FIGURE 4.15: REMS' Booms Location. Inside Red Circles.

The station consists of 4 units; Boom 1, Boom 2, Ultra-violet Sensor (UVS) and Instrument Control Unit (ICU). The booms and UVS are located on the table of Rover-TO, as shown in Fig. 4.15 and the ICU pressure sensor is located inside the rover.

The trades considered for the selection of REMS followed the backgrounds of the environmental sensors sent to Mars by NASA. The trades were done over REMS, MEDA from Perseverance, and MET from Phoenix Lander, being the last one the most favored at the beginning due to its reliability on Phoenix landing site. But it came with time to be a knowledge of the team that the barometric and thermometric technology of MET was still part of the REMS and even MEDA. The main difference consisted of the wind speed sensor of MET, which came to be more complex [64] than the booms because of its moving parts. The selection of REMS over MEDA had to do with additional capabilities MEDA had over REMS that were not key requirements for the mission and added complexity, mass and power to the overall budget.

About SHERLOC

The Scanning Habitable Environments with Raman & Luminescence for Organics & Chemicals instrument, uses spectroscopy, UV lasers and cameras to detect organic molecules belonging to past or present life. It weighs 5.16 kg and takes a total power of 48.8 W when operating [65]. The system is necessary to perform the secondary mission operations and will be a key part of the additional scientific information in the sample extraction process, where it will measure the contents of organics inside the deep ground ice, where it is possible that radiation has not prevented the presence of life.

The trade was done over the newest technologies in life detecting on Mars surface: SHERLOC, PIXL, Supercam, from Perseverance rover, and MOMA from Rosalind Franklin rover. The two last ones were discarded for complexity and

cost issues, pointing out that MOMA has to crush its samples to actually perform the study[66] which requires additional hardware and more sealed boxes like the WEB. The other two, SHERLOC and PIXL had the advantage of being non-contact instrumentation, allowing these can perform their respective goal without touching the analysis zone.

PIXL is lighter (2.615 kg) and certainly needs less power than SHERLOC (25 W) [67], but, although it is able to detect signs of past life, its main focus consists in the catalogue of minerals on Mars surface. By the other hand, SHERLOC is a more robust system with the scope of finding life signs only, consisting in an array of magnifying glasses to reach its findings to human eye with it's camera, and relying on Raman Spectroscopy, the preferred method to detect sp^2 -bonded carbonaceous materials, a pursued life detecting strategies[68] of NASA and ESA as suggested by Marshall et al. In 2014, when planning systems that integrate into this task with MOMA, inside Rosalind Franklin rover.

4.3.4 Rover Structure

Structural design is the most significant change done over the heritage components of previous rover missions. From down to top, the structure consists of the classical Rocker-Bogie suspension that gives more stability and higher speeds[69]. This suspension, developed in aluminium 7075, was designed in such a way it would drive with no problem through the most tilted slopes of the Green Valley territory corresponding to Heimdall outer ejecta crater skirt (about 5 to 10° of slope) [70]. Additional cross hill and downhill slope angle were added to the design giving margin for unusual operations.

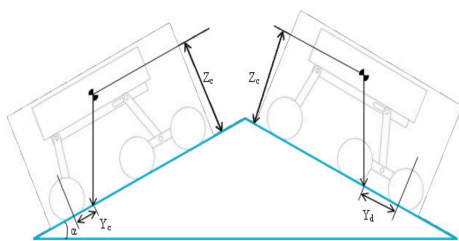


FIGURE 4.16: Downhill slope considerations [70].

$$\alpha = \tan^{-1}\left(\frac{X_l}{Z_c}\right) \quad (4.2)$$

$$\alpha = \tan^{-1}\left(\frac{Y_d}{Z_c}\right) \quad (4.3)$$

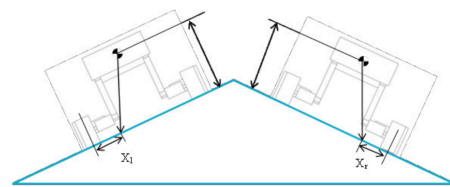


FIGURE 4.17: Cross hill slope considerations [70].

Where X_l and Y_d , correspond to the wheels offset form the rover chassis in x and y axles and Z_c corresponds to the longitude from the center of mass to the soil.

Equations 4.2 and 4.3 [70] determine how downhill and cross hill maximum slope angle were calculated for two case scenarios: the first, being worst case scenario, corresponds to sample handling operation, when drill system is erected,

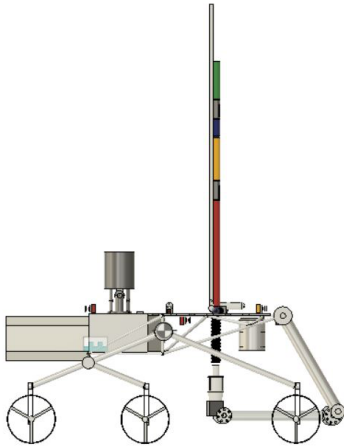


FIGURE 4.18: Position of center of mass in sample handling operations.



FIGURE 4.19: Position of center of mass in traverse operation.

drill is raised, and arm is operating under the rover table. For this scenario the maximum Downhill slope is 24° , with a maximum cross hill of 16° . The second case scenario is the traverse mode, when drill is in stowed position as can be seen in Fig. 4.19. This is the best-case scenario, when the center of mass is located as low as possible, giving a downhill and cross hill maximum of 28.66° and 20.5° respectively.

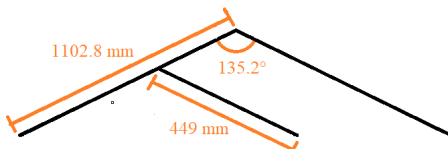


FIGURE 4.20: Calculated Rocker-Bogie dimensions.

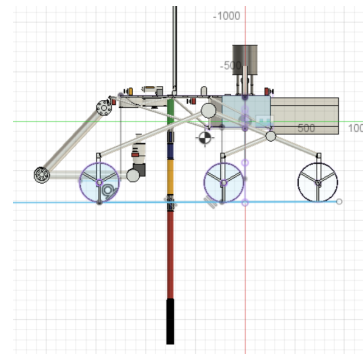


FIGURE 4.21: Drilling operations: Notice primary anchor (section in blue) has already passed the level line that represents the ground, while the drill tip just went through the rail end.

The wheels are $\varnothing 400\text{mm}$ in diameter Aluminium 2014- T6 made, with the heritage design of MSL class rovers wheels. New wheel concepts like the Shape Memory Alloy Tire were considered, but discarded due to the additional challenges and possible costs a wired wheel like this could mean to planetary protection sterilization process. The general dimensions of the calculated structure are depicted in Fig. 4.20.

An additional consideration for this suspension dimensions was the height above the ground it would give to the downwards face of the table. The suspension was calculated to offer at least 550 mm of height above the ground so it would

be possible for the robotic arm to perform its tasks under the table and for the drill primary anchor to easily get attached to the ground while the drill is still safely in contact with the table and the drill rail as it is appreciated in Fig. 4.21. Also, this height was considered so the suspension would be a structural member of the truss main frame. This decision also determined the table-truss configuration of the rover that will be explained below.

On top of the suspension, an Aluminium 2014-T6 truss was designed to keep the equilibrium between the WEB and the table. The purposed main central structure is a cantilever warren type truss. At the beginning, the lack of this technology explicitly for this requirements on a Mars rovers needed additional insight. It was found by the team that trusses existed inside the rover and lander chassis, for example Mars 2020 rover chassis, as seen in Fig. 4.22. It is analyzed that this inner trusses rely on their attachment to the skin, acting as a spar web and so, dealing with shear stress as a tension field beam, usually found in aircraft technology. Another clear example of the successful use of trusses in planetary missions is the very Descent Stage - Sky crane this Project modified as a lander.

With the eagerness of being certain of its main functionality as a cantilever, the truss was submitted to a static load study with Autodesk Fusion 360 simulation toolkit. The two scenarios studied were the total cantilever force exerted by arm and drill at the same time corresponding to 500 N, and a side momentum corresponding to 500 N as seen in at Fig. 4.24a and Fig. 4.24b, throwing a Safety Factor of about 12. A second maximum load over the truss scenario, were an overestimated load of 1,500 N was put on the structure, throwing a satisfactory 4.25 Safety Factor as seen in Fig. 4.24c and Fig. 4.24d.

Concluding the truss description, this over-designed structure serves only as a proposition to the review board for the use of a cantilever truss in the design, posterior optimization of the structure to narrow mass budget must be done in the development stage of the mission.

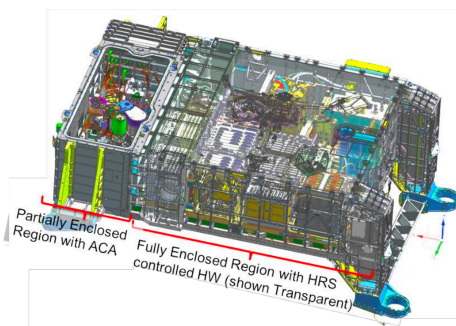


FIGURE 4.22: Mars 2020 rover chassis truss form [71].

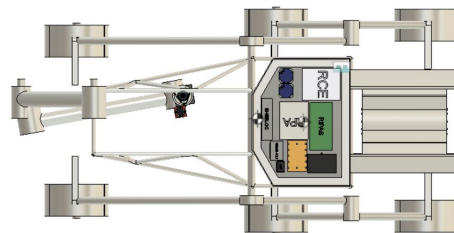


FIGURE 4.23: Rover-TO cantilever truss.

The WEB, is a set of aluminium 2014-T6 foils that serve as rear chassis providing additional shear strength to the joint wall in which WEB, truss and suspension join together and the center of mass oscillates.

The design continues with the honeycomb table, an imitation of the lander tablets found in heritage technology as Phoenix, insight, Schiaparelli and Viking landers. The 5 cm thick honeycomb table works as Tension field beam in

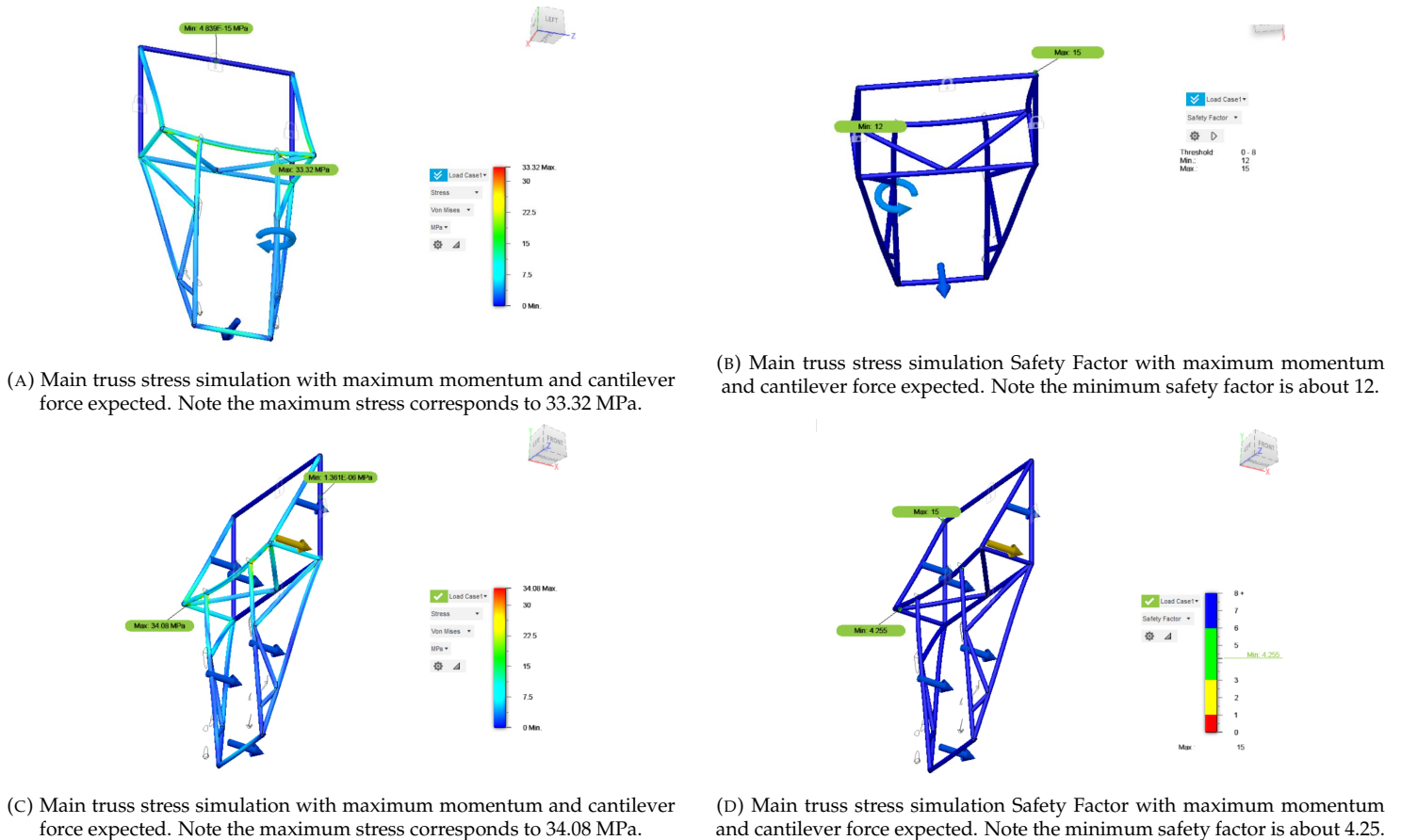


FIGURE 4.24: Main truss simulations.

cooperation with the main truss, distributes little mass on a sparse plane, thus giving more stability in case of torques due to winds hitting the drill, and most important, it guards the sample collection and drilling operations systems from radiation and sunlight.

The Auto-Gopher drill is being held by a Z axis Guide Roller Rail of Aluminium as it is found Honeybee Robotics, company in charge of its first development stages, does generally with its drills, like for example trident drill and the ROPEC [72, 73]. on the foot of the rail are rolled 10 meters of Vectran chord, heritage from skycrane [57] and ready for drilling operations. The rail can be erected by a pivot system similar to the one found in the MAV at section. This system allows for the location of the drill centrally on the table with out need of arranges that use more than one structural component like perforation cranes. This made of the positioning the drill a key trade for the design.

Ranging from various propositions like having the very arm to manipulate the drill at one side of the deck as Mars 2020 rover concept, or having an entire crane structure like kuklos [74] lander, the trade was finally based on rover stability as the drill alone represents approximately a 15% of its entire mass. The position of the drill had to be as close to the center of mass as possible so the torque would be reduced only to the torques produced by the wind speed at Phoenix landing site, of which is known may reach up to 12m/s [75], giving an overestimated value of 13.3 Nm torque using the drag coefficient

for cylindrical bars (1.2). Compared with a maximum of 273 Nm torque estimated if the drill was to be handled by the arm represents the less amount of torque for this model. This and the fact that the rover could be designed symmetrically, were the reasons why the drill was put in the longitudinal axis of the vehicle and as close to the the center of mass as possible that, with the fact that the drill will have only 1 degree of motion during drilling operations, prevents structural torques to happen besides the very low one produced by the fastest speed on Phoenix landing site, of which there are only records of it happening at daylight while the drill is stowed [75].

Finally, at the tail of the vehicle, fully recumbent lies the RTG, having this specific position with the task of balancing the rover.

4.3.5 Navigation, Guidance and Avionics

For the navigation and guidance system the rover must be able to determine its location, perform a general characterization of the place where it is located and the obstacles it may present, and have the ability to move autonomously if necessary. For this purpose, the rover's navigation system uses traditional components implemented in previous Mars rover missions [76], so its reliability and performance are already proven. The system consists of two main parts, the LN200S Northrop Grumman IMU and the NavCam and Hazcam engineering cameras.

The rover has a total of six Hazcam, of which four are used for navigation, circled in red on Fig. 4.25 These black-and-white cameras, each with a $124^\circ \times 124^\circ$ field of view [76], use the visible light spectrum to take 3D images, preventing the vehicle from sudden loss or collision with unforeseen obstacles, and their operating software makes it possible for the vehicle to make its own safety decisions [77].

The NavCams, shown in yellow in Fig. 4.25, are located at the front of the rover; these cameras black-and-white cameras use visible light to collect 3D and panoramic images. The Navcam is a pair of stereoscopic cameras, each with a 45-degree field of view, [76] to help to plan ground-based navigation. These cameras work in cooperation with the Hazcams by providing a complementary view of the landscape [77].

The LN-200S IMU is a small, lightweight and very reliable instrument, which has been used in several space missions, such as the Mars Rover Spirit, Opportunity and Curiosity. The rover will have two IMUs, however, only one will operate constantly and the other will be kept as a backup. The IMU can maintain operation down to temperatures of -62°C to 85°C , so these will be located inside the WEB of the rover, as shown in blue in Fig.4.14 [78].

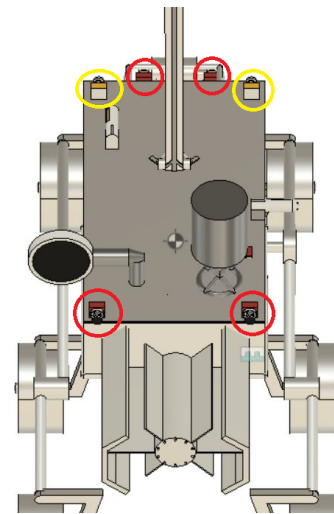


FIGURE 4.25: Rover Navigation Cameras. Circled in red the navigation Hazcams, and in Yellow the NavCams.

In addition to the above, the navigation system will be visually supported by the Martian orbiters to obtain orbital images of the rover TO locate it. In particular, the HiRISE instrument aboard MRO, working in conjunction with the NavCams, can implement a method that benefits from the improved location accuracy of IBA/BA, avoiding the inaccuracies associated with using the rover's initial position obtained by odometry. In this method, the images taken are orthorectified through triangulation of observations in orbital imagery and surface imagery of the landing site or UHF two-way Doppler tracking technology [79].

About avionics, the system will use the same reference that has been used for decades, specially on MER and as MSL class missions. Two RAD750 radiation hardened processors from BAE systems each inside a Motorola 6U VME [80] with 120 MByte DRAM and a 3 MByte EEPROM and 1 GB PROM will be put aboard the system. Only one will work at a time, the other one is just there for redundancy. This units will be found in whats its called RCE in the WEB.

4.3.6 Rover Power System

The power requirement was established by Auto-Gopher II power demand. 100 W are the necessary mimum if ice drilling operations are to be performed and thus the developers of the drill recomend the power architecture of MSL class rovers [57]. Thus, the primary power source in charge of a MMRTG (Multi-Mission Radioisotope Thermoelectric Generator). The power system constantly provides the rover with 2,000 watts of thermal power and 110 watts of electrical power 110 W at the start of the mission [81], with a 4.8% decrease each year, keeping it in operation for 14 years [82].

The reason why MMRTG was chosen is beacuse was found as the only type of RTG implemented in previous Mars missions: MSL and Mars2020 [83], [84].

The 45-kg MMRTG (4.8 kg of plutonium-238) is located at the rear of the rover and can charge two lithium-ion batteries that help meet the power demands that the MMRTG cannot satisfy during rover operations. Each battery contains eight 43 amp-hour cells in series, delivering 28 V, although they are housed in the same structure they operate independently [85]. The two batteries weigh a total of 26.5 kg and can deliver 2408 Wh at 100% capacity. However, only 1,600 Wh (66% of their capacity) is usually taken at each discharge cycle, to ensure a supply of energy to the components that must remain active while the battery completes its charge cycle, which will take approximately 20 hours (10 hours for each battery).

Depending on the activity performed by the rover, the power consumption varies, since not all components have to be active at the same time, except for the computer, the IMU and the mechanically pumped fluid loop. The Table 4.8 shows in detail the energy needs required by each rover component in both active and inactive modes. The highest energy demand corresponds to the wheels of the rover of about 200 W.

Table 4.9 shows in detail how much time was estimated for each instrument in the respective operating mode. The cells in green color imply an active power consumption while those in blue color imply a passive consumption of the components that are in idle mode. Additionally, the energy in Watts-hour that the batteries will provide in each case during the required

TABLE 4.8: Rover Instrument Power Draws.

Instrument	Active Power Draw (W)	Idle Power Draw (W)
Mechanically Pumped Fluid Loop	10	-
RIMFAX	10	4
2 NavCam	4.3	-
6 Hazcam	12.9	-
REMS	9.5	2.5
Auto-Gopher	100	-
UHF Transceiver	65	12.6
X-Band Transponder	71.8	-
Wheels	200	-
Arm	78.61	-
IMU LN200S	12	-
SHERLOC	48.8	16.6
ROM Memory	1.98	1.32
RMCA	17.1	13.2
RAD 750, 6U VME	20	5
End Effector	80	-
Total	678.19	50.22

time is shown. For each battery charging cycle, the remaining active components are expected to consume approximately 640 Wh of the 808 Wh available with the batteries at 34% of their capacity. The total cost of the power system was calculated with the help of the PCEC software, giving a total of 31 M USD, of which 28.88 M USD correspond to the RTG and 2.12 M USD to the batteries.

For the secondary mission operations it is estimated that only SHERLOC, REMS and UHF communication will be implemented, in addition to the components that must be in idle mode and active at all times, so the vehicle will be able to perform its tasks with a consumption of 1,600 Wh for 13.7 hours non-stop.

4.3.7 Rover Thermal Control

Rover- Technology Offset has to survive temperatures that can get to 181.15 k and have a mean value of 240k at noon [86][87] on primary operations and an overall range of 140 k to 280 k [88] in secondary operations and in following use. Beside lengthen Rover-TO operational life, the MMRTG provides the solution for its survival in rough temperature conditions, producing approximately 2000 W of thermal dissipation which allows this MSL class technology to reach up to $\pm 60^\circ$ latitudes [89]. The rovers use Integrated Pump Assembly Mechanically Pumped Fluid Loop system fed with Freon-11, pumped and controlled by a system of valves and a pair of bombs called RIPAS[90] from which a circuit of tubes made out of Teflon and other materials, extends to travel through the instruments inside the WEB in an special structure developed for this matter called RAMP [71]. The pertinence of using this system for this mission is visible as the instrumentation selected for the rover is almost entirely from Mars 2020 mission WEB.

TABLE 4.9: Time and Power Consumption Requirements for Rover Operation Modes.

Instrument	Geophysical Survey	Drill	X-Band Communication	UHF Communication	Displacement
Mechanically Pumped Fluid Loop	451 min	391 min	838 min	163 min	526 min
RIMFAX	451 min	391 min	838 min	163 min	526 min
2 NavCam	451 min	-	-	-	526 min
4 Navigation Hazcam	451 min	-	-	-	526 min
Arm Hazcam	-	48,8 min	-	-	-
Drilling Operations Hazcam	-	391 min	-	-	-
REMS	451 min	391 min	838 min	163 min	526 min
Auto-Gopher	-	391 min	-	-	-
UHF Transceiver	451 min	391 min	838 min	163 min	526 min
X-band Transponder	-	-	838 min	-	-
Wheels	491 min	-	-	-	526 min
Arm	-	391 min	-	-	-
IMU LN-200S	491 min	391 min	838 min	163 min	526 min
SHERLOC	451 min	391 min	838 min	163 min	526 min
End Effector	-	0,15 min	-	-	-
ROM Memory	451 min	391 min	838 min	163 min	163 min
RMCA	451 min	391 min	838 min	163 min	526 min
RAD 750 6U VME	451 min	391 min	838 min	163 min	526 min
Total power Consumption [W]	322,68	355,79	185,28	145,28	294,68
Total Power Drawn From Batteries [W]	212,68	245,79	75,28	35,28	184,68
Power Drawn From Batteries [Wh]	1600	620,00	1052,45	95,84	1600

An scheme with the basic concept of how the RIPAS hot plate-Cold plate system works is depicted in the following figures:

A passive insulation was also needed. Due to weight efficiency, MSL class rovers didn't land with any thermal insulation inside[91], instead an space between 5 to cm was left so, at mars, the mostly composed by CO_2 atmosphere would fill this gap offering a conductivity constant of only 0.01 at that low pressures [92].

With this information at hand a simple thermal equilibrium in stable state can be done to estimate the temperature that the WEB will keep during operations[39]. Usually this is done the other way around, by fixing a desired temperature to then calculate an area of radiation, but the need of a width of at least 800 mm for the rover table in order to give structural stability, gave the WEB this same transverse width which, combined with the adequate mass centering accomplished between components inside it, as seen in Fig. 4.14, left the team with a WEB of approximately $2.8m^2$ of area. With this necessity in mind, the need was to keep the WEB temperature in between the suggested range found for Perseverance WEB of $-40^\circ C$ to $50^\circ C$. [71]

Taking in account that from the original 2000 W the RTG plates already radiate approximately 800 W [90], the thermal study was done for the peak scenario 4.10, corresponding to the lowest temperature on winter, 140 K.

TABLE 4.10: Thermal Equilibrium Design for 140 K lowest heat case.

Thermal equilibrium for an outside temperature of 140 K	
Entry Power	
Power from RTG heat	2,000 W
Power from electronics dissipation	114.86 W
Outgoing Power	
Power radiated from the walls	$0.93\sigma_s T^4$
Power radiated from the RTG radiator (Cold plate)	800 W
Power conducted by the walls and through the CO_2 Isolation	$\frac{0,09(T-140)}{0,103}$

Solving the equation with the Newton Rhapsion method, the inside temperature T in the lowest temperature scenario is 264.138 K or $-11.3^\circ C$. The same exercise is done for the highest temperature scenario is 290.86 K or $17.71^\circ C$. Both of them inside the range proposed by Perseverance design team[71]. For conduction law an approximation of both materials conductivity constant was used, being 130 for Al 2014-T6 skin and 0,01 for CO_2 gas gap. For Stephan Boltzmann law, the absortivity and emissivity used were those of S13GP6NLO-1 white paint that, like on Perseverance rover, it works as coating from the hard radiation environment of Mars surface [71].

4.3.8 Sample Handling System

Arm

For this issue a mechanical arm of 68 kg Aluminium 7075, the same as the one on Perseverance and MSL missions, was selected, avoiding costs for testing and development and assuring the load capacities of the arm would be in range with those needed, effortlessly. some additional technical specifics of the arm include a joint speed of maximum 2.5 RPM which

at maximum load (about 30 kg) produces a torque corresponding to a power of 78.61 W was calculated with an upper margin [93].

The size of the bit and the core samples made unfeasible for the mass budget to count with a bit carousel like the one found inside perseverance rover, the Auto-Gopher II system is too big to replicate ROPEC drill system in a smaller rover. As will be pointed out in Drilling and Coring section, the drill was designed to achieve totally autonomous drilling and sampling tasks; further investigation led the team to the scheme thought by JPL to accomplish this goals, as it can be seen in Fig 4.28. Thus, the arm was selected as sampling system in order to fulfil Auto-Gopher requirements.

End-effector

To perform sampling the arm needs an end-effector. For this matter canadarm end-effector was chosen instead of a mechanical claw. The canadaarm end-effector can catch and constrain in all degrees of freedom, only needing to catch things smaller that its own diameter. The end effector from Rover-TO will have a rotary mechanism inside it as depicted on FIG. 4.33, the same auto-gopher rotary mechanism from FIG. 4.29, an with it, will perform the twists to clam sample tubes to OS as explained in 4.5.6.

The end effector will also mount the OS canister to MAV for which it will need a canadarm special pin attached to it as seen on.

4.3.9 Rover Communications

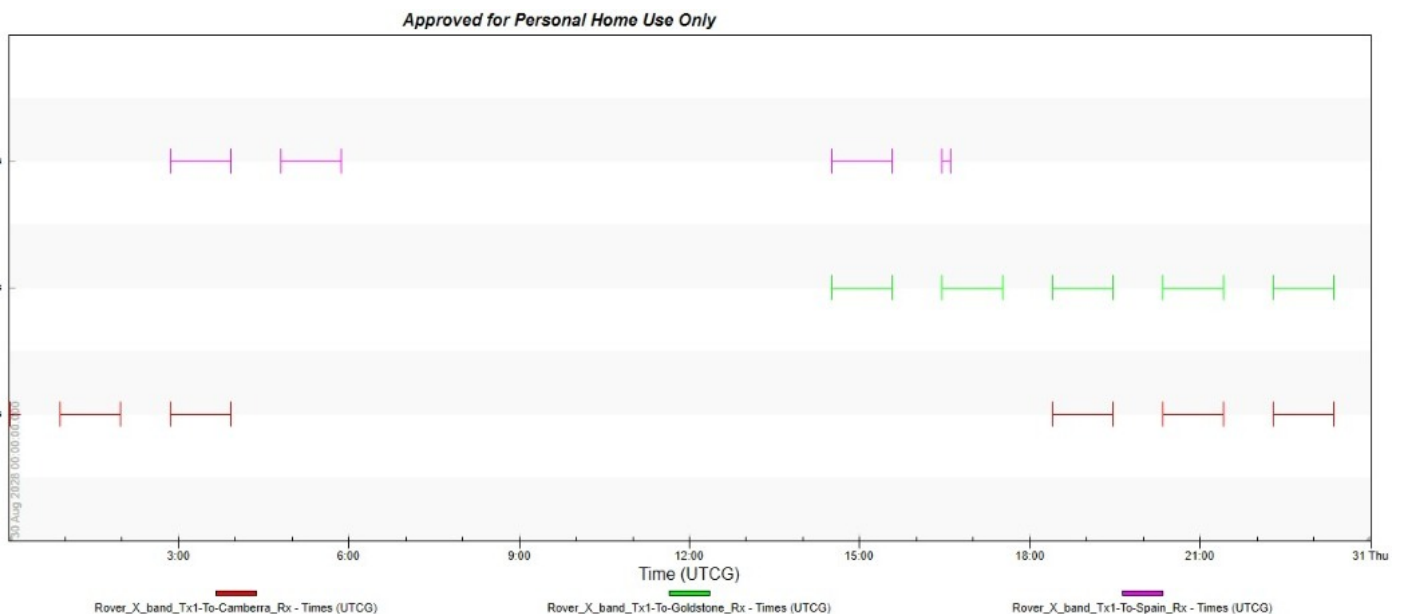


FIGURE 4.26: Rover-DSN Daily Access.

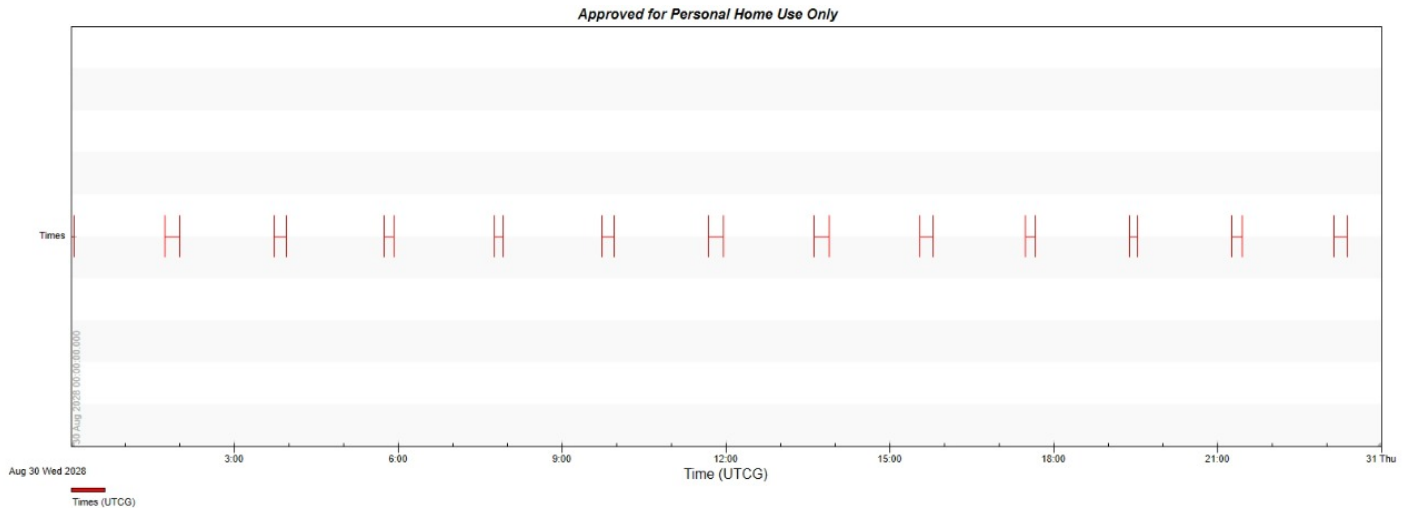


FIGURE 4.27: Rover-Orbiter Daily Access.

Constant communications with mission control is vital for promptness in data analysis and in the making of key decisions as the mission is developing. For this reason, project Haba-Sulue took the opportunity of having MSL power system to carry both orbiter relay and direct communications with Earth via DSN as explained in the orbiter communications section.

By this logic, Rover-TO carries within Perseverance’s UHF Electra Lite transceiver system, that, connected to the the UHF antenna depicted in Fig. 4.25, is capable of 2 megabits per second of data rate transmission with the relay orbiters. To accomplish this, the system draws a maximum power of 65 W and has to make use of the daily accesses to Haba-Sulue Orbiter relay that can be appreciated in Fig. 4.27. A very similar case is contemplated for the direct communication with earth via DSN, of which the daily accesses are shown in Fig.4.26. This direct communication is done via the X-band system heritage from MER missions, transmitting through the high gain antenna seen in Fig. 4.25 with a data rate that reached 28.8 kbits per second [94].

This accesses were calculated with STK communication toolkit, giving the results at Table 4.11. This allows a mean daily data traffic of 1.505352 Gbits by UHF communications, and approximately 0.55 Gbits by X-band direct communications.

TABLE 4.11: **Daily Communication Access Budget.**

Daily communication access duration. Estimated data for day 30 Aug 2028	
Rover-Orbiter UHF relay	(s)
Maximum duration	999.2
Minimum duration	199.235
Mean duration	752.676
Total duration	9,784.784
Rover-DSN X-Band direct communications	(s)
Maximum duration	3,836.731
Minimum duration	96.287
Mean duration	3,207.259
Total duration	19,243.553

4.3.10 Rover Operations

As described in this system's overview, 7 modes of operation were thought for the mission:

Geophysical Study

Before carrying out the drilling activity in each area, it is planned that the rover will be able to perform a geophysical survey like what is usually done on Earth when excavating at depth, in order to evaluate the area for ice coring and to have more precise information about the distribution of ice in the inner layers of the surface. For this purpose, Rover-TO will be equipped with the RIMFAX instrument, which is a type of GPR a non-invasive method that will provide information about the subsurface structure. REMS will also be useful to determine where drilling will be carried out.

Each geophysical borehole will take approximately 8 hours to develop covering an area of 0.171 km^2 at a speed of 152 m/h (0.042 m/s), the maximum at which RIMFAX can operate safely [61], and a power consumption of 195.53 W, as shown in Table 4.8. Additionally the geophysical survey will be carried out with the support of the rover's navigation system. In addition to providing important data on the areas where surface activities will be carried out and helping to determine the best locations for ice coring, the geophysical survey provides a very complete climatic and interior surface characterization that can be taken as additional scientific information.

Drilling Operations

In this subsection it is to be mentioned that the rover will constantly balance its own weight through the movement of the arm and the movement of the drill on deck, assuring the right position of the center mass all time. Also, as described before, the only perceivable torque on the drill will be performed by the winds on green valley. Data from Phoenix instrumentation allowed to determine prevalent wind directions are North-southlies[87]. This information and the downhill tilt angle suggest the best drilling position for the rover is with its longitudinal axis pointing Northwards or southwards

Displacement Operations

Referent to the mode in which the rover will just move in a certain direction. With a maximum operational speed of 0.2 m/s assuming a torque for 45° slopes (as upper bound torque) the rover will use this mode after landing, after geophysics mode when going to the selected spot in the studied area, and finally when going back to the MAV for the end of primary mission operations. For secondary mission operations, as the mission goal is to land as close as possible from Phoenix and EDL at this payload mass could have a landing ellipse of

Secondary Mission Operations

After leaving the OS canister inside MAV the rover will start secondary mission operations, it will immediately charge, or if charged in more than 50%, it will immediately start its journey towards Phoenix lander, guided by the reference HiRise camera aboard MRO will give as described in navigation, control and Avionics subsystem. The estimated time for arrival depends of the landing ellipse. If maximum speed is considered (0.2 m/s), taking in count displacement operations at full power can be performed in 8,76 hours, this time would be

4.4 Drilling and Coring

In this section we explain the complexity of the circumstances to be encountered and requirements to be fulfilled by the drill system, emphasizing on related aspects of the final auger selection.

4.4.1 Drilling and Coring Key Trades

The main objective of the operation is to optimize the obtaining of ice core samples respecting landing site and date selections. Either way some critical aspects led to key trades to determine the drill: ice-proof related properties such as WOB (Weight On Bit), ROP and bit materials, ice-preservation protection mechanism such as duty of cycle, operational precautions and atmosphere isolation, and the capacity to adapt to different drilling environments.

4.4.2 Ice Drilling Reference

Thanks to the experience acquired from ice drilling at polar caps on Earth it is known that, particularly at extremely low temperatures, drilling can become a challenging task, specially due to the hardness of the medium to be drilled, and possible water refreezing processes on the bit that makes the performance way slower and the need for automation and monitoring equipment to increase [95].

4.4.3 Constraint and Requirements

Environmental Conditions

Pressure, temperature, geological subsurface profile, ice deposits distributions and types are some of the parameters that are relevant to the drilling operation. The air pressure on Mars is very low, this means less heat transfer from the drill to the environment and more from the bit to the soil, meaning for some locations a possibility of flooding the borehole, when above TPW or refreezing when below TPW [3].

”Air temperatures can be as low as 140 K at the poles during winter and temperature fluctuations of over 100 K only within 6 hours, can occur” [3]. This is a critical factor for materials selection since it can expand and contract during these delta of temperature.

At the Phoenix landing site according to compiled data from this mission, pressure range is above TPW (7-10 mbar) [96], a temperature range from 175.3 K to 253.4 k [97] well below MPW, presence of rich water-bearing formations and a geological profile of soil size and form fading quickly into glacier forms. Finally during stay on Mars (springtime) there are some ”local and regional dust storms that last for a few days or weeks confined to small areas due to increased sunlight heating” but since pressure is so low dust settles quickly and a dust deflector for the rover is enough protection [96, 98].

All this implies liquid water can appear if there’s enough heat transfer from the bit to the ice and getting it stuck but also increasing the chances of cross contamination, to avoid this there are temperature sensors with high sensibility on the bit [57]. Also because high water-saturation will need more WOB the deeper the bit goes the more chances to find signs of life in the samples [3].

Technological Constraints

Material properties of the bit, WOB, power and ROP are the variables to be assessed in this section since the use of RTG is already justified in the rover’s section. These operational requirements depends on ”minimal mass, volume and energy consumption” [99] are achieved by combining rotary and percussive augers and recycling vibration energy into the drilling process [95].

For materials selection is important to take into account its properties: stiffness, erosion resistant, similar coefficient of thermal expansion because of extreme temperature changes [95]. There are three potential drill bit materials: diamond impregnated, PDC and a hybrid [3], the selection is based on the relative hardness to the drilling material.

Technical adjustments can be done to prevent the wearing of the bit such as moderate ROP, increase WOB the deeper the bit goes. Drilling torque is approximately constant, resulting in a proportional relationship between ROP and power required for rock destruction but depending on the drill bit material heating due to high rotatory speed and greater power input causes more wear of the device [3, 95].

4.4.4 Overview of Selection Process

The following are the considerations that guided the choosing of a drilling system for the mission: It was not specified, but as found in distinct sources of literature [100, 4, 101], ice cores are used as a sample when geological features of the place want to be studied, including geological history, and also atmospheric history. For other goals such as finding life in the ice, less complex drilling systems, like drilling ice chips as icebreaker-life mission [102], or other missions in the Artemis program [72] are going to make use for finding life or soil composition. The following are the considerations made for the selection of the Auto Gopher II [57, 99, 103, 104, 105]:

1. The fact that Auto Gopher can penetrate deep into the ground without considerably increasing energy supply and WOB.
2. Auto Gopher is already made by JPL and Honeybee robotics, and it has been under construction, design and testing since 2005. Information from JSC drill is scarce and didn't match the amount of bibliography to assure a TRL for its design.
3. Mass budget and the fulfill of AIAA requirements. Auto Gopher is a wire-line drill which can access big depths with no need of tube extensions, making it as very light to use drill (65 kg).
4. Sample catch and delivery system. Already planned by JPL. A concept of it can be seen at Fig. 4.28.
5. Size, in which auto Gopher constraints considerable the mission (2.5 m x 0.71 m).
6. Additional scientific information. Auto Gopher is a depth drill, which can reach the 6m depth goal established by curiosity rover, a depth in which life can survive the radiation encountered on the surface of the planet. This drill can search for life in the right place.
7. Power budget. Extremely powerful and fast, the auto Gopher has a low energy consumption in contrast to the tasks it does (100 W).

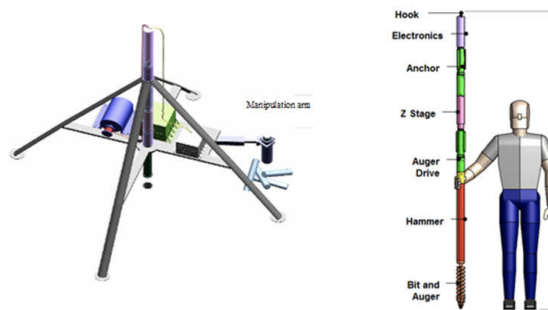


FIGURE 4.28: Auto-Gopher II concept of autonomous sampling system as proposed by JPL. Notice the arm unplugging the bit of the drill under the table.

The following table compares different aspects between NASA JSC and rotary and rotary-percussive auto gopher [105].

It is important to know that the Auto Gopher had way more data and testing information available [57], also since it has an integrated core catcher and was design for soil and ice that brings up the conclusion for the final selection.

4.4.5 Drill Design and Performance

"The Auto Gopher II is an autonomous deep wire-line drill with integrated cuttings management and drive electronics" [99] developed by JPL and Honeybee Robotics Ltd 4.29. It combines two different mechanisms a piezoelectric actuator

TABLE 4.12: Drill Comparison

	NASA JSC	Honeybee Auto Gopher II
System Mass (kg)	7	65
Drill Length (m)	2	3.9
Core Diam. (mm)	25	60
Core Length (mm)	150	100
Power (W)	50-100	< 300
WOB (N)	140-330	10-200
Penetration Rate (cm/hr)	9	80
Integrated Core Catcher	No	Yes

that works as a percussive hammer and a rotary mechanism that will work as a drill [57]. The system weights 65 kg and is expected to have a size of 2.5 m when COTS are removed from its electronics [57]. The drill functions by drilling discretely every 10 cm then the auger deposits away each core at a time as it goes deeper. The dimensions of the core are 56 mm of diameter and 100 mm of height [105].

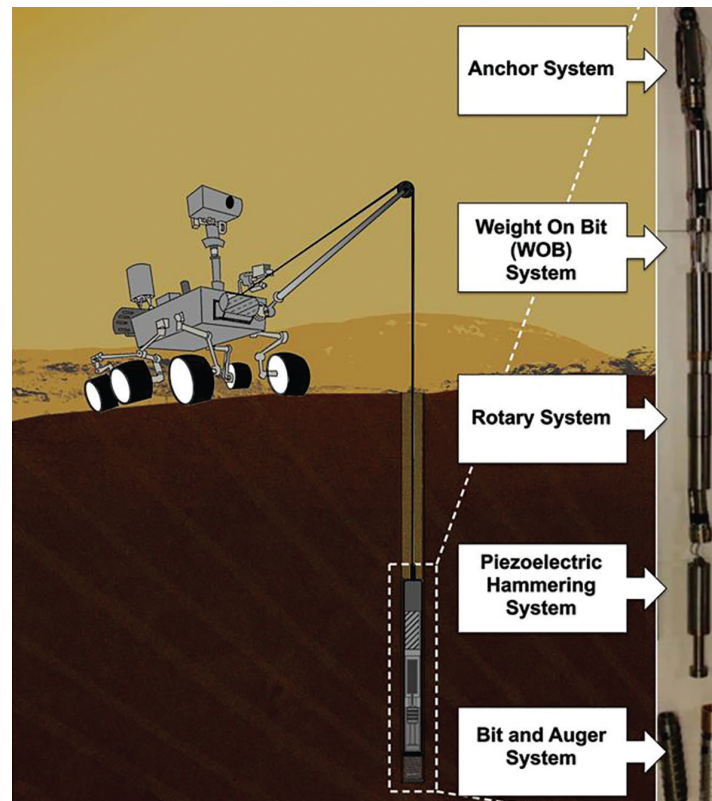


FIGURE 4.29: Auto Gopher II: Drill Parts and concept on MSL rover.

Technical Specifications

The WOB in the wireline system is provided by anchoring the drill to the borehole wall (locking the upper section) and using an internal screw to push the drilling mechanism downward during drilling. The ROP is limited to 80 cm/h [103] by

duty cycle of 50% in order to prevent overheating and excess wearing of the drill bit.

The USDC uses an intermediate free-flying mass to convert high frequency vibrations of a piezoelectric transducer horn tip into lower frequency hammering of the drill bit [57]. The wireline facilitates the ascent of the bit and maintains the integrity of the whole drill and enables drilling to greater depths without a significant increase in system mass or complexity but increases the possibility of borehole collapse and for this reason, the drilled environment should be restricted to stable formations such as ice or ice-cemented grounds as it is for the Phoenix site.

4.5 Conservation of the Ice-Core Samples

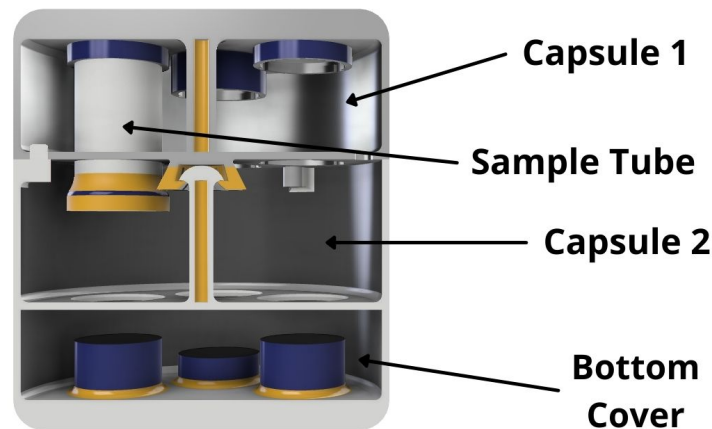


FIGURE 4.30: Cross-Section of the Orbiting Sample Sub-Assemblies.

4.5.1 OS Sub-Assemblies

The Orbiting Sample consists of three main sub-assemblies, focused on modular architecture (see Fig. 4.30) to facilitate sampling storage and the operations done by the robotic arm since if it were a single structure the rover arm would not fit in. The design functions via a Flexure Claw Mechanism (FCM), a design in which the JPL has been working on recently as it is properly fitted to withstand the mechanical loads the OS will suffer throughout the mission [106], and it can store up to 12 Sample Tubes. Although many developments like the FCM have been materializing related to OS structures, due to the current 2020 Mars mission by NASA, barely any of them have been focused towards bringing ice-core samples from mars, therefore we had the primary goal to develop an OS aimed at thermal conservation without adding much to the already present complexity. The three sub-assemblies are:

1. The capsule 1 of the OS (see Fig. 4.31a) is made up of a sample tube top/bottom restraint plate, a FCM, three security connectors and the capsule body, it can contain six encapsulated samples in a circular pattern, as it is the

optimal way for this distribution, but at two different elevations that differ by a few millimeters to avoid interference between the tubes and the robotic arm at the time of storage. The FCM connects to the capsule 2 axial rod securing the two together in a permanent way.

2. The capsule 2, shown in Fig. 4.31b, is similar to capsule 1, consisting of a sample tube retain plate, an axial rod and three security connectors that interface with those in capsule 1. The capsule axial rod is the main load-bearing part connecting to the OS FCM. This capsule serves as support for the last six sample tubes stored in the OS with its retain plate.
3. The third stage is the bottom cover which seals the OS altogether to protect the samples in the journey back to earth, it also has 6 foam cylinders to better contain and lock the Sample Tubes.

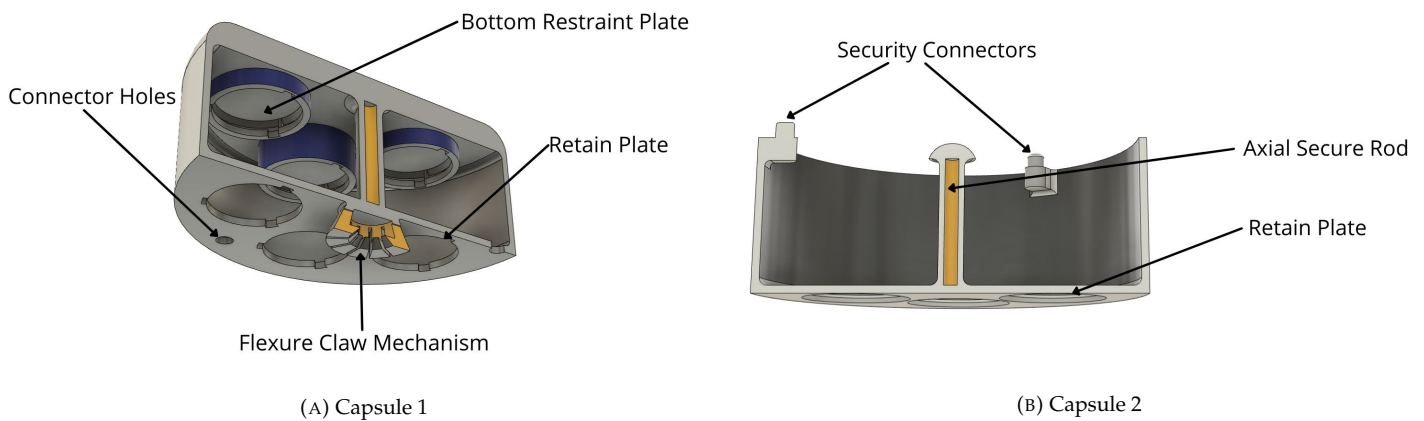


FIGURE 4.31: Cross-Sections of the Orbiting Sample Capsules

4.5.2 Top/Bottom Restraint Mechanism

When inserted, the sample tubes must be retained and secured tightly to prevent them from falling or being loose enough to compromise the stability of the whole OS, however, the retain mechanism must be reversible in case a change in samples is needed or desired. To achieve this, the sample tubes have 3 bumps that will be inserted in a specific direction at the restraint mechanism and then be rotated 120° such that the bumps are locked in place.

4.5.3 Flexure Claw Mechanism

The OS will need a strong and permanent seal to keep the samples secure, when the second capsule is inserted in the first one, the fingers of the FCM will outward and slide around the tip of the capsule 2 axial rod and snap in place to the the notch on the rod.

TABLE 4.13: OS Mass When Fully Loaded

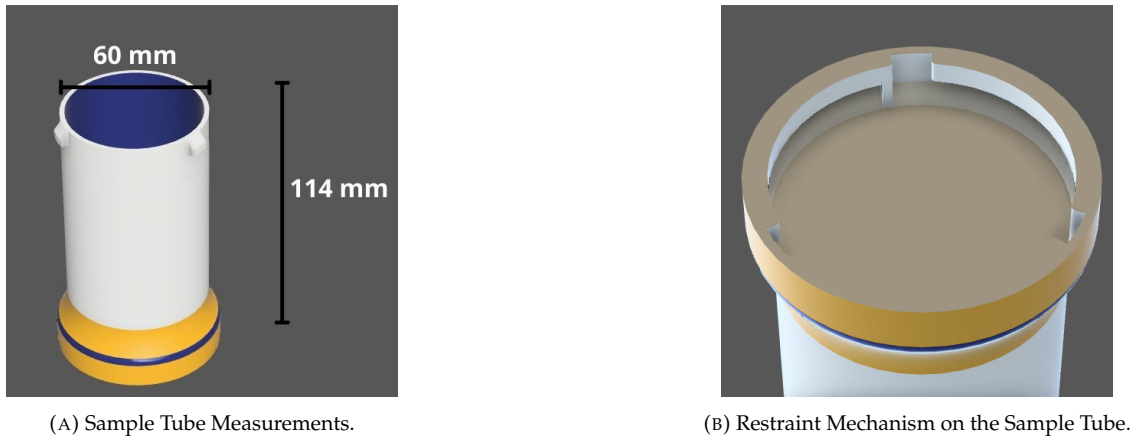
Sub-Assemblie	Materials	Volume [cm^3]	Main Density [g/cm^3]	Mass [g]
Capsule 1	Aluminum, Lithium	1,639	2.77	4,540
Capsule 2	Aluminum, Lithium	543	2.77	1,504
Low Cover	Aluminum, Lithium, Foam	1,148	2.77	3,180
12 Sample Tubes	Titanium	600	4.429	2,657
Samples	Ice	2,956	0.917	2,709
Total				14,590

4.5.4 OS Materials and Coatings

The OS structure needs to be as lightweight as possible to be within the additional mass capacity of the MAV and structurally capable of withstanding the loads in the return stage of the journey, specially in the mars ascent and the impacts of the earth entry. A mass analysis is detailed in Table 4.13. Aluminum-Lithium alloys have had an increased use in the aerospace industry for these specific properties [107], and can be used in most of the OS structure. As the OS is mostly hollow it achieves a fairly weight reduction and avoids heating due to thermal conduction of the metal. Another concern when it comes to the thermal integrity of the OS and thus the ice samples is irradiation, solar absorptance α and thermal emittance ϵ of the materials and coating layers are critical parameters in determining the OS temperature control. White coatings and films like Mylar are excellent candidates for this purpose, specially the former.

4.5.5 Tube Samples

Each tube inserted by the rover needs to be properly sealed to preserve the frozen state of the ice samples and the scientific integrity of the mission, avoiding that any contamination reaches the samples. As explained before, the Auto-Gopher-II drill will extract cylindrical samples with 5.6 cm in diameter and 10 cm in height. The goal is to bring back at least 2.5 kg of ice, and the OS will be able to carry 12 samples for a little over 2.7 kg, as the density of the ice on mars is $917 \text{ kg}/m^3$, same density as glacial ice on earth. The ice is extracted in its raw state, and then stored in a sample tube made of titanium Ti-6Al-4V, an alloy suited for protection against solar radiation and conductive heating due to its low thermal conductivity compared to other metal alloys. The sample tubes have the measures shown in Fig. 4.33a so the sample fits as perfectly as possible in the tube and the tube in the capsules, its top external surface is designed so it can be retained by a simple lock system explained above, the bottom restraint mechanism. The sample tube bottom has a design with the same geometry as the restraint plate of capsule 1 (see Fig. 4.33b), allowing another sample to be inserted and secured in it, reducing the space needed to store the 12 samples in a cylindrical shape.



(A) Sample Tube Measurements.

(B) Restraint Mechanism on the Sample Tube.

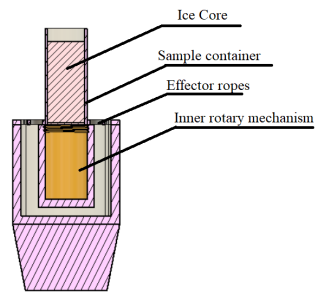
FIGURE 4.32: Sample Tubes

4.5.6 Sampling Operation Sequence: Drilling, Coring and Caching

1. The geophysical studies are done and the drilling site is selected.
2. The Auto-Gopher-II is positioned to begin the drilling procedure, which will extract 3 samples from different depths per site in four locations.
3. Once positioned, the bit starts a discreet drilling according to the operating specifications on the Auto-Gopher-II and extracting the cores from the ground, each one that won't be stored is going to be left around near the rover by the arm.
4. When a depth of 40 cm is reached, the first sample is obtained and the caching procedure is in place, and repeats at 3.2 m and 6 m. The coring speed is 80 cm/h and its non-coring speed is 190 cm/h, so the samples will be obtained at 40 minutes, 221 minutes (3.68 h) and 398 minutes (6.63 h), respectively.
5. When a core is extracted from one of the depths determined for storage in the OS, the robotic arm picks up one of the tubes and positions it directly below the drill bit so when the sample is released, the tube encapsulates it as shown in Fig. 4.33.
6. While the drill continues its operations for the next samples the rover does a brief analysis and registers a visual status of the sample with the spectrometer and HazCam on-board.
7. The rover arm identifies one empty slot in the first capsule of the OS and inserts the tube with the sample into the capsule. Thanks to the rotational properties of the rover arm it can be completely secured. To avoid any interference between the tubes and the robotic arm, the tubes are inserted first in the three upper retainers distributed in a triangular pattern, then does the same with the lower ones for the subsequent three samples.



(A) Rover Arm Receiving the Ice-Core.



(B) Cross-Section.

FIGURE 4.33: Transfer of the Ice-Core to the Sample Tubes.

8. Once the first six slots are occupied, the robotic arm loads the second capsule underneath and repeats the process until the 12 samples are secured in place, then seals the OS with the lower cover to later be transfer to the MAV. In Fig. 4.34 is a detailed sequence of the main caching steps.



(A) First three sample tubes loaded.



(B) The next three tubes.



(C) Capsule 2 loaded.



(D) Tubes in capsule 2.

FIGURE 4.34: Caching Sequence.

Transfer of the OS to the MAV

With the capsule sealed and fully loaded, the transfer of the OS to the MAV is a straightforward process, the arm is able to grab the entire capsule (see Fig. 4.35) and fixate it on the MAV nose cone inside.

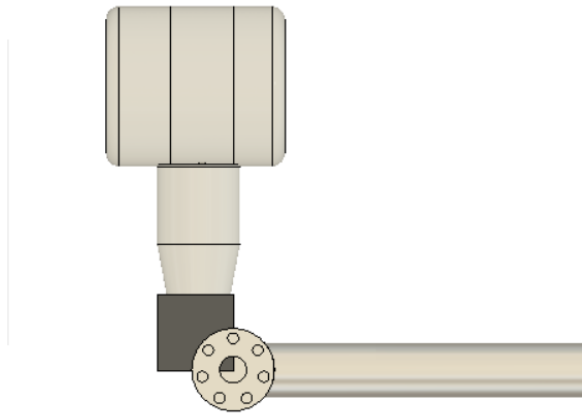


FIGURE 4.35: Rover Arm holding the OS.

4.5.7 OS Thermal Loads

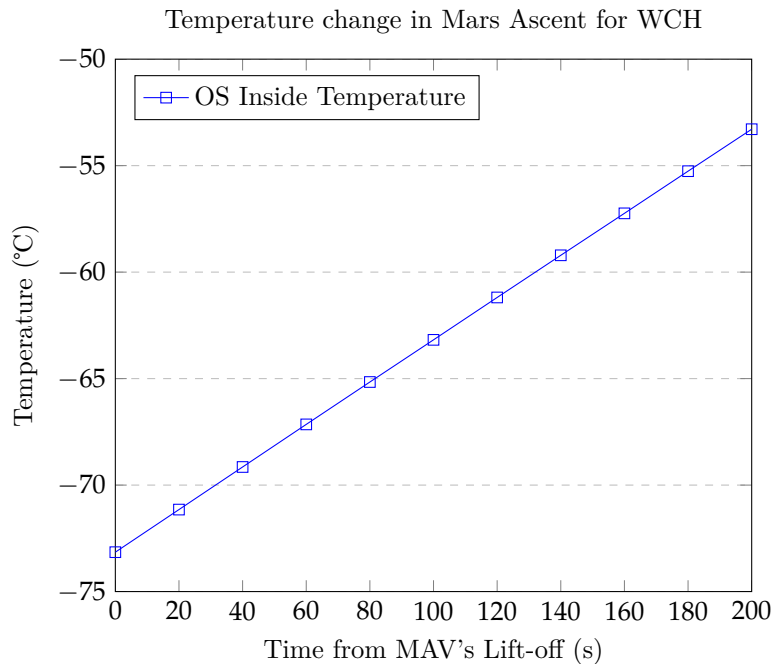
Atmospheric Conditions while on Mars Surface

The capsule will have to withstand many thermal phases with different temperatures and it needs to preserve the frozen state of the ice samples in every one of them. As the environment temperatures fluctuate between $-97.7\text{ }^{\circ}\text{C}$ and $-19.6\text{ }^{\circ}\text{C}$ and the atmospheric pressure between 724 Pa and 860 Pa [108], the samples are able to keep their frozen state, in addition the OS will be kept underneath the rover vehicle serving as a protection to direct solar radiation and its white coating will prevent almost any increase in the OS temperature due to surface albedo.

Aero-heating in the Mars Ascent

Even though the CO_2 atmosphere is very thin, the high speeds encountered during ascent would cause significant aero-thermal heating, the MAV nose cone would have a door-based opening that would allow the OS to be ejected from it and needs to have a TPS to guarantee that the OS will be thermally insulated in this critical stage. Many methods have been studied to achieve this goal, however, picking the right one is a challenging task due to the few tested options available. Polyethylene foams, film coatings and layers of aerogel have been taken into consideration, the latter being the more reliable, specially silica aerogels which present an extremely low thermal conductivity of 23.27 mW/mK [109]. As the MAV will have a solid booster, its peak flux reaches 15 W/cm^2 [110] and the WCH solar irradiation is 720 W/m^2 . Considering these values as constant to study the worst case scenario and a thickness of 3 cm for the TPS, numerical simulations show that the increase of the internal temperature (see graph below) of the OS in the an ascent time of 200 seconds is almost $20\text{ }^{\circ}\text{C}$

in the WCH, so ideally the MAV will ascent when one of the lowest atmospheric temperatures are detected by the ATS in the rover.



Orbiting Mars, Orbiter-OS Rendezvous and Journey to Earth

Once the OS is ejected from the MAV nose cone it will orbit Mars until its rendezvous with the orbiter and the EEV, the capsule will be only exposed to direct solar irradiation and it depends on the beta angle of the orbit, the altitude, and the Mars-solar distance, it fluctuates between 720 W/m^2 for the WCH and 495 W/m^2 for the WCC, only the WCH, that may put the samples at risk was considered in the analysis in which it was found that the capsule will not exceed $-20 \text{ }^\circ\text{C}$ in fact, it will gradually lose temperature due to radiative cooling, if it's desired to avoid losing too much temperature having a “zebra-stripe” of two different coatings would allow to establish a more desirable $\frac{\alpha}{\epsilon}$ ratio, for example 80% white and 20% gold. Given the recent developments in white coatings such as the synthesized Zn-MCM-41 pigment, this seems the best candidate to coat the OS, it's low solar absorption (0.154) and high thermal emittance (0.914) [111] make this coating perfect for the conditions in Mars orbit, this coating, being highly reflective in the solar spectrum, will avoid the need to implement a beacon for RF tracking, and instead facilitate detection of the capsule via optical tracking only, the minimum estimated reflectivity for this coating configuration is close to 1, which is safely above the requirement of 0.37 [106]. When detected and caught by the orbiter, is stored safely to return to earth.

Earth Entry

This is the most critical step concerning the samples integrity, the external temperature rises by orders of magnitude so special consideration were taken in mind and are better explained with the design of the Earth Entry Vehicle which holds

the OS inside.

4.6 Mass and Costs Budget

The following budget is already estimated on FY2020 M USD

TABLE 4.14: Rover Cost and Mass Budget

System	Component	Mass [kg]	Mass Margin %	Total Mass [kg]	Total Cost [M USD]
Power	MMRTG	45	0%	45	26.62
	Batteries	26.5	10%	29.15	2.36
Thermal Control	MPFL	15	0%	15	0.27
Navigation and Guidance	2 NavCam	0.44	10%	0.484	1.62
	6 HazCam	1.47	10%	1.35	1.78
Avionics	IMU LN-200S	1.5	10%	0.82	48.33
	RAD 750	2.4	10%	2.64	
	ROM Memory	6.8	0%	6.8	
	RMCA	4.896	20%	6.12	
Communications	UHF Antenna	0.1	0%	0.1	0.07
	HGA	1.1	0%	1.1	0.91
	RLGA	0.775	0%	0.775	0.72
	X-Band Transponder	4	10%	4.4	10.58
	UHF Transceiver	3	10%	3.3	8.23
Geophysical Study	REMS	2.04	10%	2.24	15.22
	RIMFAX	3	10%	3.3	3.44
Sampling and Caching System	Drill	65	20%	78	34.26
	Conservation	14.5	10%	16	6.26
	End effector	8	10%	8.8	12.58
	ARM	67	0%	67	7.68
Structure	Truss and Drill Structure	18	0%	18	10.72
	WEB Skin Plates	15	5%	15.75	
	Table	10	5%	10.5	
Rocker-Bogie	Wheels	14.94	0%	14.94	2.83
	Rocker	10.5	0%	10.5	
	Boogie	20.5	0%	20.5	
Secondary Mission	SHERLOC	4.72	5%	4.956	7.16
Total	-	366.181	-	387.525	201.64

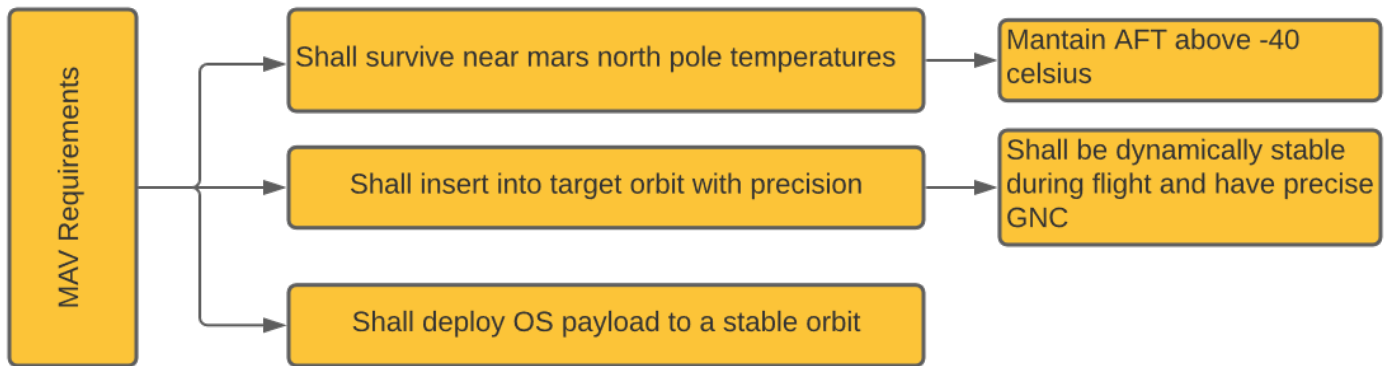


FIGURE 5.2: MAV Requirements.

5 Mars Ascent Vehicle

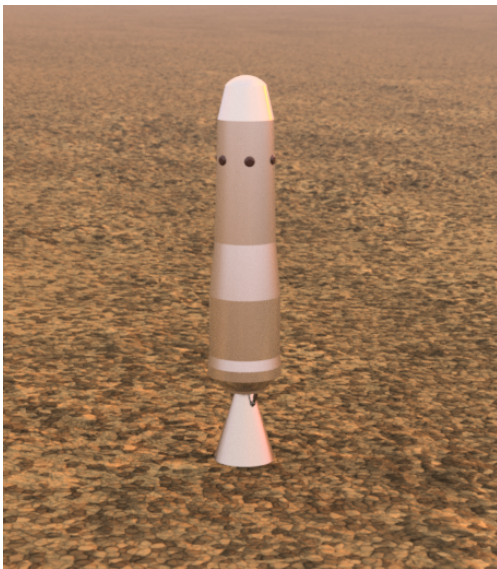


FIGURE 5.1: Haba Sulu Designed MAV at Mars Surface.

The Mars Ascent Vehicle (MAV), shown at Fig. 5.1 is a critical Mars Sample Return (MSR) mission element that is responsible for taking the samples off mars and getting them delivered into a Mars orbit for a rendezvous, where the Mars Earth Return Vehicle (MERV) will catch the Orbiting Sample (OS). However, no vehicle has ever taken off from mars carrying samples and hence it entails challenges to the design and opportunities for innovation.

The MAV selection was centered on the optimization of the motor and its propellant, Guidance, Navigation and Control (GNC), Reaction Control System (RCS), Thermal control systems (TCS) and MAV survival. Basing the decision on the mentioned design parameters, a 300 kg weight, 2.8 m height, two stage solid motor with incorporated Thrust Vectoring Control (TVC) and TPH 3062 (16% Al) propellant Mars Ascent Vehicle was selected.

The selected ascent vehicle is shown in Fig. 5.2.

5.1 Key Trades

Since the budget given for this mission is relatively low, cost optimization is paramount and thus, the main mission trade. On the other hand, considering that the MAV is so crucial to the success of the general mission, reliability and low complexity are fundamental therefore using technology that is simple and has been already demonstrated on similar environments

(flight heritage) are key to the success of the mission. Moreover, Allowable Flight Temperature (AFT) is a key trade given that the mars campaign will take place on near the north pole, making MAV survivability crucial. Another design parameter is mass. Going to mars is expensive from the standpoint of ΔV and every kilogram save is significant. Also, Gross Lift Off Mass (GLOM) is important. As a constraint, the rocket design must not exceed 400 kg.

5.2 MAV Options

Three main options were considered for the MAV, Single Stage To Orbit (SSTO) bi propellant liquid, SSTO hybrid motor and Two Stage To Orbit (TSTO) solid configuration.

5.2.1 Bi propellant Rocket

The bi propellant option, shown in Fig. 5.3 consists of a rocket with a fuel and liquid oxidant. Rockets of this type are very efficient since their specific impulse is the highest compared to hybrids and solids, and these are relatively well-known rockets. Another advantage is that they allow restartability. However, it is a complex vehicle, it takes up a lot of volume, making packaging inside aeroshell unpractical and its AFT is the lowest of the 3 options.

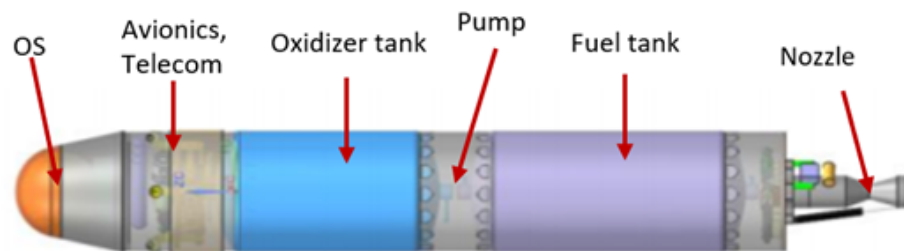


FIGURE 5.3: SSTO Bi Propellant CAD Model [112].

5.2.2 SSTO Hybrid Motor Rocket

SSTO hybrid configuration, show at Fig. 5.4 consists of a rocket with a hybrid motor, meaning that it has a liquid oxidizer and a solid fuel. Hybrid rockets are known to be more efficient than solids, but less efficient than liquids. Out of the three options, it shows several advantages. Its GLOM is the lowest of them as well as GLOM sensitivity [54]. hybrid configuration allows the best AFT value (estimate of $-72\text{ }^{\circ}\text{C}$) and allows restartability, making it more stable than the solid option. However, even though significant work has been done on this concept and technology maturity has grow, this option still has the lowest Technology Readiness Level (TRL, 5+) and considering the short time remaining for the launch of the rocket and hence short time for development and testing, there is not enough time for its full development and testing.

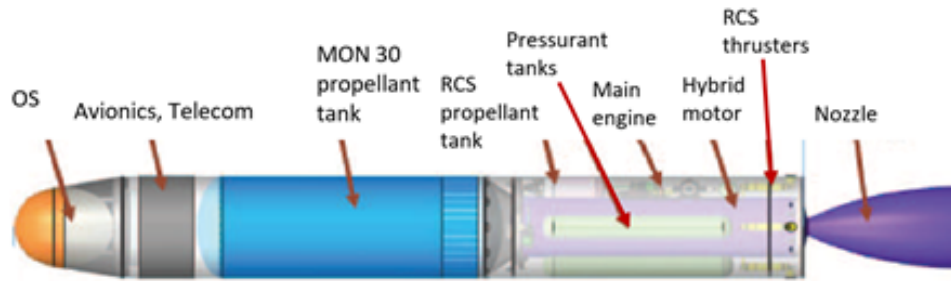


FIGURE 5.4: SSTO Hybrid Rocket Motor [113].

5.2.3 TSTO Solid Rocket

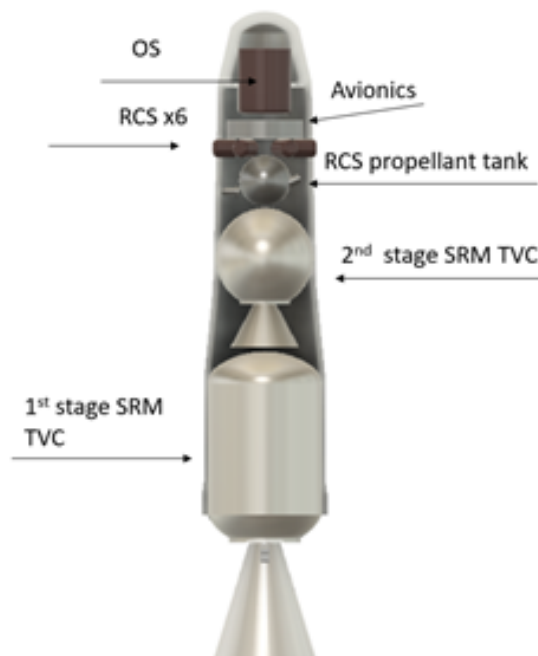


FIGURE 5.5: TSTO Solid Rocket Motor.

The TSTO solid rocket, shown in Fig. 5.5 is a two stage to orbit configuration. Considering that it is not restartable, it needs at least two stages. It also needs double avionics; it has the lowest I_{sp} (291 s) of all three options, and it is the most GLOM sensitive as well. It can potentially present stability problems on flight although adding TVC to its motors can solve this problem despite added mass. However, there is flight heritage of solid motor propulsion in Mars, it is a well-known technology, meaning it has the highest TRL (estimate of 8), it is the least complex option, it is very reliable, its AFT is acceptable (-58 °C) and it is also the least cost option.

5.2.4 MAV Selection

For the selection of the MAV configuration between the three options considered, as show at Table 5.1, and AHP study was made basing the choice on 6 key trades: GLOM, AFT, length, cost, TRL and time required for development and testing

TABLE 5.1: MAV Driver's Matrix.

	Secondary Drivers			Main Drivers		
	GLOM (kg)	AFT (K)	LENGTH (m)	COST (M USD)	TRL (1-10)	Development Time (Months)
Weight	0.083	0.251	0.054	0.161	0.260	0.191
SSTO Regular Bi Prop	285	-44	3.39	70	7	24
SSTO Pump Bi Prop	270	-44	3.21	72	7	24
Hybrid Motor	305	-72	2.89	90	5	60
Fixed Solid- Solid	317	-58	2.96	55	8	24
Solid-Solid	300	-58	2.8	55	8	24

Considering its flight heritage and relatively low complexity compared to the rest of options, the solid propulsion MAV concept is an appropriate risk reduction option. This concept allows a simpler design with significantly longer flight heritage and higher Technology Readiness Level (TRL). At the same time and as mentioned before it is mandatory that the MAV can survive the different stages of the mission, surviving the journey to Mars, the EDL and the stay on the red planet. Therefore, a ground-built propellant with a special coating has been chosen to allow the rocket to remain at -58°C without compromising its integrity. As result, the Solid -Solid configuration resulted the best option. The AHP selection process is show in the Table 5.2.

TABLE 5.2: MAV AHP Matrix.

Criteria/ Option	Cost	AFT	Reliability	Time	GLOM	Lenght	
Weight	0.161	0.251	0.260	0.191	0.083	0.054	AHP
SSTO Regular Bi Prop	0,137	0.052	0.109	0.138	0.155	0.031	0.104
SSTO Pump Bi Prop	0.137	0.052	0.135	0.129	0.303	0.075	0.124
Hybrid Motor	0.051	0.634	0.055	0.040	0,393	0.213	0.233
Fixed Solid- Solid	0.338	0.131	0.351	0.347	0.059	0.213	0.261
Solid-Solid	0,338	0.131	0.351	0.347	0.090	0.468	0.277

5.3 Fuel Selection

5.3.1 ISRU & ISPP Options

In the decision stage between liquid, hybrid or solid, ISRU and ISPP options were evaluated. However, the production plant needed for this concept added significant unviable landed mass and power requirements was beyond the possibilities. Its principles may be simple, but its implementation in space is difficult and has never been done and, in the end, the decision made was to use ground built solid propulsion motors, which eliminated the possibility of using ISRU and ISPP.

5.3.2 Solid Propellant

For the design of the propellant that will be brought to Mars from the ground (storable propellant), two main parameters were considered, its AFT and the time that it can be stored on Mars without compromising its integrity. An extensive literary review was carried out and it was found that the best option for the MAV is to use TP-H-3062 (16% Al) propellant, TP-H-3062 has extensive flight heritage. Particularly on Mars Pathfinder. SRMs used during Pathfinder's EDL phase used TP-H-3062 that successfully fired after 7 months in hard vacuum on the outbound trip to Mars [114].

5.4 Motor Design

For the motor design, an extensive literature review was made, and it was found that Northrop Grumman STAR motors fit with the concept of the mission and the conceived MAV constraints such as height and diameter, in particular, STAR 17 motor for the first stage and STAR 13B and thus, MAV motor design will be based on these two motors [115]. Technical specifications are shown in Table 5.4.

STAR 13B



FIGURE 5.6: STAR 13B. First Stage Solid Rocket Motor.

STAR 17



FIGURE 5.7: STAR 17. Second Stage Solid Rocket Motor.

Solid rocket motors also generally burn in very short durations at very high thrust levels, as with the case of selected STAR 17. Design work for a first stage solid based on a STAR 15 motor with an action time of 17 seconds showed that at the time of first stage burnout, the vehicle was in Mach 5 and 10 km in altitude, with substantial atmosphere remaining to coast through [116]. During the primary burn the Thrust Vector Control (TVC) provided enough control to maintain the

TABLE 5.4: Star 13B and Star 17 Specifications.

Star 13B		Star 17	
Motor diameter (cm)	34.29	Motor diameter (cm)	44.196
Motor length (cm)	63.78	Motor length (cm)	68.73
Effective specific impulse (s)	291.0	Effective specific impulse (s)	291.0
Burn time average thrust (N)	7597	Burn time average thrust (N)	10942.63
Maximum thrust [N]	9610	Maximum thrust (N)	12343.81
Weight (kg)		Weight (kg)	
Total located	47	Total located	155
Propellant	40	Propellant	145
Temperature limits		Temperature limits	
Operation	-20 °C	Operation	-20°C
Storage	-58°C	Storage	-58°C

vehicle's attitude. However, at MECO, the vehicle was at maximum dynamic pressure and was not dynamically stable. It would start to tumble, presenting undesirable conditions for flight. With the goal of lowering dynamic pressure at MECO, the solution found was to reduce the thrust of the motor and increase its burning time. For solid rocket motor, this can be achieved by switching the original design core burner to an end burner. Consequently, STAR 17 first stage motor core burner was changed to an end burner, achieving 45 seconds of burning time.

5.5 MAV Guidance, Navigation and Control

Mission design and vehicle constraints emphasize the need for a vehicle with high propulsive efficiency and stable, highly accurate guidance, navigation, and control systems. Successful retrieval of ice core samples from orbit around Mars depends substantially on the accuracy of the MAV orbital insertion [114, 117]. The MAV must be capable of delivering the payload to the target orbit despite the variety of unpredictable conditions. These conditions can be variations in launch azimuth or elevation, atmospheric dust or wind conditions, solid rocket motor total impulse delivered, IMU orientation error, thrust misalignments, etc. Given the high precision required for inserting the OS into a stable orbit, it is important to mitigate all uncertainties and variables that can significantly deviate the MAV from the optimal path. To achieve this, the first stage solid motor vehicle guidance employs open-loop guidance in which the MAV performs a series of roll, pitch, and yaw angles from a pre-loaded lookup table as a function of vehicle altitude [118]. Second stage guidance for the solid motor vehicle employs SXS (Simple Cross-product Steering), similar to the used in [118]. This closed-loop guidance (CLG) algorithm is based in cross-product steering (CPS) [119]. As described in [114], the algorithm is designed to target a desired semi-major

axis and orbital plane, functioning without any inherent knowledge of motor performance. The output of SXS is a V_{go} vector, which is the difference between the current vehicle's inertial velocity vector as estimated by navigation, and the inertial velocity vector calculated to achieve the semi-major axis and orbital plane of the guidance target. The simplicity of this algorithm allows it to function in a wide variety of off-nominal vehicle parameters. This condition is desirable considering the different conditions that can vary and the uncertainties that can be found on Mars regarding parameters for launch such as azimuth angle and surface inclination. Neither open-loop or SXS can manage excess energy in the solid motor vehicle. That task will be performed by energy management maneuver. Furthermore, it was found that initial attitude and position errors contributed significantly to imprecision in the trajectory [118]. For this, the mission lander avionics will act as an external system assistant and give initial state knowledge to the MAV. To achieve the requirements lower-grade IMU must be used for inertial navigation. There were various options for the selection of the IMU such as LN200S, HG 5700, HG 1930, MQ and HQ. Trade off was focused on accuracy/ weight ratio. It was found that the NG9900 by Honeywell Aerospace yielded the best trade [117]. Finally, a study that performed monte carlo analysis with 2000 individual simulations for orbit insertion precision show that using the selected IMU, the MAV reached target orbit 99.5% of the times [120].

5.5.1 Trajectory and Orbits

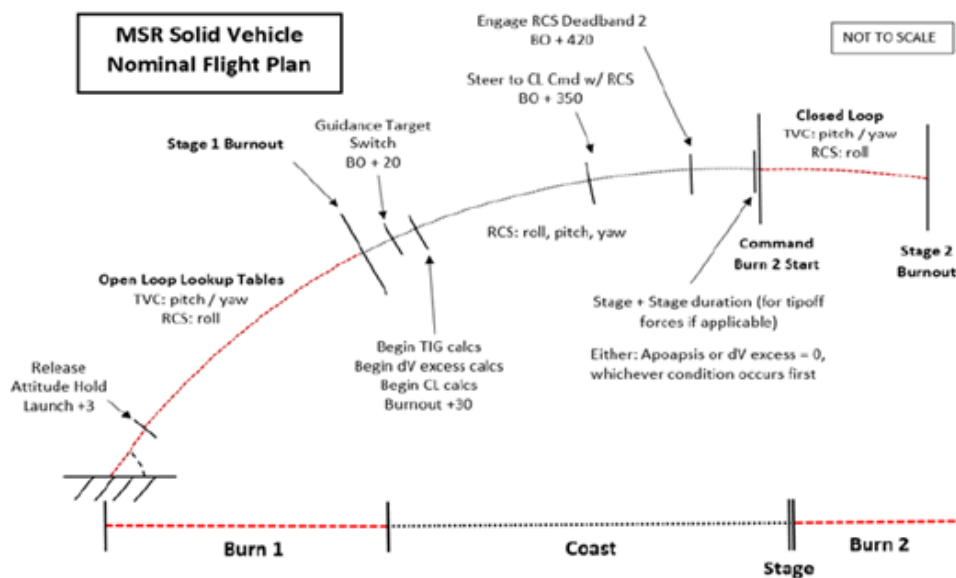


FIGURE 5.8: MSR Solid Vehicle Nominal Flight.

The selected trajectory for the two-stage solid MAV concept consists of two burns separated by a long coast, as shown in Fig. 5.8. The first stage puts the vehicle into an elliptical orbit with an apoapsis at the desired altitude of the circular orbit, but with a negative periapsis (below the surface of Mars). Once the vehicle has coasted up to nearly apogee, the second stage will fire to circularize the orbit.

It was found that increasing the altitude for the orbital insertion would increase the mass of the MAV by 0.102 kg/km or 5.1 kg per 50 km of circular orbit altitude and would reduce the mass of the orbiter by just 0.166 kg/km or 8.3 kg per 50 km. Even though the MAV mass being less mass sensitive to altitude, MERV orbit was set at 310 km and therefore this trade drove the desired insertion orbit to occur as low as possible. The lower orbit possible constrained by NASA is 300 km thus was chosen. The trajectory of Haba sulue MAV is shown in Fig. 5.9.

As mentioned, launch elevation and azimuth orientation are also important for GLOM. The greatest impact to GLOM is the launch site orientation for a TSTO vehicle [121]. If azimuth could not be controlled within a small range around the optimal launch azimuth, large growth in GLOM could be expected for off azimuth cases unless a near vertical launch can be guaranteed. If the landing system can guarantee the launch azimuth to be within approximately 70 degrees of the optimal launch azimuth, 45 degrees launch elevation could be used while maintaining the current TSTO baseline mass. If azimuth restrictions are not possible, a launch elevation near 90 is necessary to minimize GLOM growth. Consequently, a simple orientation system was added to the lander to guarantee this optimal launch azimuth and maximize mass savings and thus general mission savings.

For the calculations of the orbit, MAV, GLOM and motor parameters, a tkinter interface using python was designed using the rocket equation. Mars drag model uses AtmosModeler Simulator [122], where the density and temperature is a function of altitude. The value of the rocket drag coefficient is also modeled as a function of velocity and height and includes free molecular space and assuming a regular rocket nose geometry.

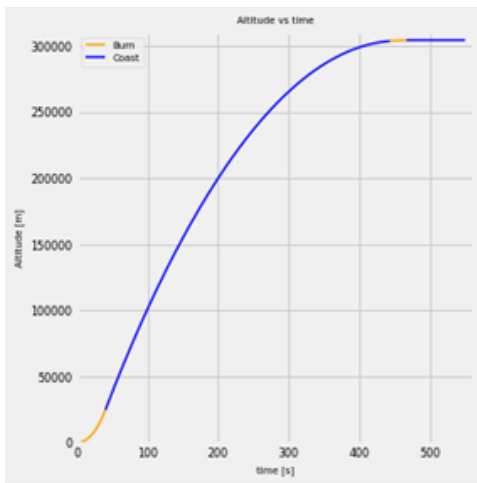


FIGURE 5.9: TSTO Solid Rocket Motor Trajectory Plot Using Designed Interface.

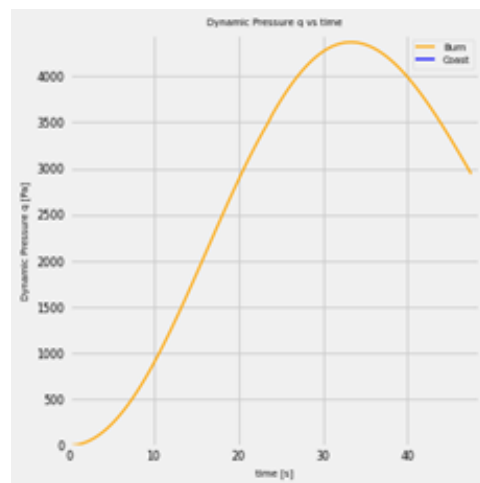


FIGURE 5.10: MAV Dynamic Pressure Plot.

From the circular orbit equation $\sqrt{\frac{GM_m}{R+h}}$ a proper 300 km circular orbit injection on mars needs 3,398.6 m/s. Several studies place ΔV requirements for orbit injection between 4,000 and 5,000 m/s using similar altitude orbits [117, 118, 119]. For MAV ΔV Budget estimation, gravity and drag losses must be considered. Despite mars atmosphere being significantly thinner than earth's, it is still a significant barrier for the rocket ascent and ΔV budget increase should be considered

around 10-15% ΔV [123]. Given the complexity of launch trajectory optimization, and analytical approach is carried out assuming that mars gravity is constant and the average angle at which the rocket travels is 22.5 degrees considering that it takes a 45 ° orientation before liftoff until it reaches 0 degrees for orbit injection. also, gravitational pull will act for approximately 475 seconds until it reaches target orbit. Considering this assumption, gravity losses can be estimated as:

$$\Delta V_{loss} = g \sin(\theta)475 \text{ s} \quad (5.1)$$

Finally, ΔV losses due to both drag and gravity are 1,007 m/s. with an estimated error of 20% and hence, estimated ΔV requirement is 4,607 m/s.

First stage trajectories are often a balance between high initial acceleration to overcome gravity losses and “throttling” back to limit maximum dynamic pressure (Max Q). The MAV ascent trajectory is no exception. Furthermore, the MAV must use the Attitude Control System (ACS) to maintain control after motor burnout. The dynamic pressure at motor burnout (Burnout Q) and its subsequent decay will drive the amount of ACS propellant required. Longer-burning motors are favored for the first stage to reduce burnout Q. To achieve this, core burner was switched to an end burner, as mentioned on the previous section. The design of the detailed motor will be discussed on the next pages.

Max Q resulted at about 4.5 kPa and around 3.5 kPa pressure at MECO. The end burner allowed switching from 17 seconds to expected 45 seconds burn time and this permitted solid rocket motor to be more stable during ascension.

From Fig5.11, a) it can be appreciated that ΔV demands are satisfied, reaching a value superior to $4700 \frac{m}{s}$ also, Fig.5.11, b) shows MAV acceleration vs time and Fig. 5.11, c) exhibits that most of the mass is lost shortly after MECO, representing approximately 55% of mass loss.

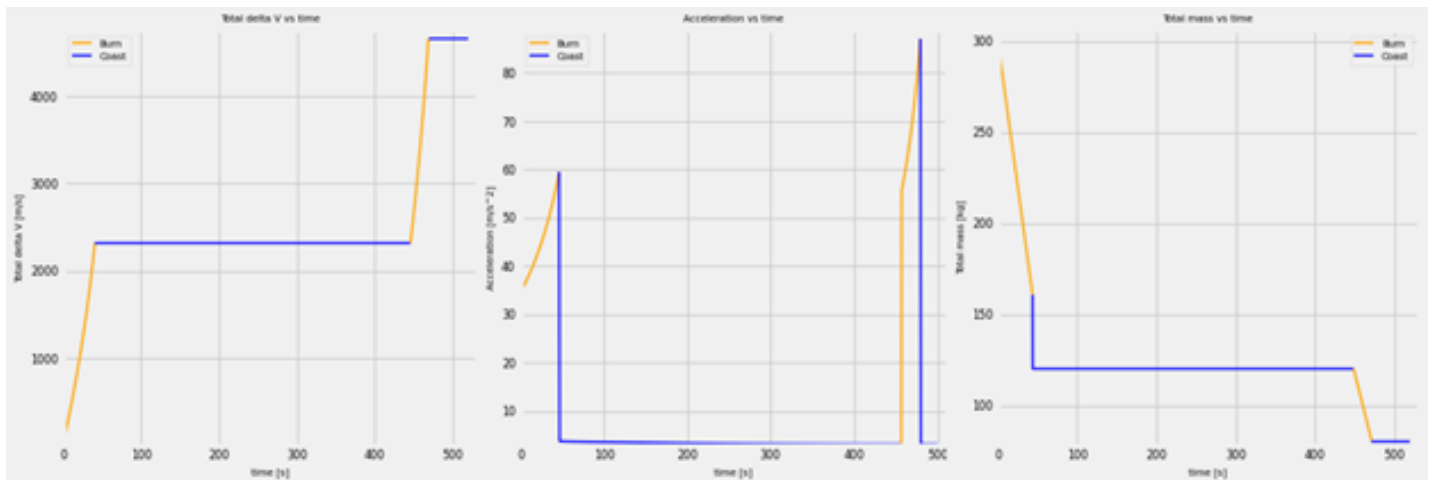


FIGURE 5.11: a) ΔV vs Time b) Acceleration vs Time c) Total Mass vs Time

5.5.2 MAV Avionics

Avionics responsible for three primary functions: Command and Data Handling (CDH), communication, and power. CDH carried out by flight computer and IMU. Communications managed by transceiver, antenna, and navigational beacon. Power managed by batteries, power distribution board, and cabling.

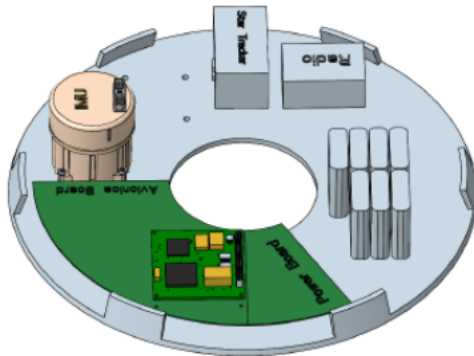


FIGURE 5.12: MAV avionics [124].

MAV system reliability is fundamental to the overall mission, but there are factors that impact redundancy such as volume and MAV mass. Consequently, the MAV baseline design chosen implements a dual-string approach for all hardware that is critical to achieving the required Mars orbit. The UHF system, only required for telemetry during ascent, was selected to be single string. This is justified due to the short operational mission duration (less than 24 hours) and flight proven reliability of the UHF system. The selected system design optimizes mass, cost and reliability.

The MAV baseline design chosen implements a dual-string approach for all hardware that is critical to achieving the required Mars orbit. The UHF system, only required for telemetry during ascent, was selected to be single string. The approach is justified due to the short operational mission duration (less than 24 hours) and flight proven reliability of the UHF system. The selected system design, show at Fig. 5.12 optimizes mass, cost, and reliability.

TABLE 5.5: MAV Avionics.

Single	Dual
UHF antenna	Flight Computer
Electra-lite Radio	Power Electronics
Telemetry Encoder	Batteries - IMU

5.5.3 Attitude Control and System Design

MAV chosen design show in Fig. 5.13 will provide roll control during motor burns and full control during coast. Thrust Vector Control (TVC) provides pitch and yaw control during (burns). Three options where considered. The systems evaluated were cold gas nitrogen, cold gas helium, and hydrazine monopropellant. The estimated system masses are tabulated below in Table 5.6.

As can be seen from 5.6, the hydrazine monopropellant system was not only the lightest of the three options but also the smallest of the three options. However, hydrazine needed to be above 2 °C AFT, and maintaining the MAV above this temperature would require a lot of power per day and this using hydrazine for RCS is non-feasible. Consequently, and based on this trade, the Nitrogen RCS option was selected given that it has lower total mass and occupies less space than the Helium option.

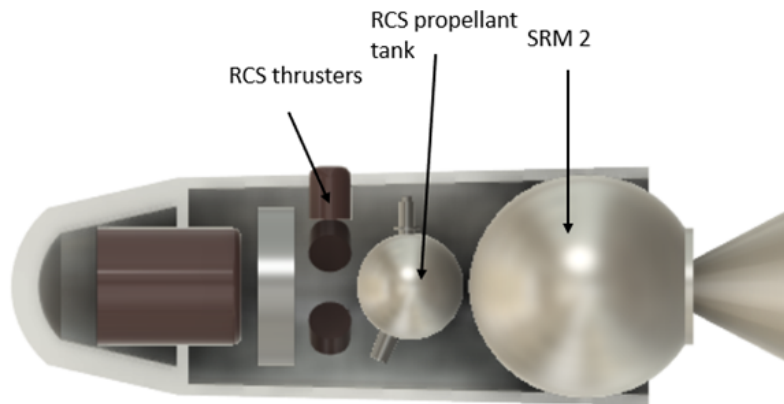


FIGURE 5.13: Second Stage RCS.

TABLE 5.6: RCS Comparison [114].

RCS System Comparison			
RCS Propellant	Nitrogen	Helium	Hydrazine
Propellant Mass [kg]	5.1	2.1	4.1
Dry Mass [kg]	10.8	27.1	5.4
Total Mass [kg]	15.9	29.2	9.4
BOL Tank Pressure [psia]	3,000	3,000	400
Tank Diameter[in]	13.3	19.1	10

5.6 MAV Systems

5.6.1 MAV Thermal Control System (TCS)

The MAV thermal control system design consists of passive and active elements onboard a system that covers the rocket called igloo.

The Igloo is a rounded square structure that surrounds the MAV and provides passive thermal control during the long duration surface stay. The MAV has an active TCS inside of the vehicle which consists of electrical heaters. They are both described in more detail below. The thermal system of the Igloo containment structure is designed to minimize heater power required for survival of the MAV systems during the worst case cold environmental conditions. The Igloo is an aluminum honeycomb structure that covers the MAV. The surface properties of the Igloo are designed to absorb heat from the sun during the day and minimize heat loss during the night. These surface properties will be achieved using a layer of aerogel covered with a high $\frac{\alpha}{\epsilon}$ ratio coating. Gold based coating was selected for this given that it has an $\frac{\alpha}{\epsilon}$ of 12.17, making it ideal for thermal control.

The selected Igloo shown in in the Fig. 5.14 makes use of the gas conduction between the Igloo and the MAV to serve as another insulating layer, taking advantage of the natural low thermal conductivity of the Mars atmosphere. As used in MSL class rovers and, in Rover-TO and OS canister for project Haba-Sulue as well. As in these cases, Mars atmosphere



FIGURE 5.14: MAV Stowed inside Igloo.

will be used as the gas filler.

A study was performed to investigate different ranges of propulsion system temperature of operation and it was found that increasing the temperature significantly increases power system mass [125]. Considering that the selected propellant can resist $-58\text{ }^{\circ}\text{C}$ to $-40\text{ }^{\circ}\text{C}$ lower limit was selected for the MAV design.

The TCS inside the igloo is employed to maintain a nonoperational temperature of $-40\text{ }^{\circ}\text{C}$ and raise igloo temperature to $-20\text{ }^{\circ}\text{C}$ for launch. The heaters will be used to maintain these AFTs and Platinum Resistance Thermometers (PRTs) to monitor the temperature and provide feedback to the lander. Different heater sizes and shapes are required to accommodate various components such as tanks and avionics. Most heater options are commercial off-the-shelf technology. The Fig. 5.15 below show the types of heaters PRTs that will be used in this application.



FIGURE 5.15: Heaters and Thermometers for Thermal Control Inside Igloo [126].

5.6.2 Mass, Power and Cost Budget

Table 5.7 shows the Mass and Power budget of MAV. Additionally, using PCEC, MAV estimation cost is set to be 52 M USD with a contingency of 10% [54, 127].

TABLE 5.7: RCS Comparisons

System Element	Mass (kg)	Average Power (W)
Structure and Mechanisms	30.00	-
Thermal Control	1.00	-
Propulsion Wet Mass	180.00	-
Propulsion Dry Mass	40.00	-
Attitude Control	5.50	4.40
Command & Data Handling	1.30	1.80
Telecommunications	3	40
Power	7.2	48.30
Cabling	2,1	-
Payload	15	-
System Contingency	7.8	-
Total	292.90	94.50

6 Earth Entry Vehicle (EEV)

6.1 System Overview

EEVs and Sample Return Capsules used in previous missions that aimed at the return of extraterrestrial samples such as NASA's Osiris Rex, Stardust mission, JAXA's Hayabusa and Kounotori missions were studied. The selected EEV design is a hybrid that takes from the Small reentry capsule concept in JAXA's Kounotori missions, the passive sample temperature control system with phase change material, and the concept that NASA has been developing mainly about the geometry and structure of EEVs for future MSR missions.

Regarding EEVs for sample return missions from Mars to Earth, NASA's Langley Research center has established a concept for EDL of a single-stage, stable and passive protection of samples [128]. This implies vehicles with the least number of subsystems that can fail during reentry such as parachutes and RCS (Reaction Control systems). A Martian sample loss probability value on return to Earth has been established by NASA of 10^{-6} due to the risk of planetary contamination and its serious implications for life on Earth [128]. The requirement of extra high reliability for this type of mission led to an EEV design without a parachute or RCS. The deceleration and conservation of the sample will be achieved with the use of suitable materials that endure the aero-heating on reentry and an energy absorption material that withstand the impact of landing. The temperature control system will be used as a phase-change material based on the JAXA's design for the Kounotori missions.

6.2 Alternatives and Decision

Initially, three alternatives were studied for the EEV, the first one is direct reentry from Mars, the second alternative performs an intersection with the ISS for a posterior descent in any commercial capsule and the last alternative consists of performing an intersection as well with ISS, but in this case, a new capsule design need to be developed for earth entry from the ISS and ship it to the orbit before the capsule reach ISS.

The process followed for the valuation of the options is an AHP by matrices. Table 6.1 corresponds to the criteria matrix where the restrictions are established and is given a weight, and through a process of comparison between restrictions, a weighted value is assigned to them. A final assessment indicates that a direct reentry from Mars should be chosen.

TABLE 6.1: EEV criterion matrix

Alternatives	System Weight	ΔV [km/s]	Integrity	ΔT [K] (Heatshield -sample)	Landing precision	Reliability [%]	Development time	Cost [M USD]	-
Weight	0.08	0.1	0.16	0.13	0.05	0.1	0.14	0.24	AHP
Direct reentry from Mars	Launch mass = 390 kg, SRC = 40 kg	0	35(300K for vibrations)	3200	100 x15 km optimal conditions	9	2 years	0	0.51
ISS interception Landing with Soyuz/Orion capsule	Launch mass = 800 kg, orion Capsule = 22700 kg, Soyuz = 7000 kg. Sample Capsule: 30 kg	7.3	5	2200	8 - 10 km	4	3-6 months	18.9	0.32
ISS interception - Landing with unmanned mission sent to ISS from Earth.3 step mission	Launch mass = 800 kg, Sample capsule = 10 kg, SRC = 40 kg	7.3	5	2173	20 km radii aprox	2	3 years	19.7	0.17

6.3 TPS and EEV Geometry

The Thermal Protection System (TPS) and geometry for the EEV were chosen based on designs developed at NASA's Langley Research center in partnership with In-Space Propulsion Technology (ISPT) and NASA Ames since 2007 [129]. The selected external geometry of the EEV is a 60° cone with a hemispherical tip on the front body and a slightly concave surface on the rear of the body. The location of the center of gravity of this geometry allows passive attitude control therefore it can maintain a stable trajectory and it can do deviation corrections in the nominal attitude without the need for Reaction Control Systems (RCS) [129].

Considering conductivity,ablative properties and flight heritage, the EEV's external material selection was carried out and is shown 6.3. These types of materials have achieved low conductivity coefficients up to $0.05 Wm^{-1}K^{-1}$ for low pressures of around 0.1 kPa (expected in high areas of the atmosphere) and for temperature differences of up to 1,000 K [130].

In Fig. 6.1a the distribution of the main components of the EEV and its materials are shown. Fig. 6.1b exhibits EEV inside the Earth Return Module (ERM) which is the module that houses the EEV protecting it from the radiation of the sun and mars in the interplanetary transition, with the sample on board from the Martian orbit to the point of ejection of the EEV that enters the Earth.

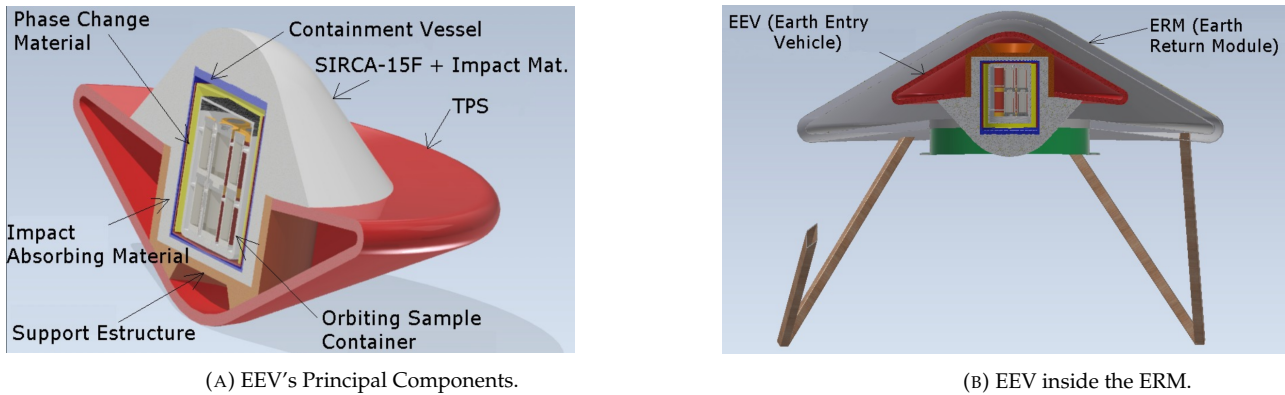


FIGURE 6.1: EEV configuration.

The dimensions of the EEV were established in a process from the inside out, the container of the ice samples after an analysis process from the sample collection area acquired a cylindrical shape with a diameter of 250 mm and a height of 300 mm. based on this sizes, the passive thermal control system was designed first and then the internal and external geometries of the EEV. Fig. 6.2 shows the overall dimensions of the EEV.

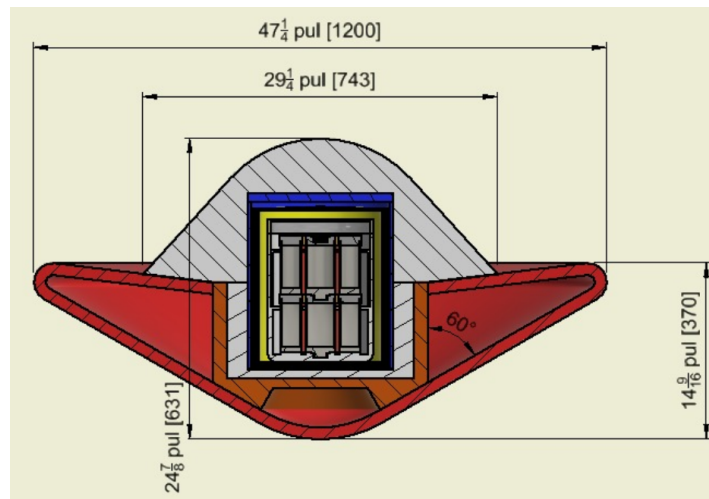


FIGURE 6.2: EEV's General Dimensions

6.4 Temperature Passive Control and External Thermal Performance

The CV is assembled with the OS inside the EEV and then the rear of the EEV's TPS is secured. It is necessary to maintain the CV with the OS attached to the transfer mechanism as it will have an active cooling system that, through a heat transfer surface, will keep the CV and OS below 0 °C in this way the phase change system will only be required during the reentry phase.

To determine the temperature peak, a comparison was made with the theoretical and experimental data of maximum temperature and/or heat flux in the ground entry vehicles of similar missions. On the Stardust and Osiris Rex missions the TPS was designed to remove over 99% of the vehicle's kinetic energy [131].

The passive thermal protection system chosen is based on the protection design developed by JAXA in its Kounotori missions (verified in 2018 [132]) because it is the only mission that has returned samples from outside the planet in which the restriction regarding the sample temperature was close to 0°C and the main restriction was to maintain protein samples from the ISS to the ground at a temperature of $4\text{ °C} \pm 2\text{ °C}$ [133]. The system consists of different multi-layer cylindrical containers called vacuum insulation packs (VIP) that cover the OS container. Between the OS container and the VIPs a phase change material is included. Heavy water with additives that allow the fusion temperature to be designed so that the latent heat used in the phase change process it is not transferred to the sample and keep it always below 0 °C. The containers of the thermal system for phase change material are made of Stainless Steel due to the need for structural resistance considering its low cost and that they will be subjected to structural loads on vacuum. CV is made of Aluminum 7075 due to its good mechanical resistance and low weight. Finally, the energy absorbing material is a graphite and Kevlar mesh honeycomb with carbon foam filling the voids, designed so that most of the impact energy is absorbed by it.

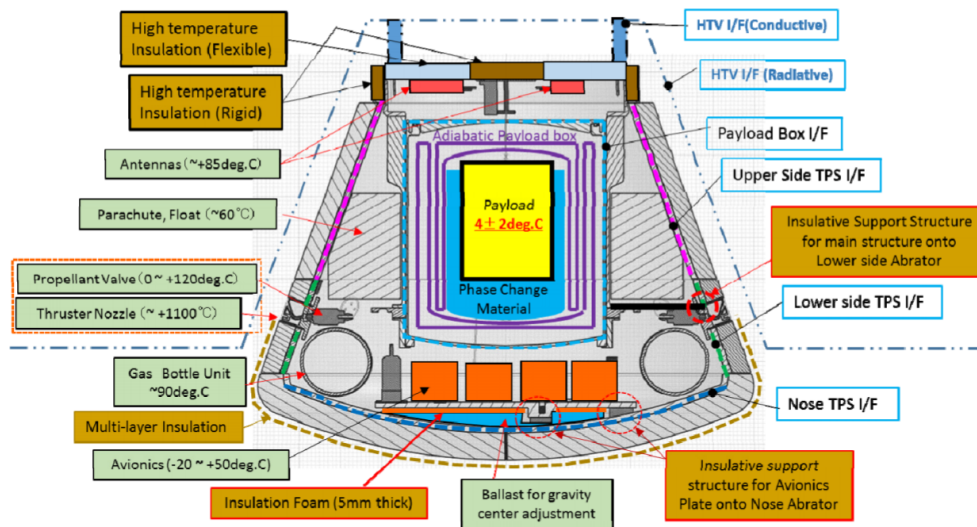


FIGURE 6.3: Thermal Design of HSRC from JAXA [133]

Figure 6.3 shows the thermal design developed by JAXA, the Haba-Sulue mission EEV design shown in Fig. 6.2 does not include RCS and parachutes and the ablative material on the top does not follow a continuous conical line from the front part but cover the rear concave surface and the exposed cylindrical part of the CV. Regarding the change of external geometry of the TPS, the tendency to change for a concave rear body for new EEVs instead of the conical one used in all the previous missions is mainly due to the better behavior in the convective Flux due to the aero-heating of the entry, these can be seen in Fig. 6.4 and Fig. 6.5a where it is seen that for the new designs reductions in convective heat of around 20%

can be achieved using the new proposed geometry [134].

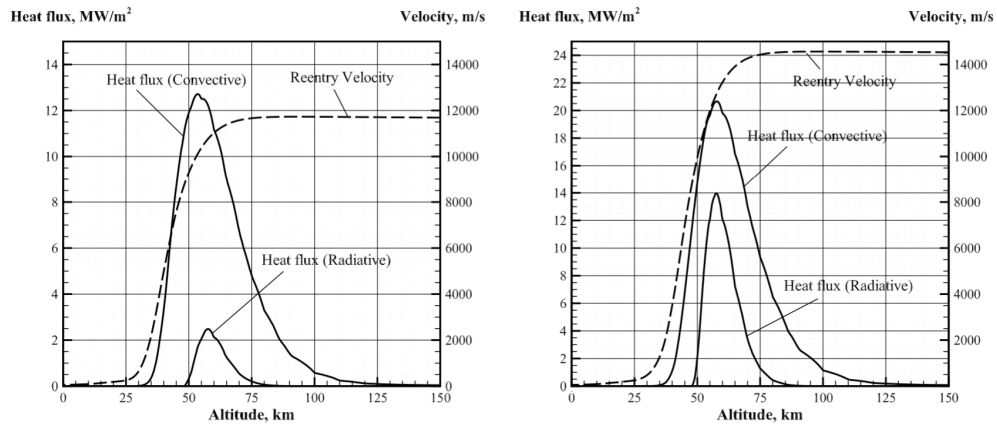
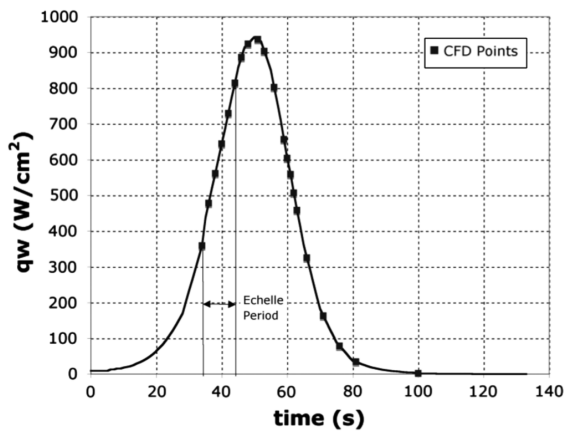


FIGURE 6.4: Heat Flux, no Rigid Flares and Rigid Flares

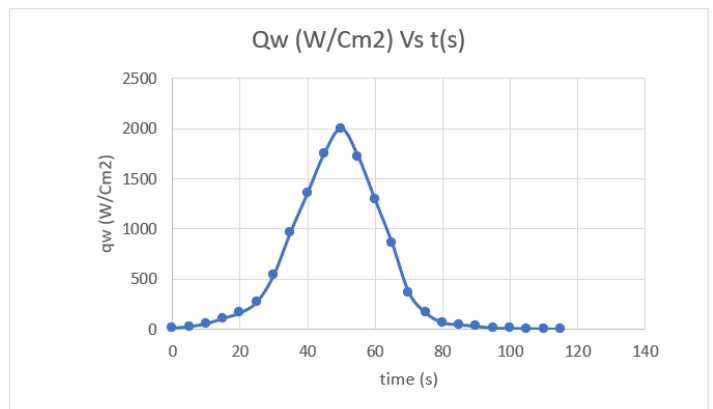
6.5 Heat Transfer Calculations

To estimate whether the ice core samples would survive reentry without melting, heat transfer calculations were performed. Total heat transfer energy balance in which the PICA stage is heated by the already known aero-thermal re-entry phenomena. The method considers the radiation heat emitted by the capsule and the conduction heat that enters and thus evaluates it towards the inner layers up to the ice core samples.

Initially, extrapolation of the thermal flux versus time curve from a CFD performed on the Sample Return Capsule reentry of Stardust [132] was made (See Fig. 6.5a). Fig. 6.5 shows the extrapolated curve for the Haba-Sulue Mission. A in 20 MW/m^2 as shown in Fig. 6.4.



(A) Stardust [132]



(B) Haba-Sulue

FIGURE 6.5: Heat Flux vs Time

Energy balance in the PICA outer layer of the TPS follows the relation $Q_{net} = Q_{in} - Q_{out}$, which derives in the equation $mC_p\Delta T = (QA\alpha - \epsilon\sigma AT^4)\Delta T$ where m is PICA outer layer mass, C_p is calorific capacity, ΔT is change in the PICA outer layer temperature, Q is heat flux extrapolated from stardust simulations, A is outer TPS superficial area, α is material absorptivity coefficient, ϵ is PICA emissivity coefficient, σ is Stephan Boltzmann constant, T is temperature at every iteration and Δt is the time interval for every iteration.

From Fig. 6.5, the heat flux acts for approximately 115 seconds, after this time heat flux is almost 0 and therefore, the calculations only took place on this time span. Consequently, taking the change in temperature every iteration, heat transfer calculation due to conduction was carried out from TPS to the ice core samples with the expression:

$$T_2 = \frac{QA\alpha - \epsilon\sigma AT^4}{mC_p} + T_1 \quad (6.1)$$

Taking temperature from the past material as T_1 , the temperature of the next material was calculated and so on until ice cores samples were reached. In next section, graphs generated from this method are shown.

6.6 Results

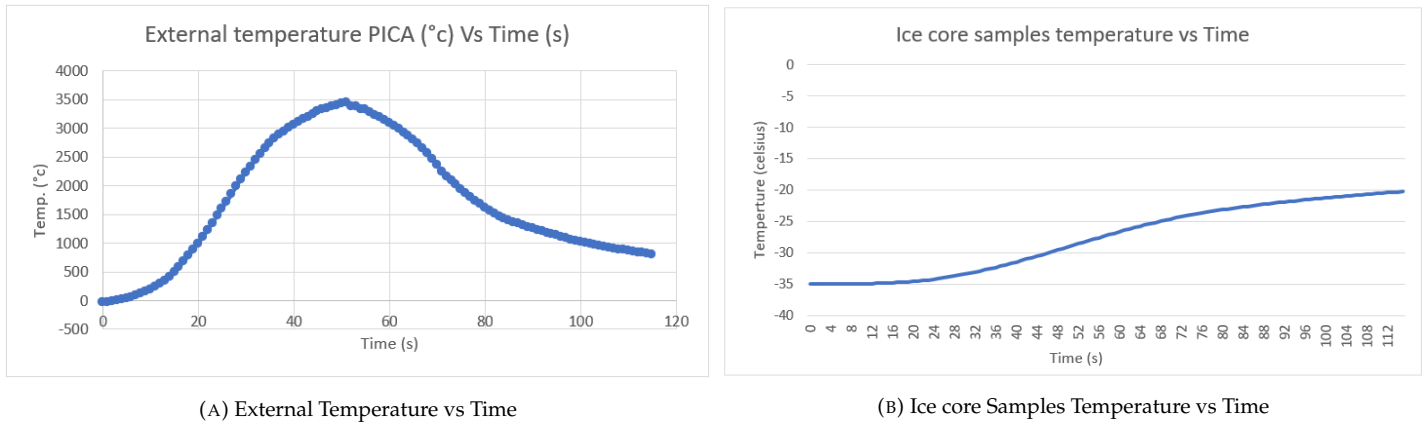


FIGURE 6.6: Temperature vs time

From the results seen on Fig 6.6a and Fig 6.6b, even though we assumed two times the heat flux from the highest re-entry capsule thermal flux in history, evaluating heat transfer on ice cores samples with the presented method shows that the samples temperature only varies from $-35\text{ }^{\circ}\text{C}$ to approximately $-20\text{ }^{\circ}\text{C}$. Therefore, ice core samples survive on earth reentry.

Table 6.2 shows a compilation of information related to the thermal performance of the Haba-Sulue mission compared to similar missions already completed or in development. It is worth mentioning that all missions used parachutes as a

TABLE 6.2: Parameters related to thermal performance with other missions that used the parachute as a reentry system.

Mission	Max. temp reentry (K)	Front diameter (m)	Vehicle mass (kg)	Reentry angle (deg)	Heat shield material
Stardust	3,500 [132]	0.81	45.7 [135]	-8.2	PICA, Phenolic Carbon
Hayabusa	3,200 [136]	0.4	16.5	0	-
OSIRIS-REx	N.D.	0.81 [137]	46 [138]	-8.2 [131]	PICA, Phenolic Carbon [131]
Kounotori (Small reentry capsule)	2,100 [133]	0.84	N.D.	N.D.	Light weight ablator [133]
Haba - Sulue	3,200	1.2	68.5	-10	PICA, Multilayer carbon based

deceleration system, in contrast to Haba-Sulue, which did not incorporate this reentry method. Additionally, Table 6.3 lists the materials selected for the EEV components and their total weight.

In Table 6.4 the estimated materials and weights of the ERM (Earth Return Module) are listed where the EEV will be installed with the sample from the orbit of Mars to approximately 40,000 km near Earth.

6.7 EEV systems and components

Regarding EEV's avionics, considering that activation and control of subsystems such as RCS or parachutes are not required, the avionics of the EEV consists only of a small lithium battery that powers two antennas, one for Iridium and another for GPS (1 W), an On-Board Computer (10 W, 14 W Diss) and an LN-200S IMU (12 W), as the one used by the Rover.

7 Mission Analysis

7.1 Mission overall cost

The costs of the mission were estimated by CER parametric models. The tool used to accomplish this was NASA's PCEC software [139], creating, in accordance to SMAD, a workbench for the systems[39], trying to price each component, and

TABLE 6.3: EEV's components material and weight

Description	Material	Thickness (mm)	Density (kg/m ³)	Weight (kg)	Thermal conductivity (W/m)
OS	Aluminum 2195 (container)	5	1,800	15	130 [128]
PCM	Heavy water (D2O)	25	1,000	3.77	0.6
Vessel 2 PCM	Stainless steel AISI 304 [129]	3	8,000	8.3	16.3
Vessel 1 PCM	Stainless steel AISI 304 [129]	3	8,000	7.64	16.3
Energy absorb material	Honeycomb grpahic and Kevlar web, ~Carbon Foam volds [130]	44	75 [136]	1.84	5
CV	Aluminum 7075	5	2,810	8.54	130
Inner structure	Carbon foam [130]	Variable	500	8	14
TPS	Front body: From inside to outside, 1st layer Carbon Fiver, 2nd~Layer Phenolic Carbon, 3rd Layer Carbon-Carbon Heat shield support structure, 4th layer Phenolic Impregnated carbon ablator (PICA-15). Afterbody protected by a low density ablator,~SIRCA~-15F (Silicon impregnated reusable ceramic ablator) [3]	25	280	15.4	0.1 [131]
Total EEV weight				68.49	

TABLE 6.4: ERM's components material and weight

Description	Material	Thickness [mm]	Density [kg/m ³]	Weight [kg]	Thermal conductivity [W/mK]
Capsule	Carbon fiber	5	500	84	14
Structure	Aluminum 7075	5	2,810	12	130
Total ERM's weight	-	-	-	96	-

when not possible due to the complexity or error to the estimation, at least of each subsystem. In tables 7.1 and 7.2 costs at system level and investment to a cost operation are found.

TABLE 7.1: Overall Mission Costs by designed system, margins were added to systems with less heritage

SYSTEMS	Cost in FY20 Millions USD	Margin	Up bound Costs in FY20 Millions USD
Modified Descent Stage	191.19	10.00%	210.31
Rover-Technology Offset	326.22	3.84%	338.77
EEV system	28.74	10.00%	31.62
Orbiter	202.88	3.00%	206.94
EDL Aeroshell	88.94	0.00%	88.94
Launch Vehicle	62.00	0.00%	62.00
MAV	54.00	10.00%	59.40
TOTAL	953,98	-	1000,00

TABLE 7.2: Percentage of investment on design activity

Activity	Investment[M USD]	Percentage of Investment
Integration and testing	127.25	13.3%
Ground systems and operations (with payroll)	144.84	15.2%
Flight Units Costs (with payroll)	255.45	26.8%
DD Costs (with payroll)	333.99	35%
Planetary Protection Costs	92.45	9.7%

7.2 Mission risks and Compliance Matrix

The space missions are a very risky domain, allowing little to no mistakes. In such cases, a risk matrix is helpful for organizations or projects that regularly encounter a high degree of risk. To increase Habasulue safety and success to levels of acceptance, mission risks were targeted and described in the Table 7.3 to describe and perform mitigation strategies considering worst-case scenarios for the most crucial mission moments and most important risk factors associated with them.

In the Table 7.4 correlates risks with its probability and the impact or severity that this risk represents to the mission. This matrix is built on two discrete scales: Consequence or Severity and Probability. Each cell has a given number that is obtained by multiplying its consequence scale number and probability scale number. Risk assessment can go from 1 (negligible/rare) to 25 (catastrophic/certain). This allowed the team to assign a risk level to each identified hazard and how each risk level established direct guidelines in terms of concrete control actions and deadlines to be met.

TABLE 7.3: Risks and Mitigation Strategic for Haba Sulue Mission

N°	Event	Status	Mitigation strategic
1	Pyrotechnic bolts deployment failure	Accept	Pyrotechnic bolts have a better than 99% of success. Hence, the risk is accepted
2	MAV flight failure	Mitigate	Perform several flights on earth to ensure MAV flight has more than 98% success
3	Planetary protection orbiter system failure	Accept	Risk accepted considering redundancy on earth.
4	OS orbit injection failure	Mitigate	Mitigation relies upon selecting the correct GNC and ACS. Several simulations and tests will be performed.
5	Orbiter OS catching/ recognition failure	Mitigate	A Time Margin has been considered. as a worst case scenario, a new rescue mission will recover the samples. The OS will keep the samples in good state.
6	Rover communications failure	Accept	Two different and independet system (direct and relay) are implemented to provide redundancy.
7	Rover Arm clog failure	Mitigate	Although mission was thought for Spring season to mitigate this problems, alternating the Arm heaters in different combinations may resolve the problem.
8	Time overrun	Mitigate	The use of heritage technologies will provide a wider time range in the design and development stage that will allow a margin of time.
9	Cost overrun	Mitigate	The expected costs are less than \$1 billion of the established budget, allowing cost overruns without affecting the development of the mission.
10	Drilling borehole colapse	Accept	The drill has the ability to get out of a collapsed borehole environment in case something like this could occur, plus Martian gravity reduces the likelihood of this risk.
11	Rover stuck on mars surface	Accept	The landing site has favorable characteristics and the navigation and guidance system helps to predict the route of travel and avoid terrain where the rover could get stuck.
12	EDL systems failure	Accept	The risk was diminished by the succes of the MSL and Mars2020 missions using this technologies.

TABLE 7.4: Risks Matrix

		Probability				
		Rare [1]	Unlikely [2]	Possible [3]	Likely [4]	Certain [5]
Consequence	Catastrophic [5]	1-6	2-5-7			
	Major [4]	12				
	Moderate [3]	9	4-8			
	Minor [2]	10-11	3			
	Negligible [1]					

TABLE 7.5: compliance Matrix

Type	Statment	Compliance state	Explanation	Pages
R	Primary goal of returning a minimum of 2.5 kg of ice core samples back to Earth	Yes	All mission requirements were successfully complied	Section 1.2. pp. 2 Section 4.5.5. pp. 60
R	The designed system should deliver a robotic system that can land on or near Martian	Yes	Fully robotic systems with landing capabilities were chosen and designed as can be seen in Mars surface Operations section	Section 4. pp. 28 Section 4.2.4. pp. 35
R	The system should be capable of performing drilling operations on Martian	Yes	Auto-Gopher II will execute the drilling tasks	Section 4.4. pp. 54 Section 4.4.2. pp. 55
C	The ice core samples should be at least 25 millimeters in diameter, and 100 millimeters in length	Yes	The delivered Ice cores are 60 mm in diameter and 100 mm in length as constrained by the core bit of Auto-Gopher II drill.	Section 4.4.5. pp. 57 Section 4.5.5. pp. 60
C	The robotic system needs to be capable of storing the ice cores in a frozen state during surface operations	Yes	The site and season chosen for landing assure stability to the samples. Additionally, location and storage materials prevent radiation sources to heat the sample. A MPFL freaon-11 pipe will roll the sample cannister, due in case of an unusual rise of atmospheric temperature it is prevent for the samples to surpass the -35rC minimum operational temperature of the thermal system.	Section 4.5.6. pp. 62 to 63
C	The system must return a minimum of 2.5 kg of ice cores in its frozen state back to Earth and accommodate the safe transfer of the ice cores to Earth-based laboratories in their frozen state	Yes	The ice core samples would be housed in the capsule designed for the thermal protection on every stage of the mission	Section 3.5.10. pp. 26 Section 6.3.5. pp. 83
R	Design and define the end-to-end mission operations, including launch, transit to Mars, entry/descent/landing, surface operation, ascent, and return to Earth	Yes	All the choices and designs were fully defined and justified based on the requirements and looking for his compliance	Section 3.5. pp. 17 Section 4.2.1. pp. 30 Section 4.3.1. pp. 38 Section 5. pp. 65 section 6.1. pp. 78
R	Select a mission architecture and vehicle design that maximizes the science data return within the cost and schedule constraints	Yes		Section 1. pp. 1 to 5 section 3.3. pp. 9
R	Discuss the selection of target locations and the values of the selected site, including the assessment criteria	Yes	Phoenix landing site is evaluated as the least risk in between mid latitudes glaciers and North pole ice caps and craters.	Section 2.1, pp.6
R	Perform trade studies on system options at the system and subsystem level to demonstrate the fitness of the chosen mission design	Yes	Trade studies based on AHP were performed for main systems. Selection analysis is found in subsystems.	Section 2.1. pp. 6 Section 3.2.2. pp. 8 Section 3.4.2. pp. 12 Section 4.3.3. pp. 39 Section 5.2.4. pp. 69 Section 6.2. pp. 79
R	Discuss selection of subsystem components, including mass, power, and volume, and how the design requirements drove the selection of the subsystem	Yes	Inside the mission	Section 1. pp. 1 to 5 Overall proposal
C	The cost for end-to-end mission shall not exceed \$1Billion US Dollars (in FY20), including launch, design development test and evaluation (DDT&E) and flight unit costs for the mission		The estimated cost is about 50 million US dollars less that the limit budget. This allows the team to have a margin for unsuspected additional costs	Section 7.1. pp. 86

TABLE 7.6: compliance Matrix

Type	Statment	Compliance state	Explanation	Pages
R	If advanced technology options are utilized in the design, estimation of technology advancement cost must be included	Yes	The most advanced technologies found in the design are found in EEV materials. A detailed estimate of the cost is found on EEV section	Section 7. pp. 86
C	The ice core sample must be returned to Earth for scientific analysis no later than December 31, 2030.	Yes	The mission delivers the ice cores for	Section 3.1. pp. 7
D	Requirements Definition	Yes		pp. 1-5
D	Requirements at subsystem level -Orbiter	Yes		
D	Requirements at subsystem level -Lander	Yes		Section 4.2, pp. 30
D	Requirements at subsystem level -Rover	Yes		Section 4.3.2, pp. 39
D	Requirements at subsystem level -MAV	Yes		section 5 pp. 67
D	Concept of Operation	Yes		p. 6, 7-27, 28- 65, 65-78, 79-85.
D	Trade Studies	Yes		as described above
D	Design Integration and Operation	Yes		pp. 1-6
D	Cost Estimate	Yes		Section 7, pp. 85-89
D	Schedule	Yes		Section 3, pp. 7
D	Executive summary	Yes		pp. 1-5
D	References	Yes		pp. 90-95
D	Compliance Matrix	Yes		pp. 88-89

Bibliography

- [1] J Garvin. "North Polar Region Craterforms on Mars: Geometric Characteristics from the Mars Orbiter Laser Altimeter". In: *Icarus* 144.2 (2000), pp. 329352. DOI: [10.1006/icar.1999.6298](https://doi.org/10.1006/icar.1999.6298).
- [2] Stephen Brough, Bryn Hubbard, and Alun Hubbard. "Area and volume of mid-latitude glacier-like forms on Mars". In: *Earth and Planetary Science Letters* 507 (2019), pp. 1020. DOI: [10.1016/j.epsl.2018.11.031](https://doi.org/10.1016/j.epsl.2018.11.031).
- [3] K. Zacny and G. Cooper. "Considerations, constraints and strategies for drilling on Mars". In: *Planetary and Space Science* 54.4 (2006), pp. 345356. DOI: [10.1016/j.pss.2005.12.003](https://doi.org/10.1016/j.pss.2005.12.003).
- [4] Issac B. Smith. "Unlocking the ClimateRecord Storedwithin Mars' Polar Layered Deposits". In: *Keck Institute for Space Studies* (2018).
- [5] Donna Viola, Alfred S. McEwen, and Colin M. Dundas. *Arcadia Planitia: Acheron Fossae and Erebus Montes*. 2015.
- [6] Donna Viola et al. "Expanded secondary craters in the Arcadia Planitia region, Mars: Evidence for tens of Myr-old shallow subsurface ice". In: *Icarus* 248 (2015), pp. 190204. DOI: [10.1016/j.icarus.2014.10.032](https://doi.org/10.1016/j.icarus.2014.10.032).
- [7] Michael T. Mellon et al. "Periglacial landforms at the Phoenix landing site and the northern plains of Mars". In: *Journal of Geophysical Research* 113 (2008). DOI: [10.1029/2007je003039](https://doi.org/10.1029/2007je003039).
- [8] Michael T. Mellon et al. "Ground ice at the Phoenix Landing Site: Stability state and origin". In: *Journal of Geophysical Research* 114 (2009). DOI: [10.1029/2009je003417](https://doi.org/10.1029/2009je003417).
- [9] G. M. Martínez et al. "The Modern Near-Surface Martian Climate: A Review of In-situ Meteorological Data from Viking to Curiosity". In: *Space Science Reviews* 212.1-2 (2017), pp. 295338. DOI: [10.1007/s11214-017-0360-x](https://doi.org/10.1007/s11214-017-0360-x).
- [10] Richard P. Kornfeld, Joe C. Parrish, and Steve Sell. "Mars Sample Return: Testing the Last Meter of Rendezvous and Sample Capture". In: *Journal of Spacecraft and Rockets* 44.3 (2007), pp. 692–702. DOI: [10.2514/1.26098](https://doi.org/10.2514/1.26098). eprint: <https://doi.org/10.2514/1.26098>. URL: <https://doi.org/10.2514/1.26098>.
- [11] NASA Online Directives Information System. *NASA Launch Vehicle Certification Requirements Matrix*. URL: https://nodis3.gsfc.nasa.gov/NPD_attachments/AttachmentA_7C.pdf.
- [12] Rachel C. Willenbring Clavert A. Staubus. *Safety Guidance for Payloads*. 2017. URL: https://tdglobal.ksc.nasa.gov/servlet/sm.web.Fetch/Safety_Guidance_for_Payloads_cas6.21.17_MB.pdf?rhid=1000&did=939757&type=released.
- [13] SpaceX. *Falcon User's guide*. 2020, pp. 3–5,36,37,52. URL: https://www.spacex.com/media/falcon_users_guide_042020.pdf.
- [14] D. A. Vallado. "Fundamentals of Astrodynamics and Applications". In: Springer, 2001, p. 318. ISBN: 0-7923-6903-3.
- [15] P. R. Escobal. *Methods of Astrodynamics*. New York: John Wiley & Sons, 1968. ISBN: 978-0-471-24528-5.
- [16] Jet Propulsion Laboratory NASA. *Basics of Space Flight*. URL: <http://www2.jpl.nasa.gov/basics/bsf4-1.php>.
- [17] Y. Song et al. "Potential Launch Opportunities for a SmallSat Mission around the Moon Injected during a Lunar Flyby En Route to Mars". In: *hindawi* (2019). Ed. by Florin Stoican, pp. 7,8. DOI: [10.1155/1245213](https://doi.org/10.1155/1245213).
- [18] Noam Izenberg et al. "Human Assisted Science at Venus: Venus Exploration in the New Human Spaceflight Age". 2020.
- [19] K. M. Hughes. "Gravity-assist trajectories to Venus, Mars, and the ice giants: Mission design with human and robotic applications". PhD thesis. Indiana: Purdue University, 2016, p. 167. URL: https://docs.lib.purdue.edu/open_access_dissertations/940.
- [20] C. Foster. *NASA Ames Research Center Trajectory Browser*. NASA Ames Research Center. URL: <https://trajbrowser.arc.nasa.gov/>.
- [21] Eric Joffre et al. "Mars Sample Return: Mission Analysis for an ESA Earth Return Orbiter". In: Nov. 2018.
- [22] Space Flight 101. *OSIRIS-REx Spacecraft*. 2021. URL: <https://spaceflight101.com/osiris-rex/osiris-rex-spacecraft-overview/>.
- [23] Autodesk. *Autodesk Inventor*. Version 2021. 2021. URL: <https://www.autodesk.com/products/inventor/overview?term=1-YEAR>.
- [24] "Qualification of the T6 Thruster for BepiColombo". In: *34th International Electric Propulsion Conference* (2015), IEPC–2015–132.
- [25] Satsearch. *ACSS - Advanced Coarse Sun Sensor*. 2019. URL: <https://satsearch.co/products/solarmems-acss-advanced-coarse-sun-sensor>.

- [26] LN-200 FOG Family Advanced Airborne IMU/AHRS. 2020. URL: <https://www.northropgrumman.com/what-we-do/air/ln-200-fog-family-advanced-airborne-imu-ahrs/>.
- [27] Phil Christensen and Lisa May. *Planetary Science Decadal Survey MSR Orbiter Mission*. 2010. URL: http://sites.nationalacademies.org/cs/groups/ssbsite/documents/webpage/ssb_059308.pdf.
- [28] Ronny Votel and Doug Sinclair. "Comparison of control moment gyros and reaction wheels for small Earth-orbiting satellites". In: *Proceedings of the 26th Annual AIAA/USU Conference on Small Satellites* (2012), pp. 1–7. URL: <http://goo.gl/V82KCB>.
- [29] Rockwell Collins. "RSI 01 Momentum and Reaction Wheels 0 . 1 Nms with integrated Wheel Drive Electronics". In: *Building* (2002). URL: http://www.electronicnote.com/media/downloads/RSI12_A4.pdf.
- [30] Aerojet Rocketdyne. "Monopropellant Data Sheet". In: 98052.425 (2004), p. 1. URL: <https://bit.ly/3hhSX1F>.
- [31] Bosh. "Travelling Wave Tube Amplifiers (TWTAs) for Space Applications". In: (2019), pp. 1,7. URL: <http://www.electronicnote.com/site/PDF/TWTA%20Brochure.pdf>.
- [32] General Dynamics. "Small Deep-Space Transponder (SDST)". In: (2019). URL: <https://gdmissionsystems.com/-/media/General-Dynamics/Space-and-Intelligence-Systems/PDF/small-deep-space-transponder-datasheet.ashx?la=en&hash=1A2E96BE0D9C0C29BD281963680DABDBEAE0E465>.
- [33] Stephen D Slobin and Christine Chang. "DSN Coverage and Geometry". In: (2016), pp. 8,16. URL: <https://deepspace.jpl.nasa.gov/dsndocs/810-005/301/301K.pdf>.
- [34] R Berger, D Artz, and P Kapcio. "RAD750 Radiation Hardened PowerPC TM Microprocessor". In: *Citeseer* (2005). URL: <http://caxapa.ru/thumbs/440955/download.pdf>.
- [35] Bae Systems. "RAD750® 6U CompactPCI Single-board computer". In: (2018).
- [36] Bae Systems. "Radiation Hardened Programmable Read Only Memory (PROM) 5 V". In: (2001). URL: <http://www.digchip.com/datasheets/parts/datasheet/568/197A807-pdf.php+>.
- [37] Anthony J Colozza and Robert L Cataldo. "Applicability of STEM-RTG and High-Power SRG Power Systems to the Discovery and Scout Mission Capabilities Expansion (DSMCE) Study of ASRG-Based Missions". In: *NASA Technical Memorandum* October (2015), p. 218885. URL: <http://www.sti.nasa.gov>.
- [38] Eagle Pincher Technologies. "SAR-10197 Aerospace Battery". In: (). URL: <https://www.eaglepincher.com/sites/default/files/EP-SAR-10197-DATA-SHEET.pdf>.
- [39] James R. Wertz, David F. Everett, and Jeffery J. Puschell. *Space mission engineering : the new SMAD / edited by James R. Wertz, David F. Everett, Jeffery J. Puschell*. 2011.
- [40] SPECTROLAB. "XTJ Prime Datasheet". In: (2018), pp. 8–9. URL: https://www.spectrolab.com/photovoltaics/XTJ-Prime_Data_Sheet.pdf.
- [41] Jhon H. Henniger. "Solar Absorptance and Thermal Emittance Thermal Emittance of Some Common Spacecraft Thermal-Control Coatings". In: *Angewandte Chemie International Edition* 6.11 (1984), pp. 951–952. ISSN: 1098-6596. arXiv: [arXiv:1011.1669v3](https://arxiv.org/abs/1011.1669v3).
- [42] NASA Dr. David R. Williams. *Mars Fact Sheet*. 2020. URL: <https://nssdc.gsfc.nasa.gov/planetary/factsheet/marsfact.html>.
- [43] Thomas Bryan, Ricky T Howard, and Jimmie Johnson. "Next Generation Advanced Video Guidance Sensor: Low Risk Rendezvous and Docking Sensor". In: *Sensors (Peterborough, NH)* (1998), pp. 1–11. URL: https://www.researchgate.net/publication/268569653_Next_Generation_Advanced_Video_Guidance_Sensor_Low_Risk_Rendezvous_and_Docking_Sensor.
- [44] Paulo Younse et al. "Concept for an On-orbit Capture and Orient Module for Potential Mars Sample Return". In: *IEEE Aerospace Conference Proceedings* (2020). ISSN: 1095323X. DOI: [10.1109/AERO47225.2020.9172814](https://doi.org/10.1109/AERO47225.2020.9172814). URL: <https://ieeexplore.ieee.org/document/9172814>.
- [45] Karl Edquist et al. "Aerothermodynamic Design of the Mars Science Laboratory Heatshield". In: June 2009. ISBN: 978-1-62410-168-7. DOI: [10.2514/6.2009-4075](https://doi.org/10.2514/6.2009-4075).
- [46] Robert Braun and Robert Manning. "Mars Exploration Entry, Descent, and Landing Challenges". In: vol. 44. Mar. 2007, 18 pp. DOI: [10.1109/AERO.2006.1655790](https://doi.org/10.1109/AERO.2006.1655790).
- [47] Brian K. Muirhead and Ashley Karp. "Mars Sample Return Lander Mission Concepts". In: *2019 IEEE Aerospace Conference*. 2019, pp. 1–9. DOI: [10.1109/AERO.2019.8742215](https://doi.org/10.1109/AERO.2019.8742215).
- [48] David W. Way et al. "Mars Science Laboratory: Entry, Descent, and Landing System Performance". In: *2007 IEEE Aerospace Conference*. 2007, pp. 1–19. DOI: [10.1109/AERO.2007.352821](https://doi.org/10.1109/AERO.2007.352821).
- [49] I. W. Ramsey et al. "The Evolution of the Viking Landing Gear". In: 1976.
- [50] J. Trautwein. "Pressurized Metal Bellows Shock Absorber for Space Applications." In: 2015.

- [51] William Gullotta et al. "RESETTABLE LANDING GEAR FOR MARS HOPPER". In: June 2014. DOI: [10.13140/2.1.1840.3524](https://doi.org/10.13140/2.1.1840.3524).
- [52] Lars Witte et al. "Experimental Investigations of the Comet Lander Philae Touchdown Dynamics". In: *Journal of Spacecraft and Rockets* 51 (Nov. 2014), p. 1885. DOI: [10.2514/1.A32906](https://doi.org/10.2514/1.A32906).
- [53] Malaya Kumar Biswal M and Ramesh Naidu Annavarapu. "Conceptual Design of Mars Lander with Novel Impact Intriguing System". In: Jan. 2021.
- [54] J. Hunter Waite and Curt Niebur. "Mission Concept Study Planetary Science Decadal Survey JPL Team X Titan Lake Probe Study". In: April (2010).
- [55] Anita Sengupta et al. "Systems engineering and support systems technology considerations of a Mars Ascent Vehicle". In: *2012 IEEE Aerospace Conference*. 2012, pp. 1–11. DOI: [10.1109/AERO.2012.6187298](https://doi.org/10.1109/AERO.2012.6187298).
- [56] *The Lander Structure*. URL: <https://mars.nasa.gov/mer/mission/spacecraft/entry-descent-and-landing-configuration/lander-structure/>.
- [57] Mircea Badescu et al. "Auto-Gopher-II: an autonomous wireline rotary-hammer ultrasonic drill test results". In: *Sensors and Smart Structures Technologies for Civil, Mechanical, and Aerospace Systems 2019* (2019). DOI: [10.1117/12.2514618](https://doi.org/10.1117/12.2514618).
- [58] Mera Fayez Horne. "Drilling on Mars Mathematical Model of Rotary-Ultrasonic Core Drilling". PhD thesis. University of California, Berkeley, 2015.
- [59] S. Hamran et al. "RIMFAX: a GPR for the Mars 2020 Rover Mission". In: *EIEE* (2017), pp. 44–50. DOI: [978-1-4799-6495-6/15/](https://doi.org/978-1-4799-6495-6/15/).
- [60] *RIMFAX for Scientifics*. URL: <https://mars.nasa.gov/mars2020/spacecraft/instruments/rimfax/for-scientists/> (visited on 03/2021).
- [61] E. Gonzales and E. Cordoba. "Compatibility Tests Between the Mars Vehicle System Test Bed and RIMFAX Radar Antenna Prototype for the Mars 2020". In: *EIEE* (2017), pp. 44–50. DOI: [978-1-5386-2231-5/17/](https://doi.org/978-1-5386-2231-5/17/).
- [62] *Radar Imager for Mars' Subsurface Exploration (RIMFAX)*. URL: <https://mars.nasa.gov/mars2020/spacecraft/instruments/rimfax/>.
- [63] J. Gómez-Elvira et al. "REMS: The Environmental Sensor Suite for the Mars Science Laboratory Rover". In: *Space Science Reviews* 170 (2012), pp. 583–640. DOI: [10.1007/s11214-012-9921-1](https://doi.org/10.1007/s11214-012-9921-1).
- [64] P.A. Taylor et al. "Temperature, pressure, and wind instrumentation in the Phoenix meteorological package". In: *Jorunal of Geophysical Research* 113 (2008). DOI: [10.1029/2007JE003015](https://doi.org/10.1029/2007JE003015).
- [65] NASA. *Scanning Habitable Environments with Raman & Luminescence for Organics & Chemicals*. Last accessed 2021. URL: <https://mars.nasa.gov/mars2020/spacecraft/instruments/sherloc/>.
- [66] A. Buch et al. "End to End MOMA (Mars Organic Molecule Analyser) Campaign with the GC-MS Engineering Test Unit (ETU)". In: *AGU Fall Meeting Abstracts*. Vol. 2019. Dec. 2019, P33D–18.
- [67] NASA. *Planetary Instrument for X-ray Lithochemistry*. Last accessed 2021. URL: <https://mars.nasa.gov/mars2020/spacecraft/instruments/pixl/>.
- [68] Olcott Marshall A. Marshall CP. "Raman spectroscopy as a screening tool for ancient life detection on Mars." In: *Phil. Trans. R. Soc.* -372 (2014). ISSN: 15311074. DOI: <http://dx.doi.org/10.1098/rsta.2014.0195>.
- [69] Yan Wang Sunxin Li. "Dynamic Rocker-Bogie: Kinematical Analysis in a High-Speed Traversal Stability Enhancement". In: *International Journal of Aerospace Engineering* 2016.Iris (2016), pp. 243–249. ISSN: 18770509. DOI: [10.1155/2016/5181097](https://doi.org/10.1155/2016/5181097). URL: <https://doi.org/10.1155/2016/5181097>.
- [70] Tabatha Heet. "Geologic Setting of the Phoenix Lander Mission Landing Site". PhD thesis. Washington University, 2009.
- [71] Keith S Novak et al. "Preliminary Surface Thermal Design of the Mars 2020 Rover". In: *45th International Conference on Environmental Systems*. Vol. 134. Albuquerque, New Mexico, 2015, pp. 1–19. URL: https://ttu-ir.tdl.org/bitstream/handle/2346/64407/ICES_2015_submission_134.pdf.
- [72] Stephen Indyk. *TRIDENT The Regolith and Ice Drill for Exploration of New ...* 2017. URL: <https://www.hou.usra.edu/meetings/leag2017/presentations/wednesday/zacny2.pdf>.
- [73] Philip Chu, Justin Spring, and Kris Zacny. "ROPEC ROTary PERcussive Coring Drill for Mars Sample Return". In: *Proceedings of the 42nd Aerospace Mechanisms Symposium*. 2014, pp. 195–210.
- [74] Anthony J Colozza and Robert L Cataldo. "Applicability of STEM-RTG and High-Power SRG Power Systems to the Discovery and Scout Mission Capabilities Expansion (DSMCE) Study of ASRG-Based Missions". In: *NASA Technical Memorandum* October (2015). DOI: [10.13140/RG.2.1.3697.1605](https://doi.org/10.13140/RG.2.1.3697.1605). URL: <http://www.sti.nasa.gov>.

- [75] J. Merrison P. Taylor C. Lange J. Davis M. Lemmon C. Holstein-Rathlou H.P. Gunnlaugsson. "Winds at Mars Phoenix Landing Site". In: *Journal of Geophysical Research* 115 (2009), p. 1548. DOI: DOI:10.1029/2009JE003411.
- [76] J. N. Maki et al. "Mars Exploration Rover Engineering Cameras". In: *Geophysical Research* 108 (2003). DOI: 10.1029/2003JE002077.
- [77] *The Rover "Eyes" and other "Senses"*. URL: "<https://mars.nasa.gov/mer/mission/rover/eyes-and-senses/>" (visited on 03/2021).
- [78] Northrop Grumman. *LN-200S IMU*. 2013. URL: "<https://satcatalog.com/component/ln-200s/>".
- [79] Y. Tao, J-P. Muller, and W Poole. "Automated localisation of Mars rovers using co-registered HiRISE-CTX-HRSC orthorectified images and wide baseline Navcam orthorectified mosaics". In: *Icarus* (2016), pp. 139–157.
- [80] BAE Systems. *RAD750 CompactPCI 6U*. URL: "<https://www.baesystems.com/en-us/product/radiation-hardened-electronics>".
- [81] NASA. *Multi-Mission Radioisotope Thermoelectric Generator (MMRTG)*. Fact Sheet. 2012.
- [82] Y. Lee and B Bairstow. *Radioisotope Power Systems Reference Book for Mission Designers and Planners*. Other. NASA, Jet Propulsion Laboratory, 2015. DOI: 20160001769.
- [83] E Lakdawalla. In: *The Design and Engineering of Curiosity. How the Mars Rover Performs Its Job*. Springer Praxis Books. Chap. Designing a Bigger Lander (2000-2003), pp. 7–8. ISBN: 978-3-319-68146-7. DOI: 10.1007/978-3-319-68146-7.
- [84] NASA. *Electrical Power-NASA Mars*. URL: "<https://mars.nasa.gov/mars2020/spacecraft/rover/electrical-power/>".
- [85] EaglePicher. *EaglePicher Batteries are Returning to Mars*. URL: "<https://www.eaglepicher.com/resources/news-and-events/eaglepicher-batteries-are-returning-mars/>".
- [86] Jet Propulsion Laboratory. *Temperature Measurements Taken by Phoenix Spacecraft*. Last accessed 30 September 2008. 2008. URL: <https://www.jpl.nasa.gov/images/temperature-measurements-taken-by-phoenix-spacecraft>.
- [87] Steven M. Nelli et al. "Simulations of atmospheric phenomena at the Phoenix landing site with the Ames General Circulation Model". In: *Journal of Geophysical Research E: Planets* 115.6 (2010), pp. 1–13. ISSN: 01480227. DOI: 10.1029/2010JE003568.
- [88] G.M. Martínez et al. "The Modern Near-Surface Martian Climate: A Review of In-situ Meteorological Data from Viking to Curiosity". In: *Space Science Reviews* 212 (2017), pp. 295–338. DOI: 10.1007/s11214-017-0360-x.
- [89] J. Kipp D. Vasavada A. Kirk R. Fergason R. Bellutta P. Calef F. Larsen K. Katayama Y. Huertas A. Beyer R. Chen A. Parker T. Pollard B. Lee S. Sun Y. Hoover R. Sladek H. Grotzinger J. Welch R. Noe Dobrea E. Michalski J. Watkins M. Golombek M. Grant. "Selection of the Mars Science Laboratory landing site". In: *Space Science Reviews* October (2012), pp. 641–737. DOI: 10.1007/s11214-012-9916-y.
- [90] Pradeep Bhandari et al. "Mars science laboratory mechanically pumped fluid loop for thermal control design, implementation, and testing". In: *SAE International Journal of Aerospace* 4.1 (2011), pp. 299–310. ISSN: 19463855. DOI: 10.4271/2009-01-2437.
- [91] Ryuta Hatakenaka et al. "Preliminary Thermal Design of the Japanese Mars Rover". In: *45th International Conference on Environmental Systems*. Washington, 2015.
- [92] Pradeep Bhandari et al. "CO2 Insulation for Thermal Control of the Mars Science Laboratory". In: *41st International Conference on Environmental Systems*. DOI: 10.2514/6.2011-5119. URL: <https://arc.aiaa.org/doi/abs/10.2514/6.2011-5119>.
- [93] Rius Billing and Richard Fleischner. "Mars science laboratory robotic arm". In: *14th European Space Mechanisms & Tribology Symposium ESMATS 2011* September (2011), pp. 363–370. URL: <http://esmats.eu/esmatspapers/pastpapers/pdfs/2011/billing.pdf>.
- [94] J. Taylor et al. "Mars Exploration Rover Telecommunications". In: chap. Chapter 7, pp. 263–376.
- [95] Mera F Horne. "Drilling on Mars - Mathematical Model for Rotary-Ultrasonic Core Drilling of Brittle Materials". PhD thesis. 2015.
- [96] G. M. Martínez et al. "The Modern Near-Surface Martian Climate: A Review of In-situ Meteorological Data from Viking to Curiosity". In: *Space Science Reviews* 212.1-2 (2017), pp. 295338. DOI: 10.1007/s11214-017-0360-x.
- [97] Canadian Space Agency. 2009. URL: https://web.archive.org/web/20110705011110/http://www.asc-csa.gc.ca/eng/media/news_releases/2009/0702.asp.
- [98] DLR - *Dust storms swirl at Mars' north pole*. 2019. URL: https://www.dlr.de/content/en/articles/news/2019/03/20190704_dust-storms-swirl-at-mars-noth-pole.html.
- [99] Kris Zacny et al. "Auto-Gopher-II: a wireline rotary-hammer ultrasonic drill that operates autonomously". In: *Sensors and Smart Structures Technologies for Civil, Mechanical, and Aerospace Systems 2018* (2018). DOI: 10.1117/12.2294560.

- [100] Robert L. Staehle. "Mars Polar Ice Sample Return Mission (Part 1)". In: *SpaceFlight* (1976).
- [101] *About Ice Cores*. 2016. URL: <https://icecores.org/about-ice-cores>.
- [102] Christopher P. McKay et al. "The Icebreaker Life Mission to Mars: A Search for Biomolecular Evidence for Life". In: *Astrobiology* 13.4 (2013), pp. 334353. DOI: [10.1089/ast.2012.0878](https://doi.org/10.1089/ast.2012.0878).
- [103] Yoseph Bar-Cohen et al. "Auto-Gopher-2 - Wireline Deep Sampler Driven by Percussive Piezoelectric Actuator and Rotary EM Motors". In: *Advances in Science and Technology* 100 (2016), pp. 207212. DOI: [10.4028/www.scientific.net/ast.100.207](https://doi.org/10.4028/www.scientific.net/ast.100.207).
- [104] Yoseph Bar-Cohen et al. "Auto-Gopher-2 An Autonomous Wireline Rotary Piezo-Percussive Deep Drilling Mechanism". In: *Earth and Space 2018* (2018). DOI: [10.1061/9780784481899.031](https://doi.org/10.1061/9780784481899.031).
- [105] K. Zacny et al. "Wireline deep drill for exploration of Mars, Europa, and Enceladus". In: *2013 IEEE Aerospace Conference* (2013). DOI: [10.1109/aero.2013.6497189](https://doi.org/10.1109/aero.2013.6497189).
- [106] Scott Perino et al. "The evolution of an orbiting sample container for potential Mars sample return". In: *2017 IEEE Aerospace Conference* (2017). DOI: [10.1109/aero.2017.7943979](https://doi.org/10.1109/aero.2017.7943979).
- [107] Karen Taminger and Stephen Hales. "Aerospace Applications of Aluminum-Lithium Alloy Thick Plate". In: June 2010.
- [108] Peter A. Taylor et al. "On pressure measurement and seasonal pressure variations during the Phoenix mission". In: *Journal of Geophysical Research* 115 (2010). DOI: [10.1029/2009je003422](https://doi.org/10.1029/2009je003422).
- [109] Luye Dou et al. "Hierarchical Cellular Structured Ceramic Nanofibrous Aerogels with Temperature-Invariant Superelasticity for Thermal Insulation". In: *ACS Applied Materials & Interfaces* 11.32 (2019). PMID: 31330101, pp. 29056–29064. DOI: [10.1021/acsami.9b10018](https://doi.org/10.1021/acsami.9b10018). eprint: <https://doi.org/10.1021/acsami.9b10018>. URL: <https://doi.org/10.1021/acsami.9b10018>.
- [110] P. Bhandari, M. Redmond, and J. Kempenaar. "Mars Sample Thermal Control During Mars Ascent and Orbit". In: 2016.
- [111] Narges Kiomarsipour, Reza Shoja Razavi, and Kamal Ghani. "Improvement of spacecraft white thermal control coatings using the new synthesized Zn-MCM-41 pigment". In: *Dyes and Pigments* 96.2 (2013), pp. 403–406. ISSN: 0143-7208. DOI: <https://doi.org/10.1016/j.dyepig.2012.08.019>. URL: <https://www.sciencedirect.com/science/article/pii/S0143720812002392>.
- [112] "Technology development and design of liquid bi-propellant mars ascent vehicles". In: *IEEE Aerospace Conference Proceedings 2016-June* (2016), pp. 1–12. ISSN: 1095323X. DOI: [10.1109/AERO.2016.7500833](https://doi.org/10.1109/AERO.2016.7500833).
- [113] "A hybrid mars ascent vehicle concept for low temperature storage and operation". In: *52nd AIAA/SAE/ASEE Joint Propulsion Conference, 2016* (2016), pp. 1–9. DOI: [10.2514/6.2016-4962](https://doi.org/10.2514/6.2016-4962).
- [114] Quincy Bean et al. "Mars Ascent Vehicle (MAV) Propulsion Subsystems Design". In: *IEEE Aerospace Conference Proceedings 2019-March* (2019), pp. 1–9. ISSN: 1095323X. DOI: [10.1109/AERO.2019.8742205](https://doi.org/10.1109/AERO.2019.8742205).
- [115] Northrop Grumman. "Propulsion products catalog". In: (2018), p. 150.
- [116] Robert Shotwell et al. "Drivers, developments and options under consideration for a Mars ascent vehicle". In: *IEEE Aerospace Conference Proceedings 2016-June* (2016). ISSN: 1095323X. DOI: [10.1109/AERO.2016.7500822](https://doi.org/10.1109/AERO.2016.7500822).
- [117] Evan Anzalone, Dane Erickson, and Carlos Montalvo. "Guidance and navigation design for a martian sample return ascent vehicle". In: *Advances in the Astronautical Sciences* 169 (2019), pp. 129–140. ISSN: 00653438.
- [118] Evan Anzalone et al. "Guidance and Navigation Challenges for a Mars Ascent Vehicle". In: *IEEE Aerospace Conference Proceedings* (2020), pp. 1–14. ISSN: 1095323X. DOI: [10.1109/AERO47225.2020.9172543](https://doi.org/10.1109/AERO47225.2020.9172543).
- [119] Richard H. Battin. *An Introduction to the Mathematics and Methods of Astrodynamics, Revised Edition*. 1999. ISBN: 1563473429. DOI: [10.2514/4.861543](https://doi.org/10.2514/4.861543).
- [120] Andrew Prince et al. "Mars Ascent Vehicle Propulsion System Solid Motor Technology Plans". In: *IEEE Aerospace Conference Proceedings 2019-March* (2019), pp. 1–12. ISSN: 1095323X. DOI: [10.1109/AERO.2019.8741851](https://doi.org/10.1109/AERO.2019.8741851).
- [121] Ian J. Dux et al. "Mars ascent vehicle gross lift-off mass sensitivities for robotic Mars sample return". In: *IEEE Aerospace Conference Proceedings April* (2011). ISSN: 1095323X. DOI: [10.1109/AERO.2011.5747505](https://doi.org/10.1109/AERO.2011.5747505).
- [122] NASA. *Mars Atmosphere Model metric Units*. Last accessed 14 May 2021. URL: <https://www.grc.nasa.gov/www/k-12/airplane/atmosmrm.html>.
- [123] John C. Whitehead. "Trajectory analysis and staging trades for smaller mars ascent vehicles". In: *Journal of Spacecraft and Rockets* 42.6 (2005), pp. 1039–1046. ISSN: 15336794. DOI: [10.2514/1.10680](https://doi.org/10.2514/1.10680).
- [124] George Story et al. "A single stage to orbit design for a hybrid mars ascent". In: *AIAA Propulsion and Energy Forum and Exposition, 2019 August* (2019), pp. 1–19. DOI: [10.2514/6.2019-3840](https://doi.org/10.2514/6.2019-3840).

- [125] John C. Whitehead. "Trajectory analysis and staging trades for smaller mars ascent vehicles". In: *Journal of Spacecraft and Rockets* 42.6 (2005), pp. 1039–1046. ISSN: 15336794. DOI: [10.2514/1.10680](https://doi.org/10.2514/1.10680).
- [126] George Story et al. "A single stage to orbit design for a hybrid mars ascent". In: *AIAA Propulsion and Energy Forum and Exposition, 2019 August* (2019), pp. 1–19. DOI: [10.2514/6.2019-3840](https://doi.org/10.2514/6.2019-3840).
- [127] W3Techs. *Usage Statistics of Content Languages for Websites*. Last accessed on 14 may 2021. 2021. URL: <https://www.nasa.gov/press-release/nasa-awards-mars-ascent-propulsion-system-contract-for-sample-return>.
- [128] M. M. Munk and L. J. Glaab. "Mars Sample Return Earth Entry Vehicle: Continuing Efforts". In: *Concepts and Approaches for Mars Exploration*. Vol. 1679. June 2012, p. 4175.
- [129] H. Price et al. "Mars Sample Return spacecraft systems architecture". In: *2000 IEEE Aerospace Conference. Proceedings (Cat. No.00TH8484)*. Vol. 7. 2000, 357–375 vol.7. DOI: [10.1109/AERO.2000.879302](https://doi.org/10.1109/AERO.2000.879302).
- [130] Kamran Daryabeigi. "Thermal Analysis and Design of Multi-layer Insulation for Re-entry Aerodynamic Heating". In: *Journal of Spacecraft and Rockets - J SPACECRAFT ROCKET* 39 (July 2002), pp. 509–514. DOI: [10.2514/2.3863](https://doi.org/10.2514/2.3863).
- [131] Thomas Ajluni et al. "OSIRIS-REx, returning the asteroid sample". In: *2015 IEEE Aerospace Conference*. 2015, pp. 1–15. DOI: [10.1109/AERO.2015.7118988](https://doi.org/10.1109/AERO.2015.7118988).
- [132] Kerry A. Trumble et al. "Post-Flight Aerothermal Analysis of the Stardust Sample Return Capsule". In: 2008.
- [133] Ryuta Hatakenaka et al. *Thermal Design of HTV Small Re-entry Capsule*. 2017. URL: <http://hdl.handle.net/2346/73102>.
- [134] Yusuke Takahashi and Kazuhiko Yamada. "Aerodynamic-Heating Analysis of Sample-Return Capsule in Future Trojan-Asteroid Exploration". In: *Journal of Thermophysics and Heat Transfer* 32 (June 2016), pp. 1–13. DOI: [10.2514/1.T4837](https://doi.org/10.2514/1.T4837).
- [135] Jaxa. *H-II Transfer Vehicle KOUNOTORI (HTV)*. URL: https://iss.jaxa.jp/en/htv/mission/htv-7/181205_interview.html.
- [136] Troy Eichmann et al. "Radiometric Temperature Analysis of the Hayabusa Spacecraft Re-entry". In: Jan. 2011. ISBN: 978-3-642-25687-5. DOI: [10.1007/978-3-642-25688-2_77](https://doi.org/10.1007/978-3-642-25688-2_77).
- [137] "OSIRIS-REx Asteroid Sample Return Mission". In: *OSIRIS-REx Asteroid Sample Return Mission Press Kit 2016* (2016). URL: https://www.nasa.gov/sites/default/files/atoms/files/osiris-rex_press_kit_0.pdf.
- [138] "Stardust Sample Return". In: *Stardust Sample Return, NASA, Press Kit, 2006* (2006). URL: https://www.jpl.nasa.gov/news/press_kits/stardust-return.pdf.
- [139] National Aeronautics and Space Administration. *Nasa Project Cost Estimating Capability*. 2018. URL: https://www.nasa.gov/offices/ocfo/functions/models_tools/PCEC/.